UNIVERSITÀ DEGLI STUDI DI VERONA

DEPARTMENT OF

Neuroscience, Biomedicine and Movement Sciences

DOCTORAL PROGRAM IN

Biomolecular Medicine

Contribution of
Piano Nazionale di Ripresa e Resilienza (PNRR)

CYCLE /YEAR

XXXVIII Cycle

α −Bisabolol Against Recurrence, Metastasis and Tumour Self-renewal in Triple Negative Breast Cancer

S.S.D. BIO-10

Coordinator: Prof.ssa Lucia De Franceschi

Signature _____

Supervisor: Prof. ssa Sofia Giovanna Mariotto

Signature_____

Co-Supervisor: Prof./ssa Elena Butturini

Signature_____

Doctoral Student: Dott. ssa Maria Mosaico

Signature _____

* Per l'elenco dei Settori Scientifico-Disciplinari (SSD) si veda il D.M. del 4 Ottobre 2000, Allegato A *"Elenco dei Settori Scientifico –Disciplinari"* reperibile sul sito del Ministero dell'Università e della Ricerca al seguente indirizzo: http://www.miur.it/atti/2000/alladm001004_01.htm

La borsa di dottorato è stata cofinanziata con le risorse del PNRR:

• per il DM 351 nell'ambito della Missione 4 ("Istruzione e ricerca") – Componente 1 ("Potenziamento dell'offerta dei servizi di istruzione: dagli asili nido all'Università"), Investimento 3.4. ("Didattica e competenze universitarie avanzate") e Investimento 4.1 ("Estensione del numero di dottorati di ricerca e dottorati innovativi per la pubblica amministrazione e il patrimonio culturale") - progetto M4C1 –Inv. 3.4 e progetto M4C1 – Inv. 4.1

• per il DM 352, nell'ambito della Missione 4 ("Istruzione e Ricerca") – Componente 2 ("Dalla Ricerca all'Impresa"), Investimento 3.3 ("Introduzione di dottorati innovativi che rispondono ai fabbisogni di innovazione delle imprese e promuovono l'assunzione dei ricercatori da parte delle imprese") – progetto M4C2 Investimento 3.3

Table of Contents

List of abbreviations

α-bis	(-)-α-bisabolol
a-bis-NPs	(-)-α-bisabolol PLGA Nanoparticles
BCSCs	Breast Cancer Stem Cells
BCSC1	Breast Cancer Stem Cells Type 1
CSCs	Cancer Stem Cells
DLS	Dynamic Light Scattering
DMEM	Dulbecco's Modified Eagle Medium
EMT	Epithelial-Mesenchymal Transition
EMSA	Electrophoretic Mobility Shift Assay
FBS	Fetal bovine serum
HBSS	Hank's Balanced Salt Solution
HPLC	High- Performance Liquid Chromatography
MFI	Median Fluorescence Intensity
NPs	Nanoparticles
PBS	Phosphate-Buffered Saline
PDI	Polydispersity index
PI	Propidium Iodide
PVA	Polyvinyl Alcohol
PLGA	Poly(Lactic-Co-Glycolic Acid)
pTyr705 STAT3	Tyrosine 705 phosphorylated STAT3
RT-qPCR	Real-Time PCR
STAT3	Signal Transducer And Activator Of Transcription 3

Abstract

STAT3, a transcription factor hyperactivated in various cancers, regulates critical processes like proliferation, apoptosis, chemoresistance, migration and invasion, epithelial-mesenchymal transition, and maintenance of cancer stem cells (CSCs). In this study, we identify (-)-α-bisabolol, a natural sesquiterpene alcohol extracted from Matricaria Chamomilla's oil, as a potential inhibitor of the STAT3 signalling cascade. The effect of (-)-α-bisabolol is evaluated in human triple-negative breast cancer cells (MDA-MB-231) and in patient-derived breast cancer stem cells (BCSCs) after exposure to sublethal doses of chemotherapeutic agents. Since STAT3 hyperactivation is implicated in multiple oncogenic pathways, the effects of (-)-α-bisabolol on proliferation, migration, and invasion are explored in both 2D and 3D cultures derived from MDA-MB-231 and BCSC1 cells. Our results show that: (1) (-)-α-bisabolol promotes apoptosis, and limits migration and invasion in 2D cultures; (2) (-)-α-bisabolol induces cytotoxic effect, decreases spheroid size, and downregulates EMT-related genes in 3D cultures. It is important to note that (-)-α-bisabolol has no effects on MCF10A, a pre-neoplastic mammary epithelial cell line. To overcome the limitations associated with the lipophilicity of (–)-α-bisabolol, we developed poly(lactic-co-glycolic acid) (PLGA)-based nanoparticles (α-bis-NPs) to improve its solubility and biological distribution. α-Bis-NPs are characterized for their chemical and physical properties, and treatment of cells with these nanoparticles resulted in enhanced effects compared to the free compound. Notably, the nanoparticle formulation produces stronger effects than the free compound when used to treat the cells. Our data suggest that (-)-α-bisabolol, particularly through nanoparticle delivery, as a promising strategy to target STAT3-dependent oncogenic features in triple-negative breast cancer and breast cancer stem cells.

Introduction

1. Breast cancer insights: incidence, classification, and therapeutic options

Breast cancer remains one of the most common tumours diagnosed in women, with an estimated 2.3 million new cases and >685,000 deaths reported in 2020, accounting for approximately 11.7% of all cancer cases. Moreover, the number of estimated deaths is only second to lung cancer, as reported by Siegel et al. (1).

Breast cancer incidence is influenced by a complex interplay of genetic and non-genetic factors. Among the non-genetic risk factors, notable contributors include increasing age, reproductive history (such as early onset of menstruation, late menopause, and nulliparity), use of exogenous hormones like oral contraceptives or hormone replacement therapy, and certain lifestyle behaviors, particularly obesity after menopause, alcohol consumption, and physical inactivity (2). Additional risk factors include prior exposure to ionizing radiation, high breast tissue density as seen on mammography, and specific benign breast conditions such as atypical hyperplasia or lobular carcinoma in situ (LCIS). Importantly, these non-genetic factors may compound or interact with genetic predispositions, such as mutations, *Brca1* or *Brca2* genes, further elevating the risk of breast cancer.

Breast cancer is a highly heterogeneous disease with various subtypes, depending on its anatomical origin. These include lesions arising from the ductal epithelium, which is the most common subtype of breast cancer, as well as those originating from the lobular epithelium or the other surrounding breast tissue. On the basis of receptor expression, they are commonly grouped into four categories: estrogen receptor positive (ER+), progesterone receptor positive (PR+), human epidermal growth factor receptor positive (HER2+), and triple-negative breast cancer (TNBC) (3). ER and PR are cytoplasmic receptors that when activated by their ligands (estrogen and progesterone) enter into the nucleus and stimulate proliferation and survival in mammary epithelial cells. Expression of ER and/or PR is often associated with less aggressive cancers and is typically responsive to endocrine therapies such as tamoxifen or aromatase inhibitors (4,5). Importantly, PR expression often reflects a fully functional ER signalling pathway, and the combined evaluation of both receptors is a key element in clinical decision-making. HER2 is a transmembrane tyrosine kinase receptor that regulates cell growth and survival (6). HER2-positive

tumours, which show gene amplification or protein overexpression of HER are associated with increased aggressiveness but also benefit from targeted therapies such as Trastuzumab and Pertuzumab (7). In contrast, TNBC lack expression of ER, PR, and HER2, thereby precluding the use of targeted therapies directed against these receptors. As a consequence, TNBCs typically display a more aggressive clinical course, limited therapeutic options, and a poorer overall prognosis (8). The high mortality of breast cancer, specifically TNBC, is largely associated with the development of lung, brain, and bone metastases (9–11). These metastatic lesions are hypothesized to originate from a subpopulation of cells characterized by both therapy resistance and metastatic dissemination, known as cancer stem cells (CSCs) (12,13).

1.1 Breast Cancer Stem Cells: Origin, Characteristics, and Therapeutic Pathways

Many types of cancers, including breast cancer, contain cells with high tumour proliferation, contributing to therapeutic resistance, metastasis, and poor differentiation. A key factor in this behaviour is the presence of CSCs, which contribute to cellular heterogeneity and can survive conventional chemotherapy and radiotherapy, thereby allowing them to persist as a reservoir for tumour regrowth and relapse. The isolation and identification of this population of cells could be a promising approach in the development of novel therapeutic strategies for cancer treatment (14). The concept of CSCs dates back to 1855, when Virchow's student Cohnheim observed a cell population with an embryonic character. In 1937, Furth demonstrated that a single cell with malignant issues can induce a tumour. This hypothesis spurred researchers to recognize a subpopulation of cells as drivers of tumour initiation and growth (15) and can lead to tumour relapses (16), exhibiting self-renewal capacity and differentiation into various and heterogeneous cancer cells in a distant organ (17–19). In 2003, Al-Hajj et al. at the University of Michigan identified the breast cancer stem cell (BCSC) for the first time, isolating a subpopulation of $CD44^{+/}CD24^{-}$ cells in immunodeficient mice (20) (Figure 1).

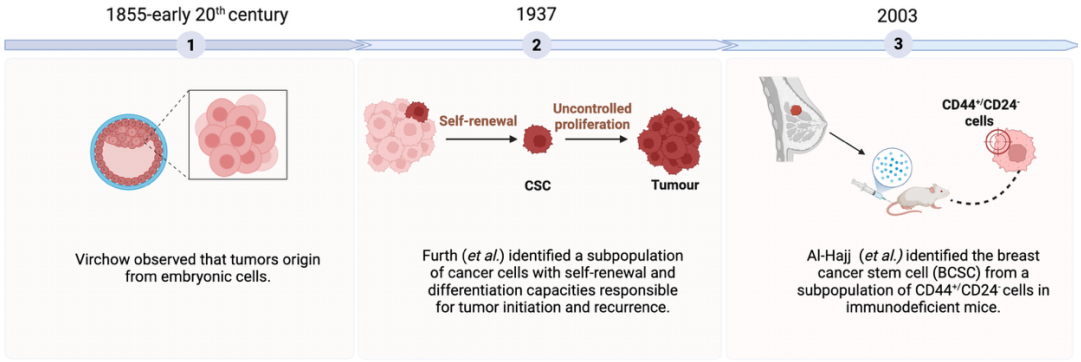

Figure 1. Developmental theory of cancer stem cells. Schematic representation of the conceptual evolution leading to the Cancer Stem Cell model. In 1855, it was hypothesized that tumours originate from embryonic-like cells with unlimited proliferative potential. In 1937, the concept of a tumour cell subpopulation capable of self-renewal and responsible for tumour growth was proposed. Finally, in 2003, the existence of CSCs was demonstrated in immunodeficient mice through the isolation of a $CD44^{+}/CD24^{-}$ cell population. Illustration created with Biorender.com.

The transition from physiological to pathological states is characterized by epigenetic and morphological changes, during which some cells undergo an epithelial-to-mesenchymal transition (EMT) (21). The acquisition of mesenchymal features enables cancer cells to invade tissue and migrate to distant sites (22). EMT not only enhances the migratory and invasive capacities of cancer cells but also confers upon them stem-like properties, contributing to therapy resistance and metastatic dissemination (Figure 2). Therapeutic strategies are increasingly focused on pathways that sustain the induction of EMT and the maintenance and survival of CSCs, such as Notch, Wnt/β-catenin, Hedgehog**,** high activity of aldehyde dehydrogenase 1 (ALDH1), and Signal Transducer and Activator of Transcription 3 (STAT3) (17,23–25)**.** Among these critical markers, STAT3 is often associated with high tumour aggressiveness and is essential for maintaining a stem-like phenotype. The STAT3 transcription factor directly promotes the transcription of genes, such as *Nanog, Oct4, Sox2, c-Myc,* and *CD44,* which are implicated in self-renewal, stemness, and in the inhibition of differentiation. Moreover, STAT3 activation upregulates EMT-related genes, including *Snail, Twist,* and *ZEB1*, facilitating cellular plasticity, invasion, and metastatic potential.

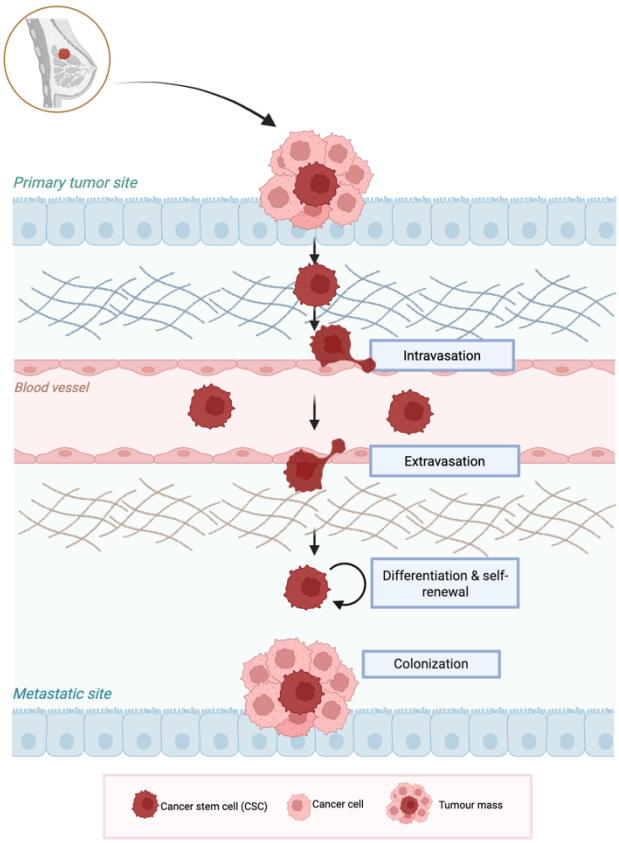

Figure 2. Schematic representation of the metastatic cascade initiated by epithelial–mesenchymal transition (EMT). At the primary tumour site, carcinoma cells undergo EMT, losing epithelial polarity and adhesion while acquiring mesenchymal traits that enhance motility and invasiveness. These EMT-activated cells infiltrate into the stroma and enter the bloodstream through a process known as intravasation. Once in circulation, tumour cells, including cancer stem cell (CSC)-like subpopulations, survive hemodynamic stress and immune surveillance until they arrest at distant tissues. Through extravasation, they transmigrate across the endothelial barrier and adapt to the foreign microenvironment. CSC-like cells subsequently undergo self-renewal and partial redifferentiation, driving the initiation and outgrowth of metastasis, ultimately forming a secondary tumor mass. Illustration created with Biorender.com.

2. Signal transducer and activator of transcription 3 (STAT3)

2.1 STAT3 signalling

STAT3 is one of the STAT family member proteins, which share similar structures and functional domains (26) (Figure 3). STAT3 exists primarily in two major isoforms: STAT3α and STAT3β, which are generated through alternative splicing of the STAT3 mRNA. Both isoforms are implicated in physiological and pathological conditions, and their relative expression balance influences cellular response, including inflammation, immune responses, and cancer progression. STAT3 protein is composed of the N-terminal domain (NTD), coiled-coiled domain (CCD), DNA binding domain (DBD), linker domain (LD), Src homology 2 (SH2) domain (SH2D), and transactivation domain (TAD), which have diverse functional roles that are summarized in Table 1 (27).

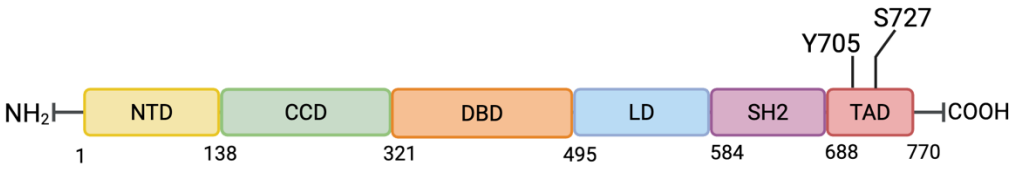

Figure 3. Structure of STAT3. Schematic representation of the six domains of STAT3, NTD (yellow), CCD (green), DBD (orange), LD (blue), SH2 (pink), and TAD (red). Illustration created with Biorender.com.

Table 1. Structural domains and functional roles of STAT3

N-Terminal Domain (NTD)	Promotes dimer-dimer interactions and nuclear import.
Coiled-Coiled Domain (CCD)	Recruits regulatory cofactors.
DNA Binding Domain (DBD),	Facilitates the recognition and binding to specific DNA sequences.
Linker Domain (LD)	Provides structural stability.
Src Homology 2 Domain (SH2D)	Responsible for receptor association and phosphorylation-dependent dimerization.
C-Transactivation Domain (TAD)	Recruits the transcriptional machinery and actives the target genes.

Table 1. STAT3 structural domains and their functional roles

The STAT3 signalling cascade comprises various phosphorylation and dephosphorylation steps (Figure 4). The activation of the canonical STAT3 pathway begins upon the binding of cytokines and growth factors to their cell-surface receptors, leading to rapid transphosphorylation and activation of Janus kinase (JAK1, JAK2, JAK3, and Tyk2). Once activated, JAKs phosphorylate specific tyrosine residues on the cytoplasmic tail of the receptors, generating high-affinity SH2 docking sites for STAT3. STAT3 is subsequently recruited to the receptor complex, where it becomes phosphorylated on tyrosine 705 by JAKs (28).

Following phosphorylation at Tyr705, the tyrosine phosphorylated monomeric STAT3 units form homodimers or heterodimers with other STAT member proteins. STAT3 dimers translocate into the nucleus, bind to specific DNA consensus sequences and drive the transcription of genes involved in multiple cellular functions including proliferation (29), metastasis promotion (30), angiogenesis (31), inflammation (32), apoptosis inhibition (33), immune response (34), TME modulation (35), CSC maintenance (34), metabolic alterations (29), chemo resistant (36), and the mediation of cancer hallmark activities through exosomes (37). In addition to JAKs, STAT3 can also be activated by non-receptor tyrosine kinases such as Src and ABL (38). The activation of STAT3 signalling has been primarily attributed to the interleukin family, including IL-6, IL-11, IL-10, and IL-23, growth

factors, such as EGF, PDGF, FGF, G-CSF, the leptin, and CNTF (39,40). Recent studies have identified additional key molecules that contribute to STAT3 signalling activation, including Toll-like (29) receptors (e.g., TLR-4 and TLR-9) and G-protein-coupled receptors (e.g., S1PR and AT1R) (39,41–43). The signal is regulated by several negative protein modulators, including the suppressors of cytokine signalling proteins (SOCS) family, protein inhibitors of activated STATs (PIAS), and several protein tyrosine phosphatases (PTPs) (38,44,45). Under physiological conditions, STAT3 activation is a transient and highly regulated process that can last from 30 minutes to several hours. After this period, the signal is switched off and STAT3 is exported into the cytoplasm. The overexpression of upstream modulators, such as IL-6 and the JAKs (46,47), or the downregulation of endogenous inhibitors, contributes to STAT3 hyperactivation (48). Thus, the dysregulation of STAT3 signalling proteins is implicated in numerous diseases, including inflammatory-related diseases, as well as haematological malignancies and solid tumours (49–52).

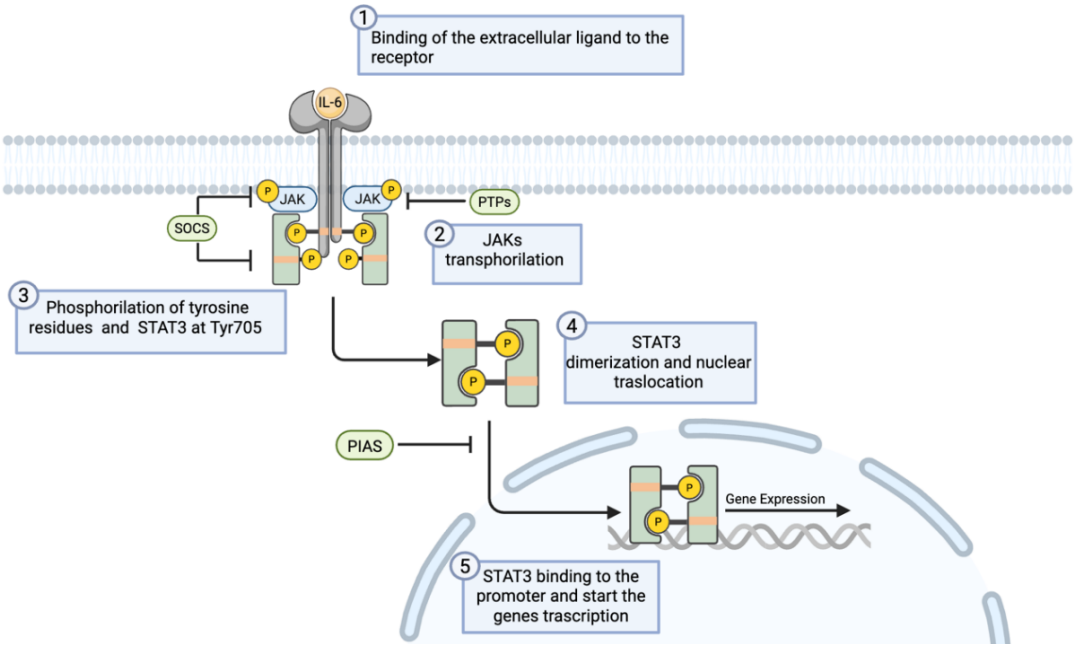

Figure 4. STAT3 signalling pathway. (1) STAT3 pathway is initiated by the binding of cytokines or growth factors to the specific receptor on the cell surface. (2) JAKs kinases, associated with the receptor, are activated through phosphorylation (3), leading to the phosphorylation of the receptor itself. STAT3 protein associates with the receptor and is phosphorylated by the JAKs at Tyr 705. (4) Phosphorylated STAT3 forms active dimers and (5) translocates into the nucleus, binding to the promoter and starting the transcription. SOCS: suppressor of cytokine signalling proteins; PIAS: protein inhibitors of activated STATs; PTPs: protein tyrosine phosphatases. Illustration created with Biorender.com.

2.2 STAT3 in cancer: focus on Breast Cancer

The oncogenic potential of STAT3 as a transcription factor has been well-investigated, due to its critical role in controlling the expression of genes involved in the oncogenic pathway (39,53,54). Notably, STAT3 not only modulates the expression of cancer-related genes but also physically interacts and functionally cooperates with other proteins (53,55). STAT3 is constitutively active in various cancers, including breast cancer (56), ovarian carcinoma (57), and pancreatic adenocarcinoma (58), as well as in haematological malignancies such as lymphomas and chronic and acute leukemia (59,60). Specifically, the elevated expression of STAT3 or p-STAT3 Tyr705 has been associated with a poor survival rate, higher tumour grade, and invasion or high chemoresistance (61–63).

Several studies have reported that the overexpression of STAT3 and its constitutive activation are strongly associated with the initiation, metastasis and progression (55). The role of STAT3 signalling in cell proliferation and survival is correlated to an increase in anti-apoptotic and proliferative genes, such as *Survivin, c-Myc, Cyclin D1, Bcl-2,* and *Bcl-xL* (64), and to the expression of metalloproteinases, including *MMP2* and *MMP9*, as well as *Twist* and *Vimentin*, involved in cell migration and invasion. Studies reveal that STAT3 protein directly binds the *Survivin* promoter, inducing its transcription, which can be blocked by Exportin 1 and CBP-mediated STAT3 acetylation (65–67). Importantly, in TNBC, the epidermal growth factor receptor (EGFR) is highly activated, contributing to the activation of STAT3 signalling (68). Furthermore, Béguelin et al. have identified that progesterone receptor-activated HER2 acts as a coactivator of STAT3, and their complex drive the activation of the *Cyclin D1* promoter, enhances *Cyclin D1* expression, and promotes the proliferation of breast tumours in *vitro* and in *vivo* (69).

Moreover, STAT3 regulates the self-renewal and maintenance of CSCs, contributing to therapy resistance in TNBC. Indeed, STAT3 cooperates with HIF-1α to sustain a CSCs population under hypoxic conditions. This effect is further stimulated by VEGF/VEGFR-2 and STAT3 signalling activation, which promotes the transcription of *Myc* and *Sox2* (70).

Taken together, all this data support the central role of STAT3 signalling in breast cancer and render it an important biomarker of aggressiveness and a promising therapeutic target in TNBC.

2.3 Targeting STAT3 for Cancer Therapy

Given the crucial involvement of STAT3 signalling in tumour progression, targeting this pathway pharmacologically represents an important approach for cancer therapy. Over the past decades, numerous direct and indirect approaches have been developed to interfere with different steps of STAT3 signalling, and several of these agents have already progressed into clinical evaluation across both solid and haematologic malignancies**.** Below, the main approaches used to shut down STAT3 signalling are described.

Targeting IL-6 or IL-6 receptor

One of the major approaches is the inhibition of the upstream regulator responsible for STAT3 pathway activation, as interleukin-6 (IL-6) or its receptor (IL-6R). Targeting IL-6 or IL-6 receptors has shown efficient suppression of STAT3 activation and inhibition of tumour growth in various studies. Siltuximab, a recombinant human-mouse chimeric monoclonal antibody targeting IL-6 and the IL-6 receptor, downregulates *Mcl-1, Bcl-Xl*, and *Survivin* in ovarian cancer cells (71), and has been tested in phase II/III clinical trials. Tocilizumab is a recombinant monoclonal antibody that targets the IL-6R and is approved by the FDA for use in patients with rheumatologic disorders (71). It demonstrates significant antitumour activity in prostate cancer by blocking IL-6/STAT3 signalling, either when used alone or in combination with the STAT3 inhibitor Stattic (71).

Targeting Tyrosine Kinases

In *vitro* and in *vivo* models have demonstrated that many small molecules, such as AZD1480 and Ruxolitinib, inhibit JAK activation and efficiently downregulate STAT3 phosphorylation through JAK inhibition (72,73). Importantly, JAK inhibition not only prevents STAT3 activation at its source but also impacts multiple oncogenic transcriptional programs downstream of JAK/STAT signalling, making this strategy particularly relevant in cancers where hyperactivation of IL-6/JAK signalling is a dominant driver.

Targeting STAT3-SH2 Domain

Another class of inhibitors has a direct effect on the SH2 domain of STAT3. The SH2 domain recognizes phosphotyrosine residues within specific sequence contexts, enabling association with activated JAKs and mediating the reciprocal phosphotyrosine–SH2 interactions between monomeric STAT proteins that drive the formation of homo- or heterodimers.

Researchers explored various peptides and peptidomimetics based on the STAT3 SH2 domain sequence, which contains a tyrosine-phosphorylation site (PY*LKTK). Despite primarily exhibiting pro-apoptotic and antitumour activity in preclinical models, these peptides are mainly restricted to research applications due to their poor stability and inefficient cellular penetration.

On the other hand, some of these small molecules, such as Stattic, OPB-31121, OPB-51602, S3I-201, SH-4-54, and STA-21, represent a more feasible and interesting strategy. These compounds impair STAT3 dimerization and nuclear translocation, ultimately leading to apoptosis and inhibition of tumour growth (74–79). However, although many SH2-targeting inhibitors have shown encouraging activity in vitro and in vivo, only a limited number have so far advanced into clinical evaluation.

Targeting DNA-Binding Activity

Inhibiting the DNA-binding activity is one approach to achieving antitumour effects, as it downregulates the expression of STAT3 target genes. Wolfrum et al. identified a peptide aptamer, DBD-1, that recognizes the STAT3 DBD, thereby inhibiting STAT3 signalling (80). Another small molecule is BBI608 (Napabucasin), an orally administered agent that suppresses the transcriptional activity of STAT3 by blocking its binding to DNA (81).

Targeting STAT3 Expression

Another class alternative approach is the control of STAT3 signalling through the use of miRNA. For example, the delivery of tumor-suppressive miRNA, such as miR-125b or miR-124-3p, inhibits STAT3 activity and impairs cancer cell survival and invasion in cutaneous squamous carcinoma and nasopharyngeal carcinoma,

respectively (82,83). Indeed, knockdown of STAT3 using small interfering RNA (siRNA) has been shown to be effective in inhibiting tumour growth in glioblastoma cells (84).

Degradation of STAT3 Protein

Finally, innovative strategies have been designed to promote the selective degradation of the STAT3 protein, utilizing proteolysis-targeting chimeras (PROTOCs), which are bifunctional molecules that can bind to STAT3 and E3 ubiquitin ligase. This complex induces the ubiquitination of STAT3 and subsequent proteasomal degradation (85,86). Preclinical studies, including SD-36, SD-91, and TSM-1, have demonstrated a strong antitumour effect of a PROTAC degrader (85,86). Similarly, small molecules such as the pro-oxidant KS10076 have been reported to induce STAT3 degradation through ROS-mediated ubiquitination, resulting in apoptosis and the elimination of cancer stem cells (87).

3. Natural Sesquiterpenes and Their Biological Activities

Sesquiterpenes are colorless, bitter, and stable compounds of terpenoids, a class of lipophilic plant secondary metabolites (88). They exhibit extensive structural diversity, including acyclic, monocyclic, bicyclic, and tricyclic frameworks, which underlie their broad spectrum of biological activities.

Sesquiterpenes exhibit a wide range of biological functions, and they are known to have been employed in traditional medicine for their anti-inflammatory, antibacterial, and immunomodulatory effects.

Among these, costunolide, isolated from the roots and rhizomes of *Saussurea lappa,* have been studied in A431 carcinoma cells, where it promotes apoptosis and inhibits cell proliferation by activating stress kinases (p38/JNK) while suppressing ERK, Akt, STAT3, and NF-kB signalling (89). Moreover, costunolide and its analogue, dehydrocostuslactone, have been shown to decrease intracellular GSH content and inhibit STAT3 phosphorylation in the human THP-1 cell line (90). Another one, helenalin, isolated from *Arnica* spp., exerts pronounced anti-inflammatory and cytotoxic actions by targeting the transcription factor NF-κB. Specifically, helenalin alkylates cysteine residues on the p65 subunit of NF-κB, thereby interrupting its

DNA binding and transcriptional activity (91). Artemisinin, a well-known sesquiterpene lactone derived from *Artemisia annua*, exhibits remarkable antimalarial and anticancer activities (92), including the suppression of cell growth (93), reduction of angiogenesis-related factors (94), and induction of ferroptosis (95). Similarly, β-caryophyllene, a bicyclic sesquiterpene found in clove and black pepper, possesses anti-inflammatory and analgesic properties through interaction with the cannabinoid receptor CB_2 (96,97).

Considering the extensive data available in the literature and the remarkable structural variability of these compounds, sesquiterpenes emerge as valuable scaffolds for the discovery and development of novel therapeutic agents derived from natural products.

3.1 (-)-α-Bisabolol

(-)-α-Bisabolol is a monocyclic sesquiterpene alcohol present in the essential oil of Chamomile, predominantly obtained by hydrodistillation from the *Matricaria chamomilla* (98,99). Literature from 2010 to 2025, based on biomedical applications of (-)-α-bisabolol, highlights the potential health benefits and considers it as one of the most therapeutically relevant plant-derived compounds. It is essential to note that (-)-α-bisabolol is not a toxic molecule, exhibiting low or no toxicity. It has been approved by the Food and Drug Administration (FDA) for use in cosmetics, personal care products, and as a food flavoring additive (98).

(-)-α-Bisabolol Structure

(-)-α-Bisabolol's IUPAC name is (6-Methyl-2-(4-methyl-3-cyclohexen-1-yl)-5-hepten-2-ol (Figure 5) . Its molecular formula is $C_{15}H_{26}O$, consisting of a 15-carbon sesquiterpene skeleton and a hydroxyl group (–OH) that confers partial polarity and contributes to biological activity. The remaining portion of the molecule is predominantly hydrophobic due to the presence of multiple methyl groups and double bonds. In nature, it may exist in four stereoisomers, which differ in the position of the hydroxyl group on the sesquiterpene backbone (100). Among these, the stereoisomer α-(-)-bisabolol is the most biologically active and, up to 50%, is the most common isolated from *M. chamomilla* (100).

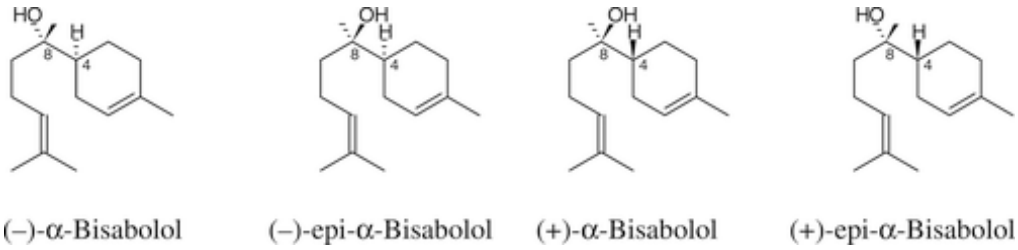

Figure 5. Molecular structure of (-)-α-Bisabolol.

Pharmacology and Bioactivity of (-)-α-bisabolol

Several studies have reported its useful pharmacological activities, including anti-inflammatory, antifungal, antimicrobial, antioxidant, and antitumour effects (98,99,101). In chondrocytes, (-)-α-bisabolol protects against AGE-induced inflammatory injury by suppressing NF-κB / MAPK signalling and decreasing catabolic enzyme expression (MMP13 / ADAMTS5) (102). Moreover, *in vivo* mouse model of LPS-induced pulmonary inflammation, (-)-α-bisabolol reduced neutrophil influx, lowered pro-inflammatory cytokines, and improved lung histology. In the same work, (-)-α-bisabolol encapsulated in lipid-core nanocapsules results in enhanced bioactivity compared to the free molecule (101). It exhibits antimicrobial and antifungal activity, inhibiting the growth of various pathogenic microorganisms. Olivera et al. observed that the inclusion complex (-)-α-bisabolol/β-cyclodextrin demonstrated a direct antibacterial effect upon *S. aureus,* in combination with gentamicin (103). (-)-α-Bisabolol's anticancer activity has been investigated in various cancer models, demonstrating the induction of apoptosis (104,105), inhibition of proliferation (104,105), suppression of the PI3K/AKT and NF-κB signalling pathways (106), and reduction of tumour invasiveness (107).

Taken together, these findings highlight (-)-α-bisabolol as a multifunctional bioactive molecule with significant therapeutic relevance. Given its favorable safety profile and broad pharmacological spectrum, particular attention has recently been directed toward its anticancer potential, which will be discussed in detail in the following section.

3.2 (-)-α-Bisabolol and anti-cancer potential

Numerous studies demonstrate that (-)-α-bisabolol is a pro-apoptotic, mitochondria-active sesquiterpene that selectively sensitizes tumour cells to cell death, with significantly lower toxicity to healthy cells compared to conventional chemotherapeutics. It is membrane–permeable, accumulates in lipid raft microdomains, perturbs mitochondrial integrity, promotes cytochrome c release, facilitates convergence of the caspase cascade, and exhibits strong synergy with conventional drugs that function through stress, DNA damage, or ER stress (104,108).

Below, each subsection will focus on specific tumour archetypes (glioblastoma, hepatocellular carcinoma, pancreatic cancer, hematologic malignancies, breast cancer), describing where the evidence is strongest, what pathways appear most relevant in each context, and how (-)-α-bisabolol behaves mechanistically in each disease class.

Glioblastoma

(-)-α-Bisabolol has been investigated in glioblastoma, one of the most aggressive and lethal primary brain tumours. The first evidence was reported by Cavalieri et al., who demonstrated that (-)-α-bisabolol induces mitochondrial apoptosis in glioblastoma cells by promoting cytochrome-c release (107). Subsequent studies confirmed and expanded this observation: (-)-α-bisabolol reduces cell viability in both human U138-MG and rat C6 glioma cells, increases extracellular adenosine production, and triggers cell death through activation of the CD73 axis, with a central role for the A3 adenosine receptor (109,110).

Hepatocarcinoma

Chen W. et al. demonstrated that (-)-α-bisabolol induces the cleavage of Caspase 3, 8, and 9, and decreases the mitochondrial cytochrome c level, resulting in an increase in cytosolic cytochrome c in HepG2 cells, a hepatocellular carcinoma cell line. This induces an upregulation of pro-apoptotic proteins, such as Bax and Bcl-2, and increases the expression of *P53, NF-Kb,* and *Fas* (111).

Pancreatic Cancer

(-)-α-Bisabolol's effect was tested in pancreatic cancer, an aggressive adenocarcinoma resistant to surgical and conventional therapies (112). The molecule suppresses AKT phosphorylation, thereby upregulating early growth response-1 (EGR1) in pancreatic cell lines (KLM1, KP4, Panc1, MIA PaCa2) without harming normal pancreatic epithelial cells. This promotes apoptosis, as confirmed by TUNEL assays (113,114). Furthermore, Masanori et al. explore its role as an anti-metastatic agent in pancreatic cells, showing an upregulation of invasion suppressors such as KISS1R, MTSS1, and TIMP2 (115). Experimental evidence suggests that (-)-α-bisabolol interacts with lipid rafts, facilitating the recruitment of the pro-apoptotic protein BID, a member of the BCL-2 family, and inducing the formation of the death complex in human pancreatic carcinoma cells (116).

Leukemia

In acute leukemia models, (-)-α-bisabolol exerts strong growth-inhibitory effects. Cavalieri et al. demonstrated that (-)-α-bisabolol acts as a pro-apoptotic agent in primary acute lymphoblastic leukemia (ALL) cells. The compound triggered mitochondrial-mediated cell death while showing minimal toxicity to normal hematopoietic cells (117). Its cytotoxic activity has been reported in B-chronic lymphocytic leukemia cells, promoting pro-apoptotic and autophagic activity (118). Additionally, it exhibits lower activity on normal B cells, monocytes, and T cells, which may contribute to an additive anti-inflammatory effect that targets the leukemia-associated pro-inflammatory microenvironment (118).

Breast Cancer

(-)-α-Bisabolol has demonstrated therapeutic potential for the treatment of breast cancer in preclinical models of HER-2/neu transgenic mice. The presented data demonstrate a reduction in tumour mass accompanied by decreased expression of key genes implicated in carcinogenesis mechanisms, such as NF-κB, Map2k, Mapk14, and HER2/neu, as well as the angiogenesis process (FGF) and apoptosis (119). However, the number of studies focusing specifically on its effects in breast cancer remains limited, and further research is required to better elucidate its mechanisms of action and therapeutic potential.

These evidences suggest the possible use of (-)-α-bisabolol for an anti-cancer treatment or in combination with conventional therapies. Moreover, further investigations are necessary to clarify the precise mechanism of (-)-α-bisabolol activity before its use in clinical applications for cancer.

4 Nanoencapsulation: Strategy for Cancer Therapy

Conventional chemotherapeutic agents such as Doxorubicin (DXN), Cisplatin, Docetaxel (DXN), and Paclitaxel (PTX) are used as monotherapies or in combination, but their poor aqueous solubility and low permeability limit the efficient delivery of effective therapeutic concentrations into tumour cells. To overcome these challenges, nanomedicine has emerged as a promising strategy, offering innovative systems for cancer prevention, diagnosis, and treatment. Nanocarriers offer improved cell targeting, reduced immunogenicity, and enhanced penetration into both tumor cells and the tumor mass. By enabling tumour-directed delivery, controlled release, surface functionalization, and reducing systemic toxicity, nanosystems can overcome solubility and biodistribution limitations while reducing systemic toxicity. In this context, several classes of nanocarriers have been engineered, each characterized by distinct composition, structure, and functional properties, enabling different delivery strategies and mechanisms of action (120–123).

Classification of nanoparticles (NPs)

The classification of NPs can be based on different physical and chemical parameters. Among the main categories, lipid-based nanoparticles (LBNPs), such as liposomes (124), solid lipid nanoparticles (SLNPs) (125), and nanostructured lipid carriers (NLCs) (126), are widely used for drug encapsulation due to their biocompatibility and high drug-loading capacity. In contrast, inorganic NPs are made of inorganic atoms linked through covalent or metallic bonds (127) and include four major groups: gold nanoparticles (128), magnetic nanoparticles (129), quantum dots (130), and silica nanoparticles (131). Another important class is carbon-based nanoparticles, such as carbon nanotubes or graphene derived structure, (132,133), which exhibit unique electrical and mechanical proprieties. Polymer-Based Nanoparticles are composed of repeated natural or synthetic monomers, can be classified into polymeric nanoparticles (134), dendrimers (135), and polymer-drug conjugates (136). Finally, hybrid nanoparticles combine an inorganic or organic core with a shell made of a different material (as a polymer or lipid), to integrate complementary properties of both classes (137). All of the nanoparticle types are summarized in Figure 6. Each type of NPs has specific properties and different advantages in tumour treatment.

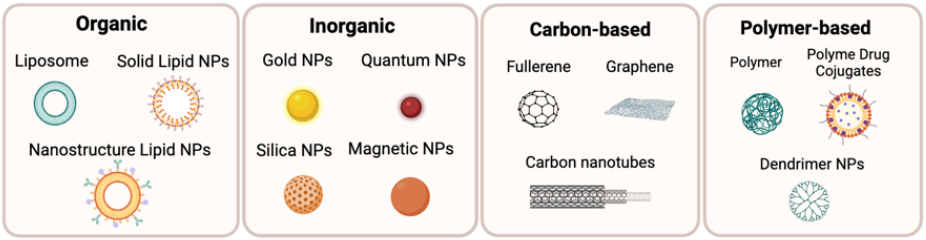

Figure 6. Classification of NPs. Illustration created with Biorender.com.

4.1 Polymeric PLGA Nanoparticles

Polymeric NPs are nano-sized delivery systems composed of biocompatible and biodegradable polymers, with a typical diameter of 100-300 nm. They can encapsulate hydrophilic or hydrophobic drugs, protecting them from degradation and improving their pharmacokinetic profile and bioavailability. These particles can be engineered through surface modification for the selective targeting of specific cells. Due to their small size, they can penetrate biological barriers and accumulate within tumour tissues via passive or active targeting. Overall, polymeric NPs allow controlled and stimuli-responsive drug release, enhancing efficacy while reducing systemic toxicity. These characteristics enable the NPs to penetrate tumour cells and infiltrate the tumour microenvironment (Figure 7).

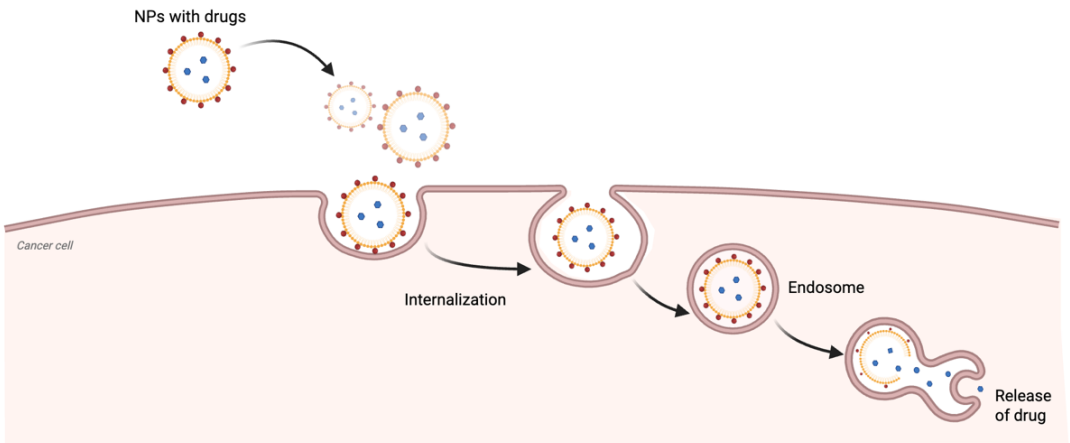

Figure 7. PLGA-NPs internalization. PLGA-NPs are internalized through endocytosis, transported between endosomal and lysosomal compartments, and ultimately degraded, releasing the drug. Illustration created with Biorender.com.

Polymeric NPs can be prepared using natural polymers such as albumin, sodium alginate, gelatin, and chitosan, as well as synthetic polymers including polylactides, poly(lactide-co-glycolide), polyglycolides, polyorthoesters, polycyanoacrylates, polyglutamic acid, and polycaprolactone (138). Among the various polymers, poly (lactide-co-glycolide) (PLGA) has garnered particular interest due to its high biocompatibility and biodegradability, which has led to its approval by the FDA and EMA for clinical use (139). Due to the intrinsic properties of PLGA, drugs release, NPs size, physicochemical stability, and surface functionalization can be precisely controlled, allowing an enhancement of tumour accumulation through both passive targeting (enhanced permeability and retention, EPR effect) and active targeting mechanisms. The versatile platform of PLGA enables the delivery of a wide range of therapies, including small-molecule chemotherapeutics, immunomodulators, nucleic acids (such as siRNA and mRNA), and antigen or adjuvant combinations (140–142). PLGA-based NPs have been utilized in solid tumors for drug and gene/siRNA, imaging, and theranostic applications (139,140,143). These types of NPs have also shown promise as carriers for nucleic acid-based therapeutics and vaccines. Sharifnia et al. developed a formulation of PLGA/PEI hybrid NPs to protect mRNA and maintain its activity *in vivo* in dendritic cells, without toxicity, highlighting their potential for antigen-encoding mRNA delivery in immunotherapy and cancer vaccine contexts (144). Moreover, in lung cancer, PEGylated PLGA NPs co-loaded with the antitumour drug gefitinib and the natural compound quercetin demonstrated synergistic antitumour activity while reducing systemic toxicity (145). Similarly, in breast cancer, paclitaxel-PLGA NPs enhanced intracellular drug accumulation and cytotoxicity compared to the free drug, thereby improving tumour regression *in vivo* (146). To overcome multidrug resistance in pancreatic cancer, gemcitabine-loaded PLGA NPs enabled controlled release and promoted drug accumulation within the tumour microenvironment. PLGA nanosystem has also been explored in combination therapy and immunotherapy. In tumour immunotherapy, PLGA carriers are used to deliver tumour-associated antigens and adjuvants in particulate form, thereby enhancing immune activation against solid tumours (147). For instance, the co-encapsulation of paclitaxel and curcumin in PLGA-NPs synergistically suppresses tumour growth and angiogenesis in murine models.

In summary, PLGA NPs represent a powerful and adaptable platform in oncology, as they enable the loading of diverse therapeutic modalities (drugs, genes, and vaccines), facilitate controlled and targeted release, and support both passive and active tumour-targeting strategies.

Aim of the thesis

TNBC is a highly aggressive breast cancer subtype, lacking expression of ER, PR, and HER2. It is characterized by elevated metastatic potential, lack of targeted therapies, and overall poor prognosis (3,148). Increasing scientific evidence suggests that BCSCs play a crucial role in tumor recurrence, metastatic dissemination, and resistance to chemotherapy, due to their enhanced capacity for self-renewal and survival (8,149–151). Central to the regulation of BCSCs survival, proliferation, and invasiveness is the transcription factor STAT3, which is frequently constitutively activated in TNBC and contributes to its malignant phenotype (51–53,152,153).

The natural sesquiterpene (-)-α-bisabolol has shown anticancer activities, including the induction of apoptosis, permeabilization of mitochondrial membrane, and inhibition of pro-survival pathways (154). Although its anticancer activity has been widely reported (119,152), no studies have yet investigated its impact on STAT3 signaling in TNBC, an aspect that could clarify the molecular mechanisms underlying its antitumoral action. Given the hydrophobic nature and limited solubility of (-)-α-bisabolol, nanoformulation strategies, such as PLGA nanoparticles, offer an opportunity to enhance delivery and improve intracellular uptake.

The aim of this thesis was to evaluate the anticancer potential of (-)-α-bisabolol in TNBC and in BCSCs, focusing on its ability to modulate STAT3 activation and suppress aggressive tumor phenotypes. Specifically, the study investigated whether (-)-α-bisabolol inhibits STAT3 phosphorylation (Tyr705) and DNA-binding activity, resulting in the downregulation of genes related to survival and proliferation (38,39). Its effects on MDA-MB-231 cells were assessed in terms of cytotoxicity, anti-proliferative activity, pro-apoptotic activity, and inhibition of migration and invasion, as well as safety in non-malignant breast epithelial cells. The study also examined the effects of (-)-α-bisabolol in CSC-enriched spheroids derived from MDA-MB-231 and patient-derived BCSC1 cells, evaluating spheroid growth, EMT, stemness-associated gene expression, and clonogenicity. Finally, PLGA-loaded (-)-α-bisabolol nanoparticles (α-Bis-NPs) were produced and characterized for their physicochemical properties, cellular uptake, and biological efficacy in both 2D and

3D models. Overall, this thesis aimed to provide a comprehensive assessment of (-)-α-bisabolol as a potential anti-STAT3 agent in TNBC and to determine whether α-Bis-NPs enhance its pharmacological activity against tumour and stem-like cancer cell populations.

Materials and Methods

1. Cell Lines and Culture Conditions

The human breast cancer cell line MDA-MB-231 was purchased from the American Type Culture Collection. The cells were maintained in Dulbecco's Modified Eagle's Medium (DMEM) (Life Technologies, Carlsbad, CA, USA), adding 10% FBS, 100 IU/mL penicillin, 100 µL/mL streptomycin, and 40 µg/mL gentamycin (Life Technologies, Carlsbad, CA, USA),). MCF10A and BCSC1 cells were provided by the Department of Obstetrics and Gynecology at RWTH University Hospital Aachen (Germany), and the experiment was conducted there. MCF10A was purchased from the American Type Culture Collection. These cells were cultured in DMEM/F12 (Thermo Fisher Scientific, USA/MA) supplemented with 5% horse serum, 20 ng/mL endothelial growth factor (EGF), 0.5 µg/mL hydrocortisone, 100 ng/mL cholera toxin, 10 µg/mL insulin, and 1% penicillin-streptomycin. BCSC1 were isolated from TNBC patients treated with sequential chemotherapy regimens, as described in (12). These cells were established by transfection with a stable e-GFP protein. BCSC1 were cultured in mammary epithelial cell growth basal medium (MEBM) (Lonza, Switzerland) supplemented with 1% B27, 1% amphotericin, 1% penicillin-streptomycin, 20 ng/mL EGF, 4 µg/mL heparin, 20 ng/mL, fibroblast growth factor (FGF), 35 µg/mL gentamicin, and 500 nmol/L rho kinase inhibitor. BCSCs were subcultured once a week and propagated in culture media containing 2% Cultrex in a 60 cm culture dish. All cells were maintained at 37 °C and 5% CO2 except BCSC1 under 3% O_2/5% CO_2. BCSC1 cells with a passage number lower than 40 were used.

2. Treatment with (-)-α-bisabolol

(-)-α-Bisabolol at a purity ≥95 % (Sigma-Aldrich, St. Louis, MO) was dissolved in ethanol, and a 500 µM stock solution was prepared in cell culture medium, as reported previously (105,154).

3. Cell Viability, Cell Proliferation and Clonogenic Survival

Viability with Trypan Blue

The viability of MDA-MB-231 and cancer stem-like cells derived from MDA-MB-231 cells were evaluated with the 0.1% Trypan Blue exclusion test using a TC20 Automated Cell Counter (Bio-Rad).

Cell Proliferation with IncuCyte

MCF10A (2 x 10^4 cells/well) and BCSC1 (2 x 10^3 cells/well) cells were seeded in 96-well plates and their growth was observed using the IncuCyte® Live-Cell analysis system (Sartorius, Ann Arbor, MI, USA) with a scan every 24 hours. After 1 week, growth curves were obtained considering the 'cells percentage of confluency' for MCF10A or 'green object count per image' for BCSC1.

Limiting Dilution Cloning

BCSC1 cells were seeded in monolayer culture in triplicate in 96-well plates pre-coated with 2% Cultrex. For dilution cloning, cells were counted and seeded at densities of 200, 100, and 50 cells per well. (-)-α-bisabolol treatment was added immediately after planting, and cell growth was monitored using the IncuCyte® Live-Cell Analysis System (Sartorius, Ann Arbor, MI, USA) with image acquisition every 6 hours over 7 days.

4. Western Blot Analysis

Cells were washed with ice-cold phosphate-buffered saline (PBS) and lysed at 4 °C in 20 mM HEPES (pH 7.4) buffer containing 420 mM NaCl, 1 mM EDTA, 1 mM EGTA, 1% Igepal, 20% glycerol, and protease and phosphatase inhibitor cocktails. Protein concentration was quantified using Bradford reagent (Thermo Fisher Scientific). 50 µg/lane of total protein extracted was resolved by 7.5% or 10% SDS-polyacrylamide gel electrophoresis and transferred to a polyvinylidene difluoride

(PVDF) membrane (Immobilon P, Millipore, Bedford, MA, USA). Membranes were blocked with 5% fat dry milk or BSA in Tris-buffered saline with 0.1% Tween 20 (TBST) at room temperature (RT) for 1 hour and then incubated with primary antibodies specific for pTyr^{705}STAT3, Caspase-3, PARP1 (Cell Signalling Technology, Beverly, MA, USA), and STAT3 (Santa Cruz, Santa Cruz Biotechnology, Dallas, TX, USA). After washing with TBST, the membranes were hybridized with anti-rabbit or anti-mouse IgG peroxidase-conjugated secondary antibody (Cell Signaling Technology) and developed using Western Chemiluminescent HRP Substrate (Millipore) on a ChemiDoc MP Imaging System (Bio-Rad, Hercules, CA, USA). Blotted proteins were quantified using ImageLab (Bio-Rad).

5. Electrophoretic Mobility Shift Assay (EMSA)

Ten micrograms of nuclear extract from MDA-MB-231 cells, prepared according to Osborn et al., were incubated in the dark for 20 minutes at room temperature with 2 µL of STAT3 IRDye™ 700 infrared dye-labeled oligonucleotides (LI-COR) in a 20 µL reaction mixture, following the manufacturer's instructions. The following double-stranded oligonucleotides were used as specific labeled probes or unlabeled cold competitors: 5'-GAT CCT TCT GGG AAT TCC TAG ATC-3' , 3'-CTA GGA AGA CCC TTA AGG ATC TAG-5'. Reaction products were separated by electrophoresis on a non-denaturing 5% polyacrylamide gel. Gels were scanned using the ChemiDoc MP Imaging System (Bio-Rad, Hercules, CA, USA) with the Cy5.5 application (Excitation: 683 nm, Emission: 703 nm), and band intensity was quantified using ImageLab 6.1.0 software (Bio-Rad).

6. Cell Migration and Invasion Analysis

Migration analysis

MDA-MB-231 cells were seeded in 60 mm dishes at a density of 1 x 10^6 cells. After 24 hours, a linear scratch was created through the mono-layer. After washing with Hank's Balanced Salt Solution (HBSS), the medium was replaced with fresh medium containing the indicated concentration of (-)-α-bisabolol. At 0, 16, and 24 h of treatment, the cells were observed, and the degree of wound healing was evaluated using microscope imaging and analysed using ImageJ software.

Invasion analysis

The cell invasion assay was performed using the 3D Matrigel Drop Invasion assay (155). Matrigel (BD Biosciences) was thawed overnight (O.N.) at 4°C and diluted in serum-free DMEM to a final concentration of 3 mg/mL. Briefly, 5 x 10^4 cells were mixed with 10 µl of cold Matrigel and seeded in plates precisely in the center of the well of a 24-well plate. The Matrigel drops were solidified in a 37°C incubator with 5% CO_2 for 30 min, and 2 ml of cell-type-specific media was added to each well. The cells were kept in culture for six days, and the media were changed every other day. The cell invasion analysis was conducted using imaging with an Evident microscope. For quantification, the area of cell migration beyond the Matrigel drop was measured using ImageJ. Using the freehand selection tool, two separate areas were outlined: the total area, which included both the Matrigel drop and the adjacent migrated cells, and the second area, corresponding to the Matrigel drop only. The area of cell migration was calculated by subtracting the Matrigel area from the total area. Finally, pixel-based measurements were converted into square millimetres by calibrating the scale in ImageJ.

7. Real-Time Analysis (RT-qPCR)

For STAT3-regulated genes, stemness, and EMT-related genes, the same PCR procedure was carried out, and RPL13a was used as the internal control. RNA extraction was performed using the PureLink Total RNA kit (Qiagen) according to the manufacturer's instructions, and the RNA was quantified using a plate reader (Infinite 200 PRO, Tecan). Following the manufacturer's protocol, 1 g of total RNA was reverse-transcribed using the SuperScript VILO cDNA synthesis kit (Life Technologies). Aliquots of the cDNAs (corresponding to 25 ng of the original RNA) were used for real-time PCR with the GoTaq qPCR Master Mix (Promega, USA) on QuantStudio™ 3 Real-Time PCR System (Thermo Fisher Scientific). The specificity of the amplified products was monitored by performing melting curves at the end of each amplification reaction. All amplicons generated a single peak, thus reflecting the specificity of the primers. The sequences of the forward and reverse primers used for PCR are reported in Table 2.

Table 2. List of primer sequences.

Cd44	CCAGAAGGAACA GTGGTTTGGC	ACTGTCCTCTGG GCTTGGTGTT
Oct4	CCTGAAGCAGAA GAGGATCACC	AAAGCGGCAGAT GGTCGTTTGG
Sox2	GCTACAGCATGA TGCAGGACCA	TCTGCGAGCTGG TCATGGAGTT
Nanog	CTCCAACATCCT GAACCTCAGC	CGTCACACCATT GCTATTCTTCG
Klf4	CATCTCAAGGCA CACCTGCGAA	TCGGTCGCATTT TTGGCACTGG
Snail	TGCCCTCAAGAT GCACATCCGA	GGGACAGGAGA AGGGCTTCTC
E-Cadherin	GCCTCCTGAAAA GAGAGTGGAAG	TGGCAGTGTCTC TCCAAATCCG
N-Cadherin	CCTCCAGAGTTT ACTGCCATGAC	GTAGGATCTCCG CCACTGATTC

8. Cancer Stem Cells and Spheroid Formation: MDA-MB-231 and BCSC1

MDA-MB-231 cells were grown in non-adherent conditions in MammoCult medium (Stem Cell Technologies, Vancouver, Canada) supplemented with hydrocortisone (0,48 μg/mL) and heparin (4 μg/mL)(Stem Cell Technologies, Vancouver, Canada) in 6-well or 96-well plates. The plates were coated with BIOFLOAT™ FLEX solution (faCellitate, Mannheim, Germany) for 10 mins, followed by air-drying the solution under laminar flow for 30 mins and removing excess.

BCSC1 cells were cultured using two different anchorage-independent cancer stem cell sphere assays, depending on the type of analysis performed: (1) for spheroid size analysis, BCSC1 cells (100 cells/well) were seeded in 100 μL of culture medium in U-bottom 96-well plates and allowed to form spheroids over three days; (2) for spheroid formation efficiency analysis, BCSC1 cells (200 cells/well) were resuspended in 2% Cultrex and seeded as a drop in flat-bottom 96-well plates. After Cultrex solidification, culture medium was added, and spheroids were grown for 7–10 days.

9. Flow Cytometry

Dual staining with Annexin V–FITC and propidium iodide

Apoptosis was assessed using the Annexin V-FITC/Propidium Iodide (PI) Apoptosis Detection Kit (Invitrogen) according to the manufacturer's instructions. 2 x 10^5 cells were washed with PBS and resuspended in 200 μL of Binding Buffer (1x). Cells were then stained with 5 μL of Annexin V–FITC for 10 minutes at RT in the dark. After incubation, the cells were resuspended in Binding Buffer (1x), and 10 μL of PI was added immediately before acquisition on a flow cytometer BD FACSCanto™ II (BD Biosciences, San Jose, CA, USA). Data were analysed with FlowJo v10 software (BD Biosciences).

Immunophenotype

1 x 10^5 cells were washed in PBS, and stained with anti-human CD44-PE (BD Pharmingen, San Jose, CA, USA) and CD24-FITC (BD Pharmingen, San Jose, CA, USA) at 37°C for 15 mins. After incubation, the cells were washed with PBS, acquired on a BD FACSCanto II (BD Biosciences, San Jose, CA, USA), and analyzed using FlowJo v10 software (BD Biosciences). Data were expressed as the Median Fluorescence Intensity (MFI) difference between stained and unstained cells.

(-)-α-Bisabolol PLGA Nanoparticles (α-bis-NPs) Cellular Uptake

MDA-MB-231 cells were grown in non-adherent conditions and were treated with NPs stained with Rhodamine B for 24 hours. 1 × 10^^{5} cells treated and untreated with Rhodamine B-NPs were washed in PBS and labelled with anti-human CD44-PE (BD Pharmingen, San Jose, CA, USA) at 37°C for 15 mins. After incubation, the cells were washed in PBS, acquired using a BD FACSCelesta (BD Biosciences, San Jose, CA, USA), and analyzed with FlowJo v10 software (BD Biosciences). Data were expressed as the Median Fluorescence Intensity (MFI) difference between stained and unstained cells.

10. Preparation of (-)-α-bisabolol Nanoparticles (α-Bis-NPs)

(-)-α-Bisabolol-loaded PLGA nanoparticles (α-Bis-NPs) were prepared using the single emulsion solvent evaporation method, as described previously (156). The nanoformulation of α-Bis-NPs was performed in collaboration with Nanomnia s.r.l. (Figure 8).

(-)-α-Bisabolol was loaded into the particles by using an organic phase that became entrapped inside them during formation. 20 mg of PLGA (7–17 kDa, PLGA 50:50, Sigma-Aldrich, St. Louis, MO, USA) and 2,5 mg of (-)-α-bisabolol were dissolved in 2 mL of dichloromethane. The organic phase was emulsified in 1% (w/v) aqueous polyvinyl alcohol (PVA, 1%) aqueous solution using a high-shear homogenizer (Ultra-Turrax, IKA®, Germany), to make oil in water emulsion, which was followed by sonication with a microtip probe sonicator (Benchmark Scientific, Sayreville, NJ,

USA) set at 30% of amplitude, pulse ON for 15 secs and pulse OFF for 10 secs for 10 min over in ice. The emulsion was kept stirring overnight on a magnetic stir plate at RT to evaporate the organic solvent. The produced nanoparticles were collected by centrifugation at 13,000× g for 20 min at 10 °C and washed several times with water to remove residual solvents. Finally, 5% mannitol was added as a cryoprotectant, and the NPs were lyophilized for storage and stored at 4°C until use. Empty nanoparticles were prepared by the same procedure without (-)-α-bisabolol. To make the particles visible in immunofluorescence analysis, 500 µg of Rhodamine B was dissolved in the organic phase, and PLGA nanoparticles were prepared as described.

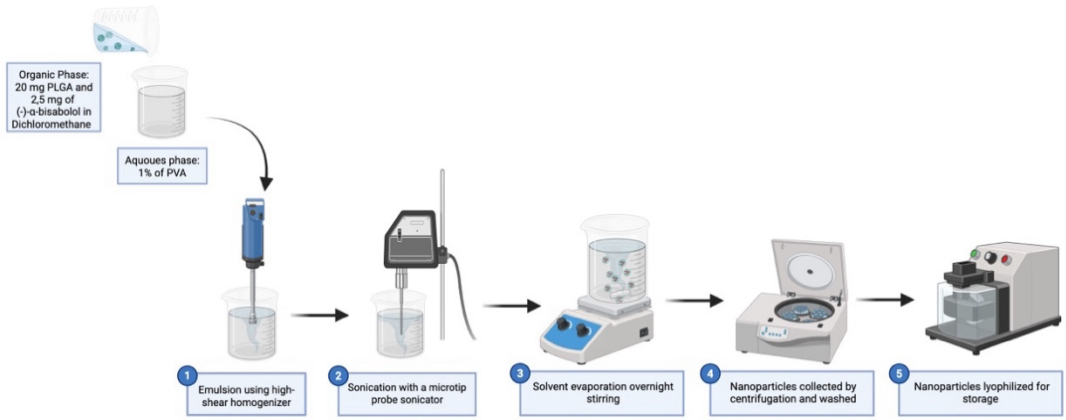

Figure 8. Preparation of α-Bis-NP by the single emulsion solvent evaporation method. (1) PLGA and (-)-α-bisabolol dissolved in dichloromethane were emulsified into a 1% PVA aqueous phase using a high-shear homogenizer. (2) The emulsion was further sonicated with a microtip probe sonicator to obtain a stable nanoemulsion. (3) Organic solvent was removed by overnight magnetic stirring at room temperature. (4) Nanoparticles were collected by centrifugation and washed. (5) Mannitol (5%) was added as cryoprotectant, and the nanoparticles were lyophilized for storage. Illustration created with Biorender.com.

11. Physico-Chemical Characterization of α-bis-NPs

Dynamic Light Scattering (DLS)

The Particle Size, Size Distribution, and Zeta Potential of NPs were determined by dispersing them in Milli-Q water and analyzing by Dynamic Light Scattering (DLS) using a particle size analyzer (Nano Zetasizer ZS, ZEN3600, Malvern Instruments Ltd, Worcestershire, England) at controlled temperature. DLS, through light scattered by particles, determines the diffusion coefficient of the particles and thus their size distribution. Polydispersity index (PDI) refers to the relative variance in the NP size distribution and varies from 0.0 for a sample that has uniform particle size to 1.0 for a sample that has multiple particle size populations. Values lower than 0.2 are considered acceptable for polymer-based nanoparticles (157). For drug delivery, a suitable zeta potential is between -30 mV (anionic) and +30 mV (cationic), indicating that the nanoparticles are more stable in liquid and biocompatible. The majority of biological membranes have a negative charge, and cationic nanoparticles exhibit greater toxicity due to their ability to break down cell walls and pass through membranes. The NPs were analyzed in triplicate.
The mean diameter of the samples was measured in triplicate with 10–20 readings per sample and the results were expressed as mean size + SD. When the PDI values ranged from 0.01 to 0.7, the particle distributions were narrow. Zeta potential was measured after diluting the nanoparticle suspensions to 1 mg/mL with 1× phosphate-buffered saline (PBS).

High Performance Liquid Chromatography (HPLC)

The amount of (-)-α-bisabolol incorporated into PLGA-NPs was quantified by HPLC equipped with a UV detector system (JASCO, Cremella, LC, Italy) using a C18 column (250 x 3 mm; 5 μμm Phenomenex Luna). Elution was performed at a flow rate of 0.5 mL/min using linear gradient elution for 30 min. Mobile phase A was composed of H_2O:CH_3CN: H_3PO_4 with a ratio of 80:19:1, while mobile phase B consisted of 100% CH_3CN. The detection wavelength was set at 200 nm. The amount of (-)-α-bisabolol was calculated using a calibration curve. All samples were analyzed in triplicate.

α-bis-NPs were suspended in CH_3CN, centrifuged at 1500 rcf for 20 mins, and the amount of (-)-α-bisabolol was quantified in the supernatant by HPLC, as described above. The encapsulation efficiency (EE%) was calculated by using the following formula:

$$EE\% = Wf / Wi \times 100$$

Where Wf= amount of (-)-α-bisabolol entrapped in α-bis-NPs; Wi= amount of (-)-α-bisabolol added.

In vitro drug release

In vitro drug release of (-)-α-bisabolol entrapped in α-bis-NPs was performed, in PBS at physiological pH (pH 7.4) at 37°C, with continuous shaking for a specific time period ranging from 1 to 120 hours (158) . At specific time points, the solutions were centrifuged at 13,000 g for 30 min, and the supernatant was collected and replaced with fresh PBS. Finally, the supernatant was collected and precipitated, dissolved in CH_3CN. The amount of drug released in the supernatants or recovered in the precipitate was measured by HPLC analysis. Release data were expressed as the cumulative drug percentage of the drug analyzed at each time point compared with the total amount. All experiments were performed in triplicate.

12. Immunofluorescent for cellular uptake

5 × 10^4 MDA-MB-231 cells were seeded on glass-bottomed 6-well plates and treated with empty PLGA nanoparticles stained with Rhodamine B. After 24 hours, the medium was removed, and the cells were incubated for 15 minutes to fix them with 4% paraformaldehyde. The cells were incubated with DAPI (Life Technologies) at 1:2000 in PBS for 20 minutes at room temperature. Cell images were captured using a fluorescence microscope (Evident, Zeiss Microsystem) at 60x magnification and processed using Adobe Photoshop.

13. Statistical analysis

Results are presented as mean ± standard deviation (SD) of at least three different biological replicates. Statistical differences were determined by Student's t-student two-sided and one-way analysis of variance (ANOVA) for multiple comparisons. Data were analyzed using GraphPad Prism 10, and statistical significance was defined as $p < 0.05$.

Results and Discussion

1. (-)-α-Bisabolol modulates constitutive STAT3 signalling in MDA-MB-231 cells

STAT3 is constitutively activated in highly malignant solid and haematological tumours, where it plays a critical role in cell proliferation, angiogenesis, chemoresistance, and metastasis. One of the critical steps leading to the activation of STAT3 is its phosphorylation at a specific tyrosine residue (Tyr 705), dimerization, and successive translocation into the nucleus. To determine whether (-)-α-bisabolol could inhibit the constitutive activation of STAT3, the level of Tyr705 phosphorylated STAT3 was assessed by western blotting analysis after treatment of MDA-MB-231 cells with the indicated concentration of (-)-α-bisabolol. As shown in Figure 9A, STAT3 is constitutively phosphorylated in these cells, and (-)-α-bisabolol treatment dose-dependently reduced STAT3 Tyr705 phosphorylation without affecting STAT3 protein level. To evaluate the binding activity of STAT3, an electrophoretic mobility shift assay (EMSA) was performed, using a fluorescent probe containing the STAT3-specific consensus sequence. The assay revealed a progressive decrease in STAT3–DNA binding activity over time with 125 μM (Figure 9B). Specifically, a reduction is evident 15 minutes after treatment, and persists for up to two hours. To further investigate whether the reduction in STAT3 phosphorylation leads to a decrease in STAT3 signalling activity, we analyzed the mRNA expression of several STAT3-dependent genes after (-)-α-bisabolol treatment. These genes are involved in cell cycle progression (*Cyclin-D1*), and inhibition of apoptosis (*Survivin, Mcl-1, Bcl-2, Bcl-xl*) (38,159). Notably, (-)-α-bisabolol significantly downregulated the expression of *Bcl-xl*, *Mcl-1*, *Survivin*, *Bcl-2,* and *Cyclin D* after 24 hours (Figure 9C). This study highlights that (-)-α-bisabolol inhibits the constitutive activation of STAT3 and effectively downregulates the transcriptional activity of its downstream targets, thereby potentially reducing the proliferative and survival capacity of cancer cells.

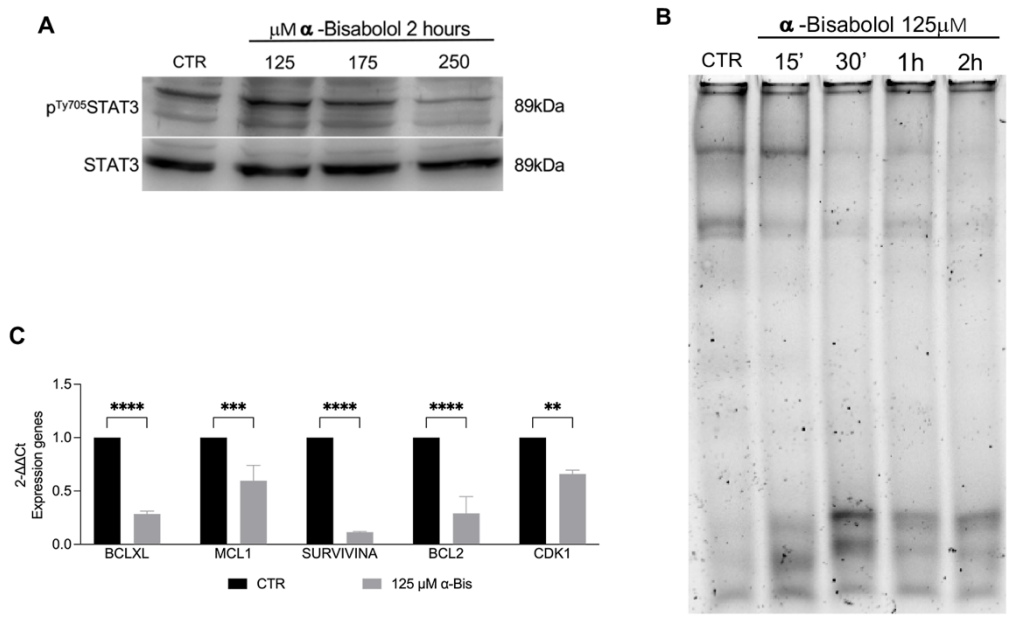

Figure 9. (-)-α-Bisabolol modulates constitutive STAT3 signalling in MDA-MB-231. **(**A**)** Western blot analysis of pTyr705STAT3 and STAT3 after 2 hours of treatment. The image shown is representative of three independent experiments (B) EMSA analysis of STAT3–DNA binding activity with 125 μM using IRDye™ 700 infrared dye-labeled oligonucleotides. The image shown is representative of three independent experiments. C) qPCR analysis of STAT3-related gene expression. The data were normalized against RLP13A RNA, and the levels of mRNA are expressed as the value relative to the untreated control. Each bar represents the mean±SD of four independent experiments performed in triplicate, and a Two-way ANOVA test was performed to determine statistical significance, $p < 0.00001$ (****), $p < 0.0001$ (***), $p < 0.001$ (**), $p < 0.01$(*).

The cytotoxicity of (-)-α-bisabolol has been investigated in various cancer cell lines. Several studies have reported modulation of Bcl-2 family proteins, reduction of XIAP levels, and suppression of NF-κB activity (160), which collectively contribute to its pro-apoptotic profile. However, the hypothesis that (-)-α-bisabolol may inhibit the activation of STAT3 remains unexplored. For these reasons, the potential involvement of the STAT3 pathway is particularly intriguing, especially in the context of TNBC, where STAT3 plays a crucial role in maintaining the disease's aggressiveness and stemness. The current study provides important preliminary results.

2. (-)-α-Bisabolol induces apoptotic cell death in MDA-MB-231 cells with no cytotoxic effect in non-transformed breast cells

To investigate the biological effect of the anti-STAT3 compound, we first assessed the cytotoxic effect of (-)-α-bisabolol by incubating MDA-MB-231 cells with increasing concentrations of the compound for 24 and 48 hours. As shown in Figure 10A, (-)-α-bisabolol reduced cell viability in a dose-dependent manner, with an EC_{50} ~125 μM after 24 hours, and an EC_{50} ~100 μM after 48 hours. To investigate whether this loss of viability was related to apoptosis, cells were treated with 125 μM of (-)-α-bisabolol for 5 and 24 hours, stained with Annexin V/PI, and analyzed by flow cytometry. The results showed a time-dependent increase in cells Annex V^+/PI^- (early apoptosis), revealing the irreversible onset of the apoptotic cascade (Figure 10B). Additionally, the cleavage of caspase-3 and PARP1 further confirmed the (-)-α-bisabolol-induced apoptotic damage (Figure 10C). These data confirm the induction of apoptosis previously described in other studies, which have shown that (-)-α-bisabolol activates Caspase 3 and Caspase 9 (152) or permeabilizes mitochondrial membrane, leading to cytochrome c release (153).

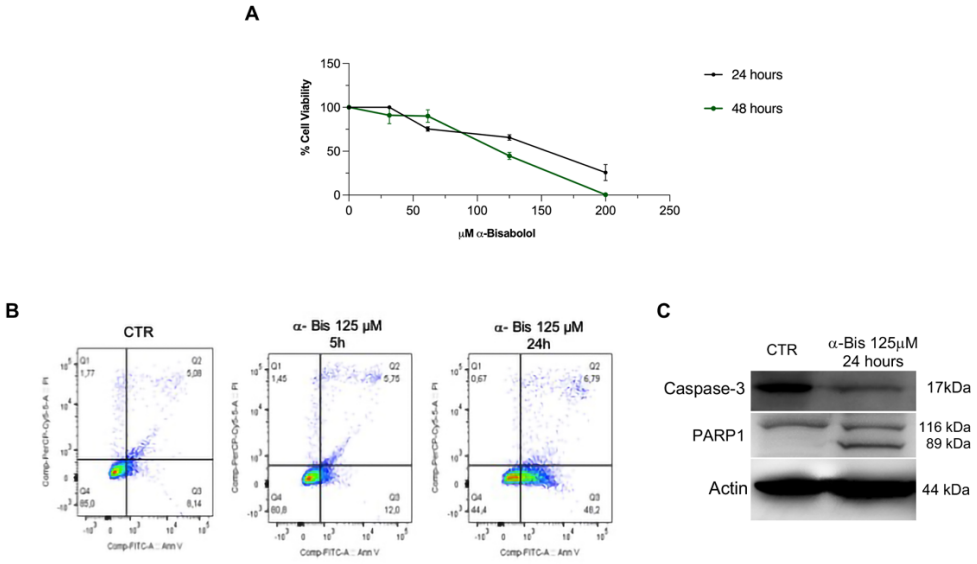

Figure 10. Apoptotic effect of (-)-α-bisabolol in MDA-MB-231 cells. (A) Cell viability assay at 24 h and 48 h after (-)-α-bisabolol treatment in MDA-MB-231 cells. Data are shown as mean ± SD from three independent experiments. (B) Flow cytometry analysis of Annexin V/PI quantifying apoptotic cells upon (-)-α-bisabolol treatment. The plots represent the population of cells in different quadrants (Q1- Dead/Necrotic cells, Q2- Late apoptosis, Q3- healthy live cells, Q4- Early apoptotic cells). (C) Western blot analysis for the expression of caspase-3 and cleavage of PARP-1. β-Actin was used as the internal loading control. Data are representative of three independent experiments.

The cytotoxic effect of (-)-α-bisabolol on non-transformed cells was evaluated using the epithelial breast cell line, MCF10. The cells were treated with increasing concentrations of the compound, and cell proliferation was monitored using live-cell imaging (Incucyte) over a 6-day period. As shown in Figure 11, (-)-α-bisabolol did not induce cytotoxic effects at any of the tested concentrations. These data are consistent with previous reports, which demonstrate a non-cytotoxic effect of (-)-α-bisabolol on non-transformed cells, such as PBMCs or fibroblasts (105,161). Data suggest that (-)-α-bisabolol is well tolerated by non-transformed cells and may exhibit tumour-selective activity.

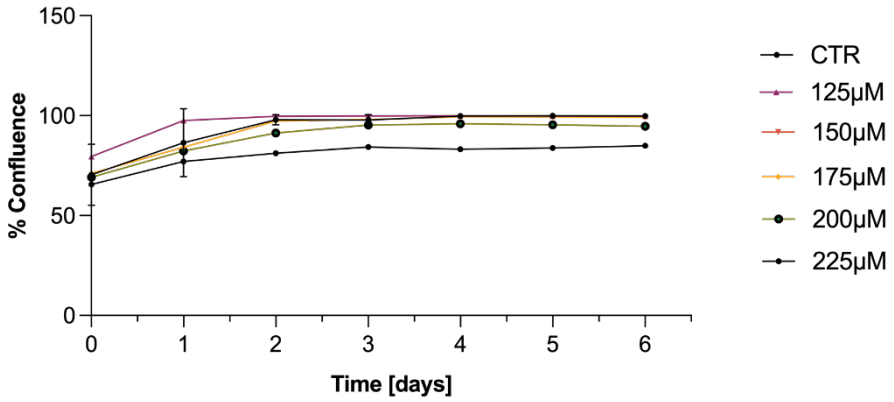

Figure 11. (-)-α-Bisabolol in non-transformed breast epithelial cells, MCF10A. Proliferation assay in MCF10A cells over 6 days following treatment with (–)-α-bisabolol. Data are shown as mean ± SD from four independent experiments.

3. (-)-α-Bisabolol impairs the migration and invasion of MDA-MB-231 cells

Abnormal differentiation, migration, and metastasis are representative biological features of tumour cells, often associated with hyperactivation of STAT3 signalling. STAT3 transcriptionally regulates a set of genes involved in epithelial–mesenchymal transition (EMT) and extracellular matrix remodelling , which promote tumour cell motility and invasiveness. Therefore, the effect of (-)-α-bisabolol on cell migration and cell invasion was evaluated using the wound-healing assay and 3D Matrigel drop assay, respectively. As shown in Figure 12, (-)-α-bisabolol inhibits the migration of MDA-MB-231 cells in a dose- and time-dependent manner, reducing wound closure by up to 90% after 24 hours at a concentration of 125 μM. Moreover, the 3D Matrigel Drop assay demonstrated that (-)-α-bisabolol down-regulated the invasive potential of MDA-MB-231 cells in a dose- and time-dependent manner, as indicated by a significant reduction in the invasion area (Figure 13).

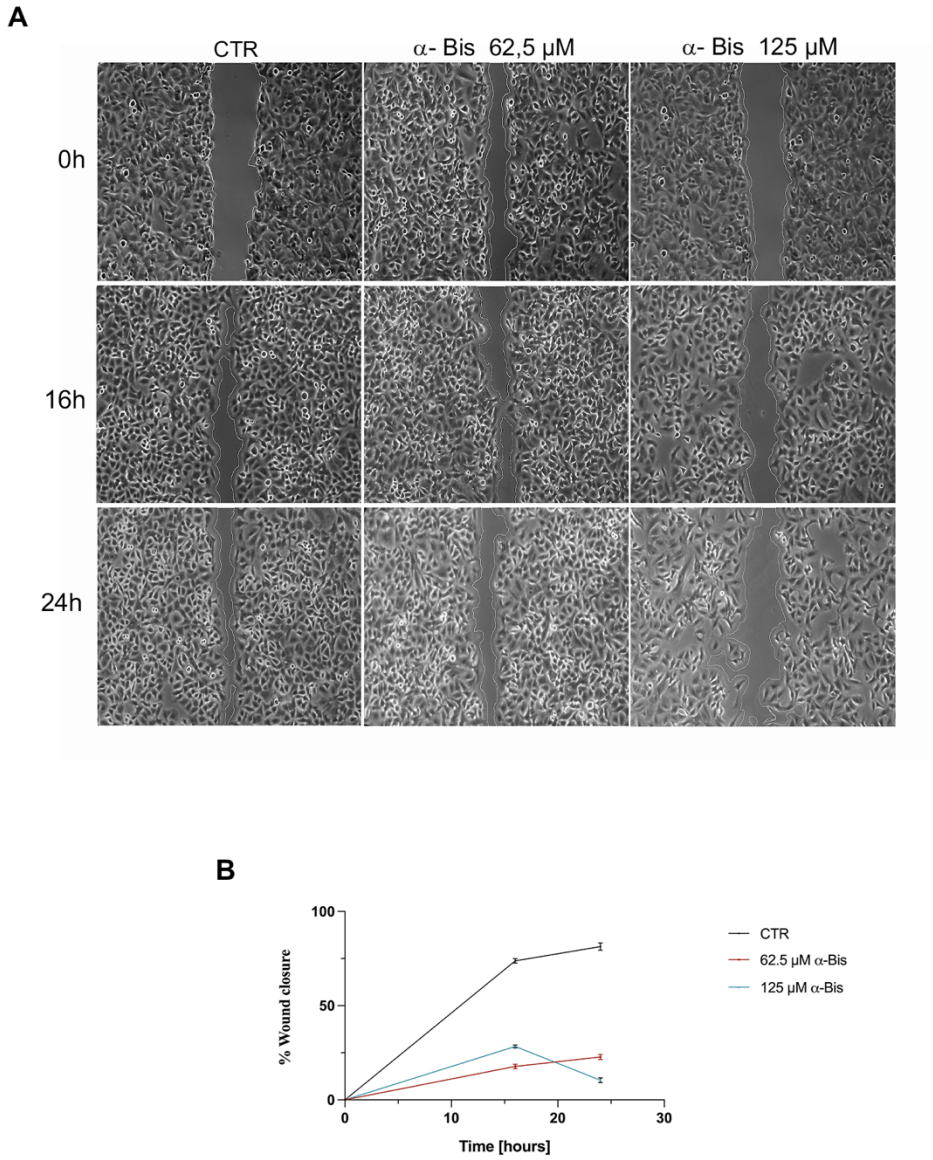

Figure 12. Scratch-wound assay and wound-closure quantification in MDA-MB-231 cells after (-)-α-bisabolol treatment. (A) Representative images at 0, 16, and 24 hours and (B) quantification of wound closure percentage at 16 hours and 24 hours. Data are presented as mean ± SD from 3 *i*ndependent experiments.

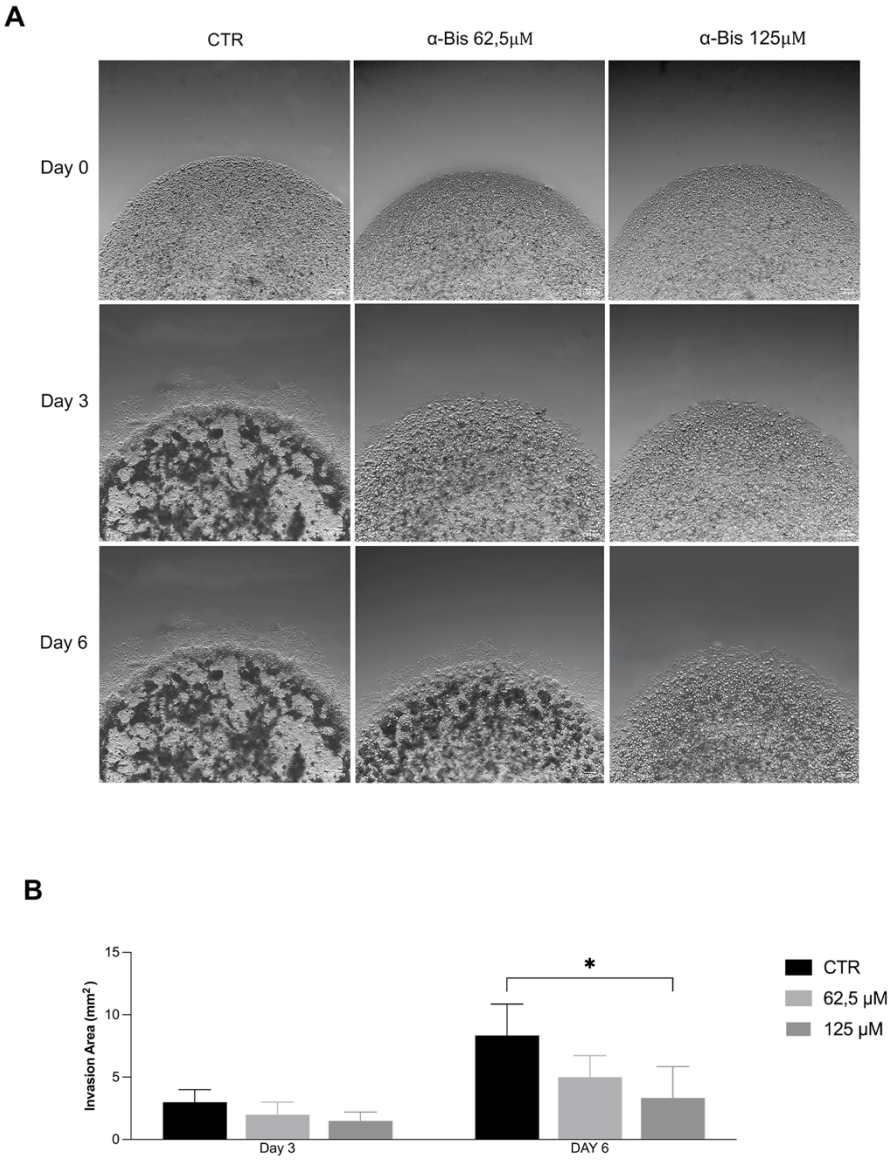

Figure 13. 3D Matrigel Drop assay in MDA-MB-231 cells following (-)-α-bisabolol treatment. (A) Representative images of 3D Matrigel Drop invasion at 0, 3 and 6 days after of (-)-α-bisabolol treatment, followed by quantification of invasion area (mm²) at (B) 3 days and (C) 6 days. Data are presented as mean ± SD from three independent experiments.

Evidence for the involvement of STAT3 in the mechanism by which (-)-α-bisabolol inhibits migration and invasion is limited**,** whereas the literature provides much stronger support for its association with mitochondrial targeting and induction of apoptosis, rather than blockade of the STAT3 pathway. Only Wu et al. described that (-)-α-bisabolol inhibits the migration of lung cancer cells A549 in a dose-dependent manner (149). The present study confirms the potent inhibition of migration and invasion by (-)-α-bisabolol in MDA-MB-231 cells, driven by the STAT3 pathway, suggesting a possible effect on metastasis development.

4. Effect of (-)-α-bisabolol on Cancer Stem Cells Derived from MDA-MB-231 Cells

STAT3 regulates several important features of CSC phenotypes, including their ability to self-renew, survive, and resist conventional therapies. The hyperactivation of STAT3 signalling has been documented to support the maintenance and expansion of CSC populations in various tumour types, contributing to tumour progression and recurrence (150,151).

Since the key role of STAT3 in regulating CSC phenotype, we established an *in vitro* model of CSC to test the effect of our anti-STAT3 compound.

As described in the literature, cells grown under non-adherent conditions form spheroids that are highly enriched in CSCs, making this model relevant for investigating the molecular mechanisms underlying CSC biology. To evaluate the effect of (-)-α-bisabolol on CSCs, we cultured MDA-MB-231 cells in MammoCult medium under non-adherent conditions to promote the formation of spheroid structures. The cells were cultured for 7 days until the spheroids reached a diameter of 200 - 600 µm. Due to their irregular shape, diameters were measured using ellipse fitting in ImageJ (Figure 14A). CSC enrichment was confirmed by flow cytometry, which analyzed the expression of canonical surface markers, $CD44^{+}/CD24^{-}$ (Figure 14B), and by qRT-PCR analysis for stemness- and EMT-associated genes, such as *KLF4, SNAIL, SOX2, OCT4* and **NANOG** (Figure 14C).

Altogether, these findings confirm the enrichment of CSC-like populations in these spheroid cultures.

Consistent with the literature, which indicates STAT3 as a key regulator of breast cancer stemness in 3D models (162), we investigated STAT3 phosphorylation in CSC-enriched spheroids derived from MDA-MB-231 cells. Direct evidence of high p-STAT3 in CSC-enriched 3D MDA-MB-231 spheroids is limited in the literature. To date, only Erdogan Ö et. al (163) have demonstrated that the growth and maintenance of 3D models of TNBC spheroids are sustained by elevated p-STAT3 levels, whereas spheroid models derived from non-TNBC cell lines show minimal STAT3 phosphorylation in the absence of paracrine stimulation or oncogene overexpression (e.g., HER2) (164). Therefore, investigating STAT3 activation in our spheroid system is particularly relevant, as it may provide novel insights into STAT3-dependent mechanisms in 3D TNBC spheroid models.

As shown in Figure 14D, Tyr705-phosphorylated STAT3 is higher in the 3D MDA-MB-231 model with respect to parental cells.

This spheroid culture provides a suitable model for evaluating the impact of our anti-STAT3 compound on CSCs viability and its potential as a therapeutic intervention.

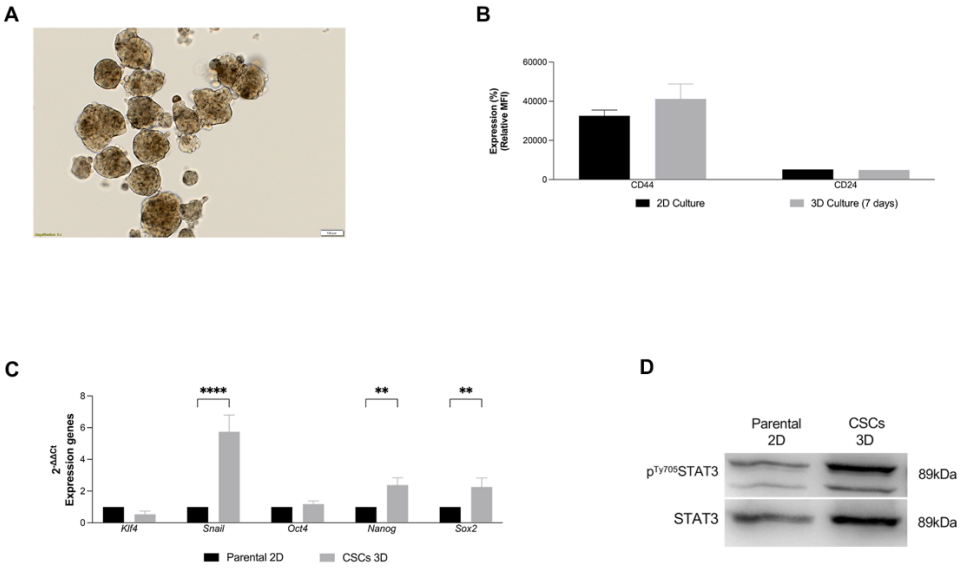

Figure 14. Characterization of CSCs from MDA-MB-231 Cells. (A) Representative brightfield image of MDA-MB-231 spheroids acquired at 10× magnification. (B) Flow cytometry analysis of the immunophenotype of the $CD44^{+}/CD24^{-}$. Data are presented as mean ± SD from three independent experiments. (C) qRT-PCR analysis of stemness- and EMT-related gene expression. The data were normalized against RLP13A RNA, and the levels of mRNA are expressed as the value relative to parental 2D cells. Each bar represents the mean±SD of four independent experiments performed in triplicate, and a Two-way ANOVA test with Dunnett's multiple comparison was performed to determine statistical significance, $p < 0.00001$ (****), $p < 0.0001$ (***), $p < 0.001$ (**), $p < 0.01$(*). (D) Western blot analysis of pTyr705-STAT3 and STAT3. The image shown is representative of four independent experiments.

The CSC-like spheroids were then treated with the indicated concentration of (-)-α-bisabolol for 48 hours, resulting in a cytotoxic effect with an estimated EC_{50} of ~150 μM (Figure 15A). Morphological evaluation and quantitative image analysis demonstrated a significant reduction in spheroid area following treatment, suggesting that (−)-α-bisabolol not only reduces cell viability but also affects the 3D growth capacity of CSC-like cells (Figure 15B).

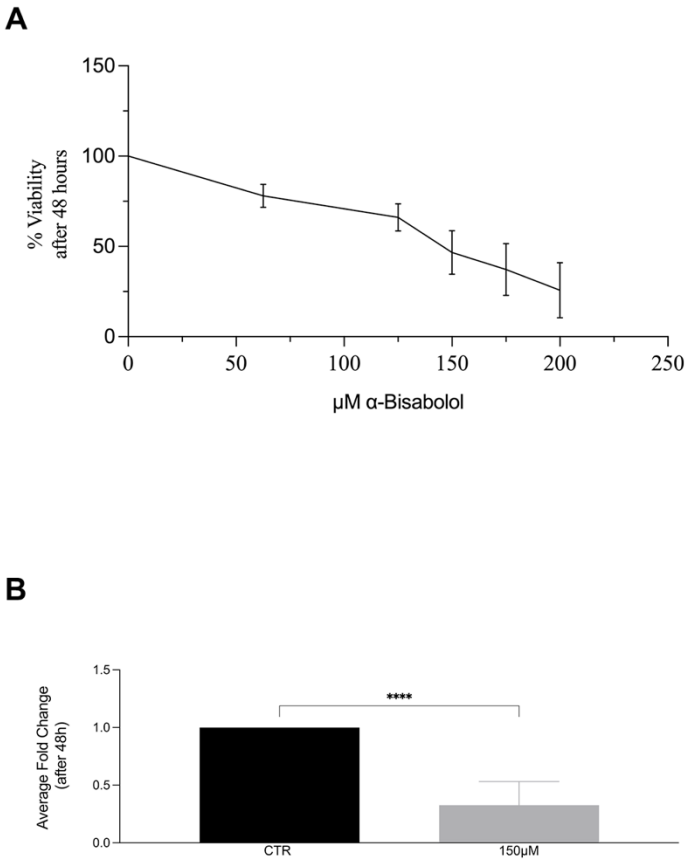

Figure 15. Effect of (-)-α-bisabolol on CSC 3D model of MDA-MB-231. (A) Cell viability assay at 48 h after (-)-α-bisabolol treatment in CSC 3D model of MDA-MB-231 cells. Data are presented as means ±SD of four independent experiments. (B) Morphological analysis of CSC 3D model of MDA-MB-231 cells after (-)-α-bisabolol treatment. The data were compared with untreated 3D spheroids. Each bar represents the mean±SD of four independent experiments performed in triplicate.

The observed cytotoxic effect of (-)-α-bisabolol on CSC-enriched spheroids indicates that this compound can effectively target the survival of the stem-like 3D model of MDA-MB-231 with an EC_{50} of approximately 150 μM. The transcriptional changes induced by (-)-α-bisabolol suggest an impact on both stemness and EMT features. However, these data do not directly link the STAT3 cascade to EMT regulation, which remains unexplored. This dual effect (reduction in CSC survival and in 3D growth capacity) supports the potential of this compound to impair aggressive features of BCSCs in 3D models.

5. PLGA-NPs as Drug Delivery System of (-)-α-bisabolol

To overcome the solubility limitation and improve the delivery of (-)-α-bisabolol, we formulated PLGA nanoparticles (α-Bis-NPs). Marongiu et al. reported that the encapsulation of (-)-α-bisabolol into PLGA nanoparticles enhanced its cellular uptake and biological effect in dendritic cells compared to the free compound (168). More recently, α-Bis-NPs have been reported to exert pro-apoptotic effects in lung cancer cells, further highlighting the potential of PLGA-based delivery systems to improve the efficacy of (-)-α-bisabolol (169).

Based on these findings, we produced α-Bis-NPs using an emulsion solvent evaporation technique, as described in the Materials and Methods Section.

The biological performance of PLGA-NPs is influenced by various parameters, including particle size, polydispersity index (PDI), and zeta potential. According to the literature, nanoparticles with a diameter between 100-200 nm, a negative surface charge, and a PDI value of around 0.1-0.2, exhibit good stability and efficacy for anticancer applications (170–172). The produced α-Bis-NPs had an average particle diameter of 160.3 ± 30.0 nm and a PDI of 0.114 ± 0.080, which reveals a monodisperse preparation (Figure 16A). In comparison, the empty PLGA-NPs were slightly larger and more monodispersed, with an average size of 180.7 ± 30 nm and a PDI ranging from 0.047 to 0.021 (Figure 16B). Figure 16A and 16B show the particle size distribution by number and PDI evaluation of one representative preparation.

The charge on the surface of the particles is characterized by measuring the zeta potential of the suspension. The zeta potential of α-bis-NPs and empty NPs was around – 2.00 mV, consistent with previously reported values for PLGA nanoparticles.

The amount of entrapped (-)-α-bisabolol was determined by HPLC analysis using a standard curve, as shown in Figure 16C (insert). The measurement of (-)-α-bisabolol content in the nanoparticles was interpolated from this curve to calculate the encapsulation efficiency, equivalent to 50% ± 10%. Although the encapsulation efficiency obtained for our α-Bis-NPs is modestly lower than the values commonly reported for PLGA nanoformulations, typically between 60-80% (depending on polymer composition, drug solubility, and formulation method) (157), this reduction does not compromise the overall functionality of the system. However, optimization studies will be necessary to improve this parameter. Notably, the PLGA nanoparticles used in this study displayed no intrinsic cytotoxicity, consistent with the well-established biocompatibility and FDA-approved safety profile of PLGA carriers (173).

The *in vitro* release of (-)-α-bisabolol from α-Bis-NPs was evaluated in PBS at 37 °C using the cumulative drug release method. Approximately 20% of the compound was rapidly released from the NPs within the first hour, and the release increased up to 70% after 24 hours, remaining at this level for the subsequent 48 hours. As observed for other PLGA-loaded NPs, the formulation exhibited a biphasic release profile, characterized by an initial burst release followed by a phase of constant drug release (Figure 16D).

These data represent a release profile that suggests a diffusion-controlled mechanism.

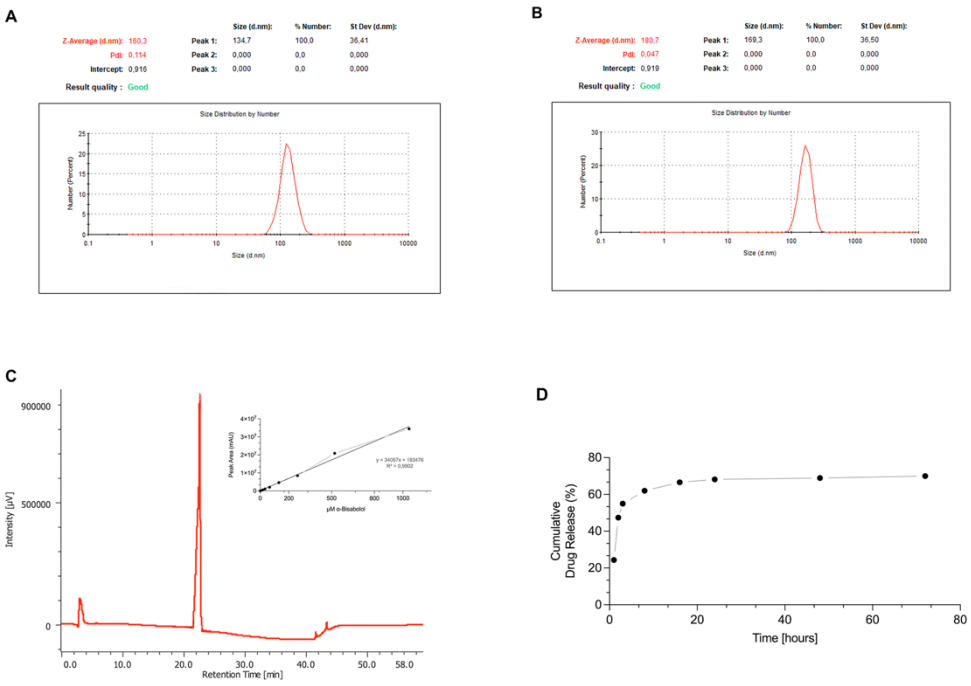

Figure 16. Characterization of α-Bis-NPs and PLGA-NPs. Representative image of the size distribution of α-Bis-NPs (A) and empty PLGA-NPs (B) by DLS analysis. (C) HPLC profile of α-Bis-NPs . Insert**:** standard curve of (-)-α-bisabolol by HPLC analysis. (D) *In vitro* drug release profile at physiological pH. Data are presented as mean ± SD from three independent experiments.

Overall, the results indicate that the nanoparticles produced in our laboratory display physicochemical characteristics consistent with those described in the literature.

6.PLGA-NPs and α-Bis-NPs on 2D culture of MDA-MB-231

In order to investigate the biological effects of the PLGA NPs produced in this study, the cellular uptake of empty PLGA-NPs was tested in the 2D model using fluorescent microscopy and flow cytometry. Previous studies indicate that PLGA-NPs are internalized through energy-dependent endocytosis, transported between endosomal and lysosomal compartments, and ultimately degraded, releasing the drug.

The MDA-MB-231 cancer cell line was incubated with two different concentrations of empty PLGA-NPs conjugated with Rhodamine B, followed by nuclei staining with DAPI. The images show that the unloaded nanoparticles were internalized by cells after 24 hours of incubation (Figure 17A). To quantify the nanoparticles internalized, flow cytometry analysis was performed at 24 hours. The data showed that 53.5% of cells present fluorescent nanoparticles inside after 24 hours (Figure 17B). The observed efficient internalization of PLGA nanoparticles in MDA-MB-231 cells confirms the suitability of these drug delivery systems in TNBC models. Flow cytometry demonstrated that more than 50% of cells internalized the nanoparticles within 24 hours, indicating rapid uptake and potential for efficient intracellular delivery.

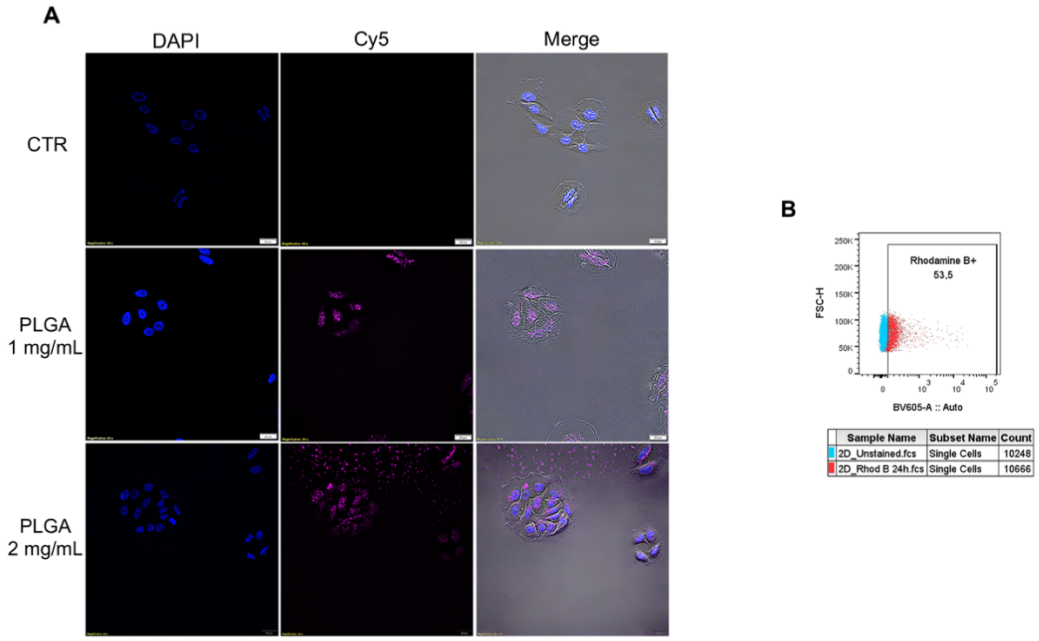

Figure 17. Cellular uptake of PLGA-NPs in a 2D model of MDA-MB-231. (A) Immunofluorescence of MDA-MB-231 cells stained with DAPI and treated with empty PLGA-NPs conjugated with Rhodamine B acquired at 60× magnification. (B) Flow cytometry analysis of internalization of PLGA-NPs stained with Rhodamine B. Data are presented as mean ± SD from three independent experiments.

Then, the cytotoxicity of empty PLGA-NPs was tested in MDA-MB-231 cells using a concentration range corresponding to the same amount of particles used in the subsequent experiments. The results showed that after 48 hours, the NPs are safe and non-cytotoxic at all tested concentrations (Figure 18A).

Finally, the cytotoxicity of α-Bis-NPs was analyzed in MDA-MB-231 cells and compared with that of free (-)-α-bisabolol. The results showed that α-Bis-NPs reduced cell viability in a dose-dependent manner, with an EC_{50} of approximately 100 µM, similar to that observed for the free (-)-α-bisabolol (Figure 18B). These results indicate that α-Bis-NPs do not enhance the cytotoxic efficacy in 2D culture conditions but rather maintain the same activity as the free compound. The main advantages of nanoparticle delivery are therefore expected in 3D cultures or *in vivo*, where improved penetration, enhanced stability, and controlled release become critical determinants of therapeutic efficacy.

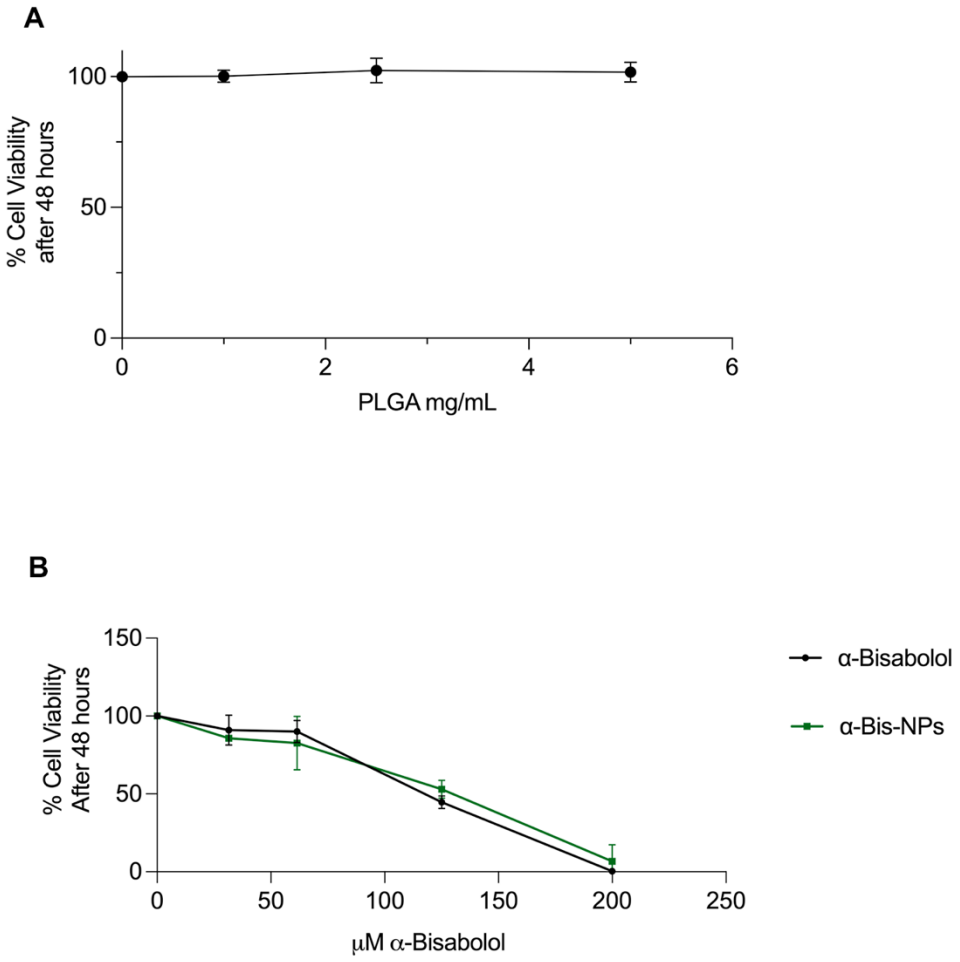

Figure 18. Cytotoxicity of PLGA-NPs and α-Bis-NPs on 2D model of MDA-MB-231. (A) Cell viability assay at 48 hours after empty PLGA-NPs treatment in a 2D model of MDA-MB-231 cells. (B) Cell viability assay at 48 hours after (-)-α-bisabolol and α-Bis-NPs treatment in a 2D model of MDA-MB-231 cells. Data are presented as mean ± SD from three independent experiments.

7. PLGA-NPs and α-Bis-NPs on 3D culture of MDA-MB-231

To quantify the NPs internalized into CSC-like 3D structure, the spheroids were treated with empty PLGA nanoparticles conjugated with rhodamine B, and cellular uptake was evaluated using flow cytometry. After 24 hours of treatment, only 16.2% of the cells internalized the nanoparticles (Figure 19A). In comparison with monolayer cells, the penetration of NPs in this structure is approximately 3 times lower. These data are in line with the literature, which reports low tumour penetration of nanoparticles due to the properties of the tumour mass (174,175). As previously described, cell packing and the extracellular matrix present in the *in vitro* spheroids limit the passage of particles larger than 120 nm (176), similar to the *in vivo* environment (175). These phenomena explain why nanoparticles often exhibit high internalization efficiency in 2D systems but limited penetration and accumulation in 3D tumor-like structures.

Then, the cytotoxic effect of α-Bis-NPs was tested in 3D cultures of the MDA-MB-231 cell line. As shown in Figure 19B, α-Bis-NPs induced a dose-dependent cytotoxic effect with an EC_{50} of around 125 μM after 48 hours of treatment (Figure 19B). Moreover, α-Bis-NPs had an enhanced cytotoxic effect in a 3D model compared to the free compound at the same time point. Interestingly, even if the internalization is lower than in the monolayer, the (-)-α-bisabolol-loaded formulation is more cytotoxic than the free molecule in spheroids, suggesting that nanoparticle encapsulation enhances the drug's cellular internalization and bioavailability.

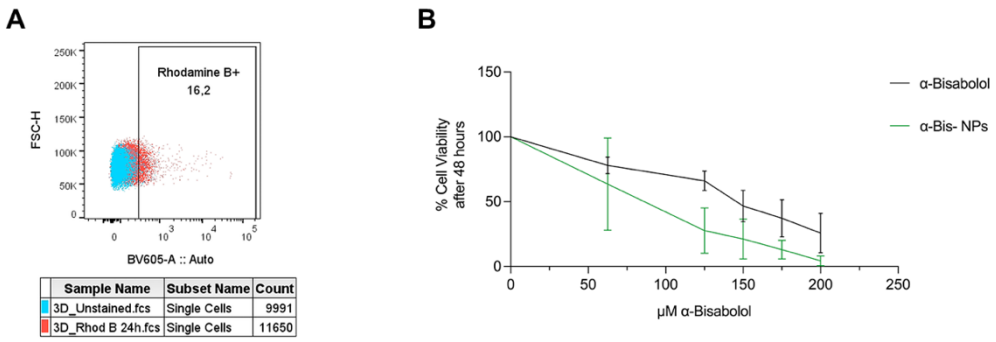

Figure 19. Effect of PLGA-NPs and α-Bis-NPs on 3D culture of MDA-MB-231 cells. (A) Flow cytometry analysis of internalization of PLGA-NPs stained with Rhodamine B. Data are presented as mean ± SD from three independent experiments. (B) Cell viability assay at 48 h after (-)-α-bisabolol and α-Bis-NPs treatment in a 3D model of MDA-MB-231 cells. Data are presented as mean ± SD from three independent experiments.

8. (-)-α-Bisabolol Inhibits STAT3 Activation, Proliferation, and Clonogenic Potential in BCSC1

To evaluate the translational applicability of (-)-α-bisabolol, we extended our studies to primary tumour cells derived from TNBC patients, designated BCSC1. The BCSC1 cells were isolated and characterized at RWTH University Hospital Aachen (Germany) in the laboratory of Dr. Jochen Maurer.

These cells originate from breast tumour samples lacking ER, PR, and HER2. The BCSC1 cells were isolated from a patient who had received preoperative treatment with sequential chemotherapy regimens, including FEC (5-fluorouracil, epirubicin, and cyclophosphamide), FAC (5-fluorouracil, doxorubicin, and cyclophosphamide), TAC (docetaxel, doxorubicin, and cyclophosphamide), TC (docetaxel and cyclophosphamide), and cisplatin. This cell line is an example of heavily pretreated tumours, potentially reflecting the clinical course of the disease after the first recurrence and sequential treatment lines following further progression (177). BCSC1 cells have already been demonstrated to be valuable tools for studying TNBC in general and cancer stem cells in particular (12,177). According to previously published results (12,177), BCSC1 cells were cultivated in 2D, exhibiting epithelial clusters (Figure 20).

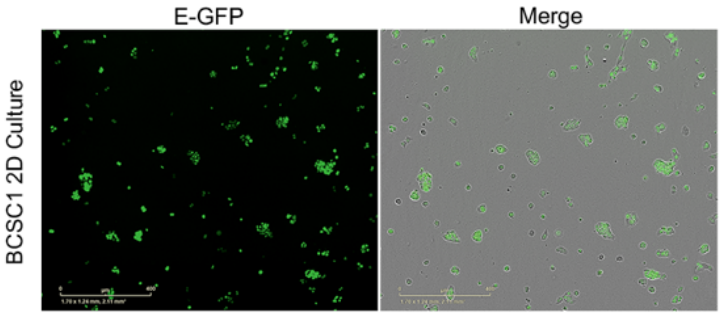

Figure 20. Representative images of the 2D culture of BCSC1. BCSC1 cells marked in E-GFP (left) and E-GFP overlaid with brightfield (right) to visualize fluorescence and morphology.

BSCS1 cells exhibit stem-like features, characterized by a high level of *Nanog, Sox2, Oct4,* and *Klf4*, which are stemness genes regulated by STAT3 transcriptional activity.

To analyze STAT3 activation in these cells, Tyr705-phosphorylated STAT3 in 2D-cultured BCSC1 was assessed using western blot analysis with a specific anti-pTyr-STAT3 antibody. As shown in Figure 21 (lane 1), these cells exhibited constitutive STAT3 activation, providing an excellent model for testing our anti-STAT3 compound. BSCS1 were then treated with the indicated concentration of (-)-α-bisabolol for 2 hours, and protein extracts were analyzed by western blot. As shown in Figure 21, treatment resulted in a dose-dependent decrease in STAT3 phosphorylation at Tyr 705).

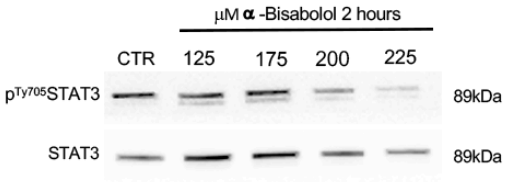

Figure 21. Effect of (-)-α-bisabolol on pTyr-STAT3 in BCSC1. Western blot analysis for the expression of pTyr705 STAT3 and STAT3 after 2 hours of treatment. The shown image is representative of three independent experiments.

To further investigate the effect of (-)-α-bisabolol on BCSC1 cells, cell proliferation was analyzed over 6 days following treatment with (-)-α-bisabolol at the indicated concentration. While control cells continued to proliferate over the 6-day period, (-)-α-bisabolol-treated cells exhibited a significant dose-dependent reduction in proliferation starting from day 3, with a plateau corresponding to around 50% proliferation observed in the following days starting from 175 μM (-)-α-bisabolol (Figure 22A).

To assess whether (-)-α-bisabolol impacts the stem cell potential of BCSC1, we performed limiting dilution cloning assays *in vitro*. This approach allowed us to quantify the clonogenic capacity of single cells, a hallmark of stemness (178). The results demonstrated a significant, dose-dependent decrease in colony formation after 7 days of treatment (Figure 22B-22C), indicating that (-)-α-bisabolol effectively impairs the self-renewal capacity characteristic of these cells. Interestingly, this effect is also valuable at the lowest concentration used. The combined reduction in proliferation and clonogenic potential suggests that (-)-α-bisabolol targets both growth and stem-like characteristics of BCSC1 cells, features that are critical for tumor initiation, progression, and resistance to therapy. Importantly, this dual effect of (-)-α-bisabolol represents a novel contribution to our understanding of its mechanism of action in BCSC1 cells.

Given that our system is characterized by high STAT3 phosphorylation, it is possible to speculate that (-)-α-bisabolol exerts its cytotoxic effect, at least in part, by reducing STAT3 activation**,** thereby targeting the transcriptional programs that sustain CSC-like traits.

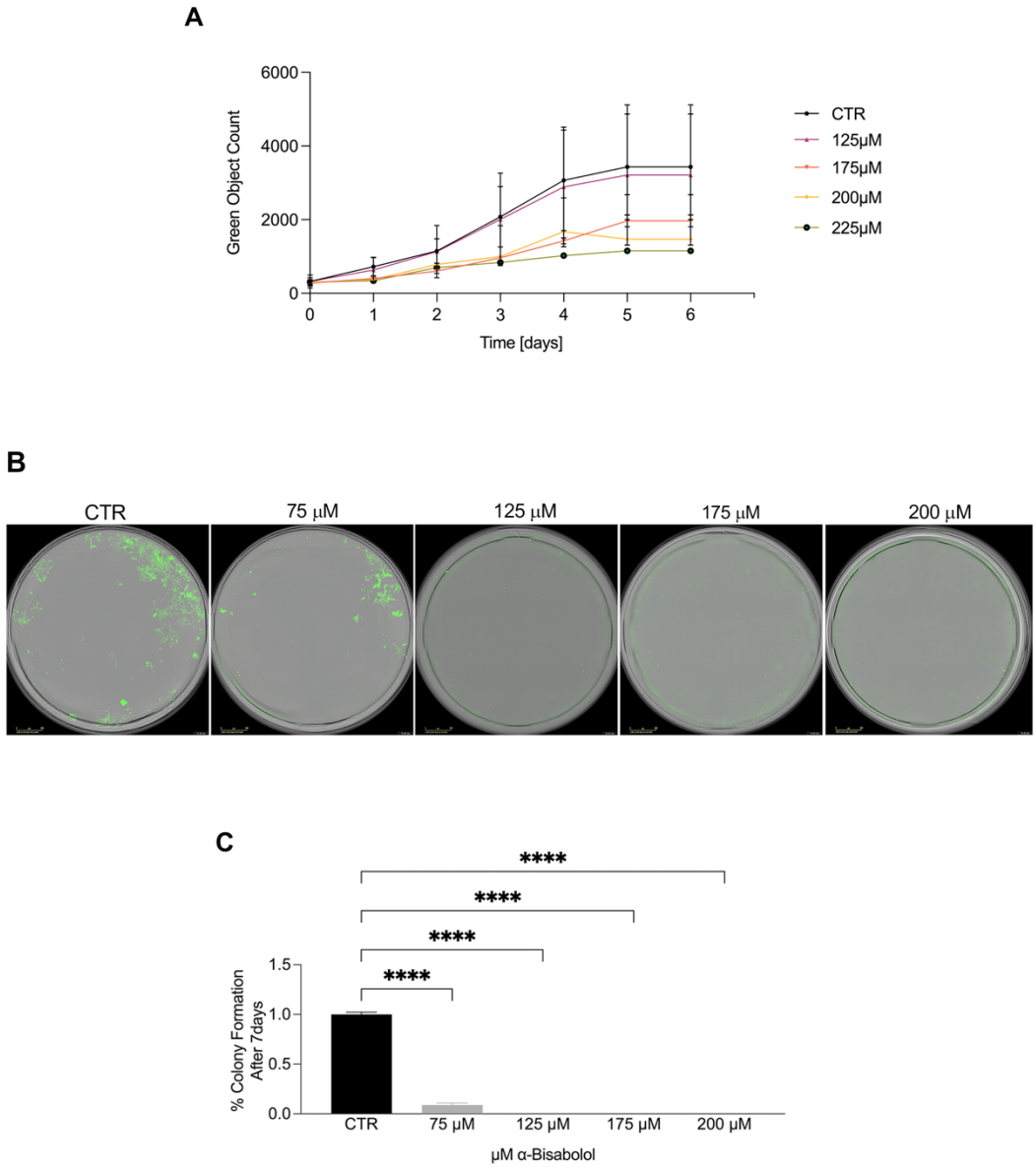

Figure 22. Effect of (-)-α-bisabolol on proliferation and stem cell potential in BCSC1
(A) Proliferation assay in BCSC over 6 days following treatment with (-)-α-bisabolol. Data are shown as green object count mean ± SD from five independent experiments. (B) Representative images of dilution cloning assay with 200 cells after 7 days of treatment and (C) graph of data presented as mean ± SD from three independent experiments. Analysis with Incucyte Live System.

9. (-)-α-Bisabolol Impairs Spheroid Growth in BCSC1

BCSC1 were cultivated in a 3D culture model to better mimic the malignant condition *in vivo*, making them a valuable system for evaluating the efficacy of anticancer treatments (Figure 23).

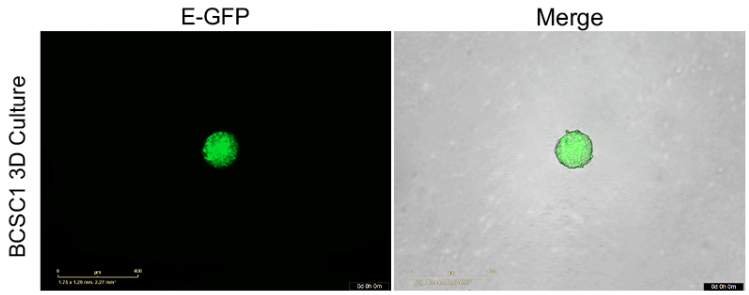

Figure 23. Representative images of the 3D culture of BCSC1. BCSC1 cells marked in E-GFP (left) and E-GFP overlaid with brightfield (right) to visualize fluorescence and morphology.

In cancer research, the reduction in spheroid size is commonly used as an indicator of damaged tumour growth and therapeutic effectiveness.

To investigate the impact of the (-)-α-bisabolol treatment on CSC-like structures, we assessed spheroid size at 24 and 48 hours after treatment with the indicated concentration of compound. Quantitative analysis of spheroid area revealed no significant size reduction at 24 hours, indicating that the treatment did not inhibit spheroid growth (Figure 24A). On the other hand, at 48 hours, (-)-α-bisabolol affected spheroid growth, inducing a significant reduction at 175 μM (Figure 24B). Spheroids are known to exhibit increased drug resistance due to strong cell–cell contacts and microenvironmental gradients, which limit the penetration and consequently the impact on overall size. Nevertheless, these events do not exclude the possibility of molecular or functional alterations in the CSC population after (-)-α-bisabolol treatment, which still requires further investigation. Considering the limited penetration of it into BCSC1 3D spheroids, the use of α-Bis-NPs, may improve intracellular drug accumulation and overall therapeutic efficacy.

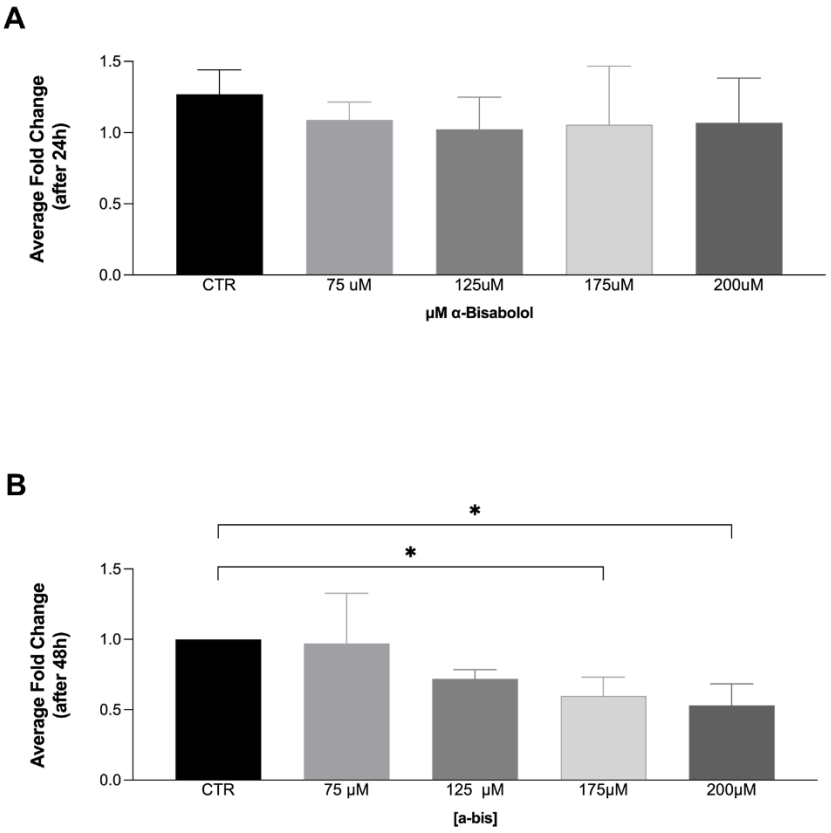

Figure 24. Effect of (-)-α-bisabolol treatment on BCSC1 spheroid size at 24 and 48 hours. (A) Graph of size analysis of BCSC1 spheroids at 24 hours, presented as the average fold change relative to the 0 h time point. (B) Graph of the size analysis of BCSC1 spheroids at 48 hours is presented as the average fold change relative to the 0 h time point. Spheroid size was quantified using ImageJ, with a standardized macro applied. Data are presented as mean ± SD from three independent experiments.

10. PLGA- NPs and α-Bis-NPs on 2D and 3D culture of BCSC1

Empty NPs were tested for their cellular uptake by 2D and 3D BSCS1 models.

The 2D and 3D cultures were treated with empty NPs stained with Rhodamine B and analyzed at 24 and 48 hours using Incucyte Live Image System (Figure 25A-25B). The images showed internalization of empty PLGA- NPs in both systems.

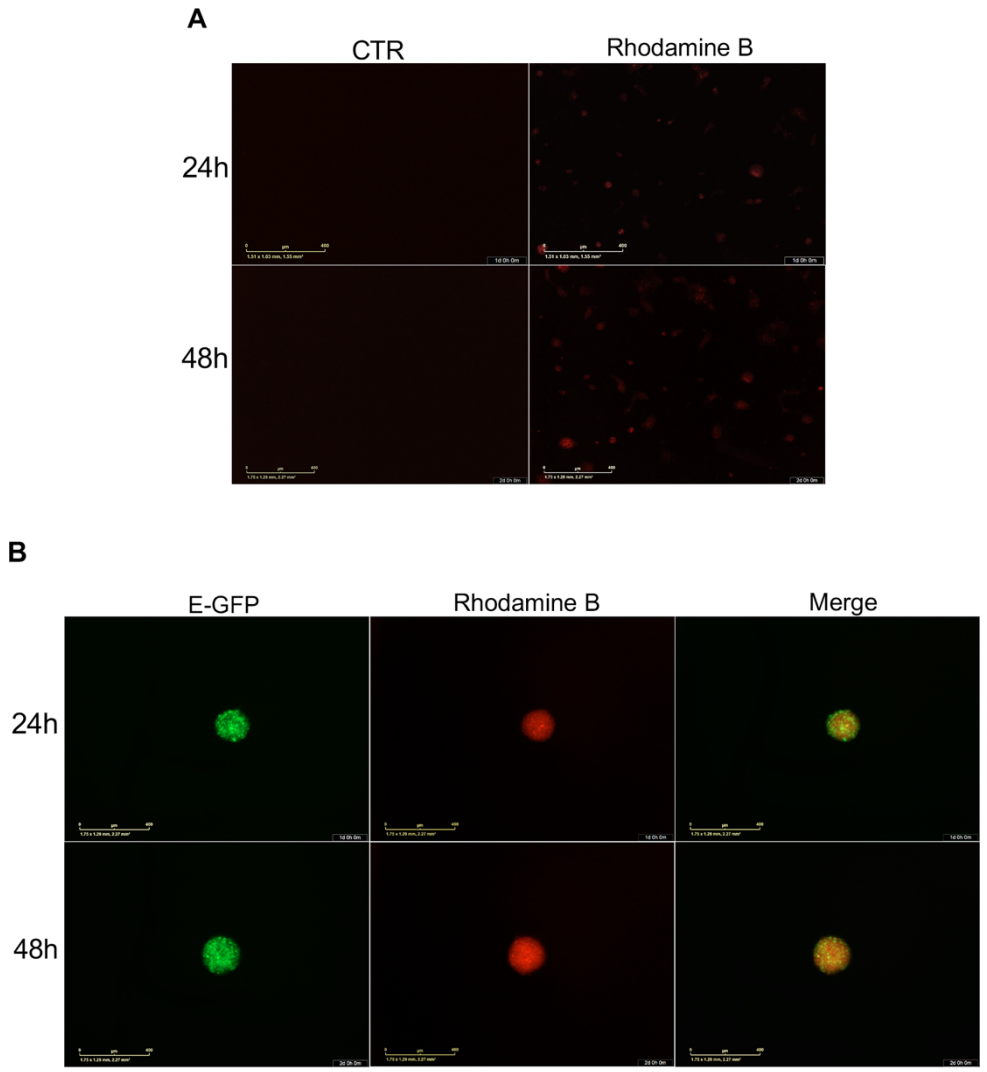

Figure 25. PLGA-NPs conjugate with Rhodamine B cellular uptake in 2D and 3D models of BCSC1. (A) Representative images of cellular uptake of empty PLGA-NPs conjugate with Rhodamine B (red) in 2D culture of BCSC1 after 24 and 48 hours. (B) Representative images of cellular uptake of empty PLGA-NPs conjugate with Rhodamine B (red) in 3D culture of BCSC1, marked with E-GFP protein (green) after 24 and 48 hours.

Given the absence of cytotoxic effects previously demonstrated in this study on MDA-MB-231, the empty PLGA-NPs were used in BCSC1 to confirm their safety. Figure 26A shows that PLGA-NPs don't have any cytotoxic effect on BCSC1.

The cytotoxicity of α-Bis-NPs was analyzed in 2D cultures of BCSC1 and compared with the cytotoxic effect of the free molecule. The results showed that (-)-α-Bis-NPs, reduced cell viability in a dose-dependent manner, with an EC_{50} of 81.7 μM. A similar dose-dependent effect was observed after treatment with (-)-α-bisabolol with an EC_{50} of 175 μM (Figure 26B). The encapsulated formulation exhibited approximately a twofold increase in cytotoxicity against these aggressive breast stem cancer cells.

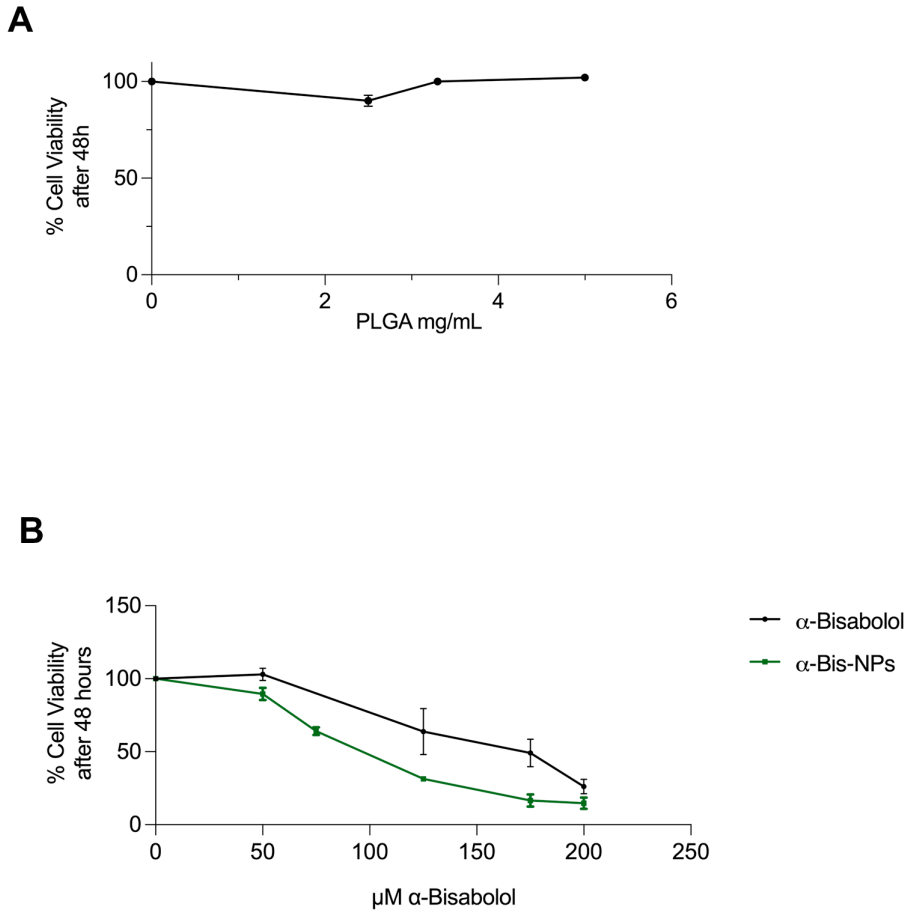

Figure 26. Cytotoxicity of PLGA-NPs and α-Bis-NPs on 2D model of BCSC1. (A) Cell viability assay at 48 hours after empty PLGA-NPs treatment in a 2D model of BCSC1. (B) Cell viability assay at 48 hours after (-)-α-bisabolol and α-Bis-NPs treatment in a 2D model of BCSC1. Data are presented as mean ± SD from three independent experiments.

These data demonstrate that the NPs are efficiently internalized by BCSC1 cells without any cytotoxic effect, and α-Bis-NPs reduce the cell viability more than the free compound. This improvement is particularly relevant considering that BCSC1 cells represent a highly aggressive and therapy-resistant model, as previously reported (177). The nanoparticle formulation reflects improved cellular uptake, protection of the molecule from degradation, and more efficient intracellular release.

The effect of α-Bis-NPs was then evaluated in 3D BCSC1 culture, which displays a smooth and compact spheroid structure, a condition under which the free compound showed a low reduction in tumor mass size. As shown in Figure 27, the treatment with α-Bis-NPs resulted in a statistically significant dose-dependent reduction in spheroid size already after 24 hours, with the most pronounced effect observed at the highest dose.

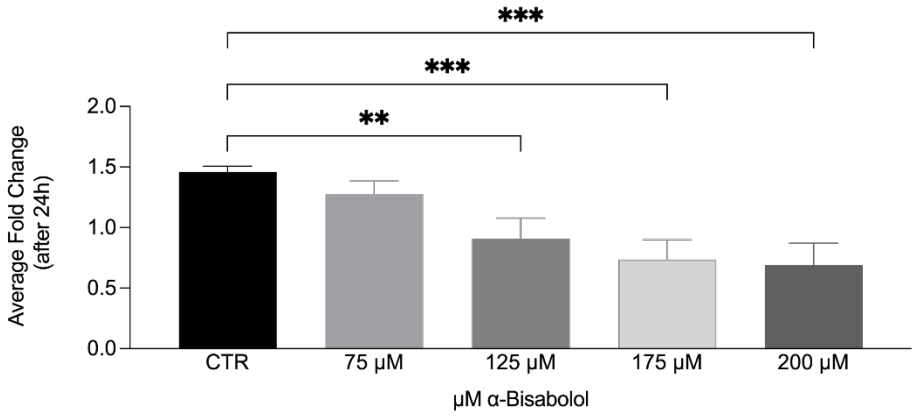

Figure 27. Effect of α-Bis-NPs treatment on BCSC1 spheroid size at 24 hours. (A) Graph of size analysis of BCSC1 spheroids at 24 h presented as average fold change relative to the 0 h time point. Data are presented as mean ± SD from three independent experiments.

These results suggest that the encapsulation of (-)-α-bisabolol in PLGA-NPs can effectively overcome the structural barriers of compact BCSC1 spheroids. This approach is particularly promising for targeting aggressive, stem-like TNBC cells that are typically resistant to conventional therapies. Overall, these findings support further investigation of α-Bis NPs as a strategy to improve the efficacy of (-)-α-bisabolol in 3D cancer models.

Conclusion

In this thesis, the natural compound (–)-α-bisabolol was proposed as an inhibitor of STAT3-driven signaling with antitumor capabilities in TNBC and BCSCs.

Firstly, (-)-α-bisabolol decreases STAT3 phosphorylation and inhibits its DNA-binding activity, resulting in the downregulation of genes involved in survival, proliferation and apoptosis (38,159). The ability of (-)-α-bisabolol to induce apoptosis in MDA-MB-231 cells was also confirmed, in line with its well documented pro-apoptotic activity, which involve caspase activation and mitochondrial damage (104,107,179) . Importantly, no toxicity was observed in non-transformed breast epithelial cells, indicating a favorable therapeutic proposal. In addition, as an anti-STAT3 compound, (-)-α-bisabolol reduced cell migration and invasion, processes strongly associated with TNBC metastasis (180,181), suggesting its potential in the reduction of tumour metastasis.

In CSC-enriched 3D spheroid models derived from both MDA-MB-231 cells and BCSC1, (-)-α-bisabolol decreased spheroid viability and size. Moreover, in 3D MDA-MB-231 cells (-)-α-bisabolol modulated key stemness and EMT markers, such as *Sox2, Oct4, Snail*, and *Klf4*,. These alterations could be consistent with a disruption of STAT3-driven stemness programs, suggesting that (-)-α-bisabolol may target CSC populations that are often resistant to conventional therapies.

To overcome the pharmacokinetic limitations of (-)-α-bisabolol, α-Bis-NPs were formulated. These NPs exhibited optimal physicochemical characteristics, efficient encapsulation, and stable release profiles, which are in line with those described in the literature (171,170,172). Notably, these NPs demonstrated enhanced efficacy than the free molecule in both monolayer and spheroid models.

In conclusion, this work supports (-)-α-bisabolol as a promising natural compound capable of inhibiting STAT3 signalling, reducing the

aggressiveness of TNBC cells, and targeting CSC-enriched populations. Furthermore, PLGA nanoencapsulation has been demonstrated to be an effective strategy for enhancing the biological activity of (-)-α-bisabolol. Overall, these findings provide a solid preclinical basis for future studies evaluating (-)-α-bisabolol, either alone or in nanoparticle formulations, as a potential therapeutic agent targeting the STAT3/CSCs axis in TNBC.

References

1. Sung H, Ferlay J, Siegel RL, Laversanne M, Soerjomataram I, Jemal A, et al. Global Cancer Statistics 2020: GLOBOCAN Estimates of Incidence and Mortality Worldwide for 36 Cancers in 185 Countries. CA: A Cancer Journal for Clinicians. 2021;71(3):209–49.

2. Danaei G, Vander Hoorn S, Lopez AD, Murray CJ, Ezzati M. Causes of cancer in the world: comparative risk assessment of nine behavioural and environmental risk factors. The Lancet. 2005 Nov 19;366(9499):1784–93.

3. Molecular Classification of Breast Cancer Utilizing Long Non-Coding RNA (lncRNA) Transcriptomes Identifies Novel Diagnostic lncRNA Panel for Triple-Negative Breast Cancer [Internet]. [cited 2025 June 5]. Available from: https://www.mdpi.com/2072-6694/13/21/5350

4. Ali S, Coombes RC. Endocrine-responsive breast cancer and strategies for combating resistance. Nat Rev Cancer. 2002 Feb;2(2):101–12.

5. Group (EBCTCG) EBCTC. Relevance of breast cancer hormone receptors and other factors to the efficacy of adjuvant tamoxifen: patient-level meta-analysis of randomised trials. The Lancet. 2011 Aug 27;378(9793):771–84.

6. Mineo JF, Bordron A, Isabelle QR, Maurage CA, Virginie B, Séverine L, et al. Increasing of HER2 Membranar Density in Human Glioblastoma U251MG Cell Line Established in a New Nude Mice Model. J Neurooncol. 2006 Feb;76(3):249–55.

7. Use of Chemotherapy plus a Monoclonal Antibody against HER2 for Metastatic Breast Cancer That Overexpresses HER2 | New England Journal of Medicine [Internet]. [cited 2025 June 5]. Available from: https://www.nejm.org/doi/full/10.1056/NEJM200103153441101

8. Human Primary Breast Cancer Stem Cells Are Characterized by Epithelial-Mesenchymal Plasticity [Internet]. [cited 2025 June 5]. Available from: https://www.mdpi.com/1422-0067/22/4/1808

9. Takai K, Le A, Weaver VM, Werb Z. Targeting the cancer-associated fibroblasts as a treatment in triple-negative breast cancer. Oncotarget. 2016 Oct 14;7(50):82889–901.

10. O'Sullivan CC, Davarpanah NN, Abraham J, Bates SE. Current challenges in the management of breast cancer brain metastases. Seminars in Oncology. 2017 Apr 1;44(2):85–100.

11. Jiang F, Li Y, Si L, Zhang Z, Li Z. Interaction of EZH2 and P65 is involved in the arsenic trioxide-induced anti-angiogenesis in human triple-negative breast cancer cells. Cell Biol Toxicol. 2019 Aug 1;35(4):361–71.

12. Metzger E, Stepputtis SS, Strietz J, Preca BT, Urban S, Willmann D, et al. KDM4 Inhibition Targets Breast Cancer Stem–like Cells. Cancer Research. 2017 Oct 31;77(21):5900–12.

13. Reya T, Morrison SJ, Clarke MF, Weissman IL. Stem cells, cancer, and cancer stem cells. Nature. 2001 Nov;414(6859):105–11.

14. Calcagno AM, Salcido CD, Gillet JP, Wu CP, Fostel JM, Mumau MD, et al. Prolonged Drug Selection of Breast Cancer Cells and Enrichment of Cancer Stem Cell Characteristics. JNCI: Journal of the National Cancer Institute. 2010 Nov 3;102(21):1637–52.

15. Capp JP. Cancer Stem Cells: From Historical Roots to a New Perspective. Journal of Oncology. 2019;2019(1):5189232.

16. Desai A, Yan Y, Gerson SL. Concise Reviews: Cancer Stem Cell Targeted Therapies: Toward Clinical Success. Stem Cells Translational Medicine. 2019 Jan 1;8(1):75–81.

17. Ricardo S, Vieira AF, Gerhard R, Leitão D, Pinto R, Cameselle-Teijeiro JF, et al. Breast cancer stem cell markers CD44, CD24 and ALDH1: expression distribution within intrinsic molecular subtype. Journal of Clinical Pathology. 2011 Nov 1;64(11):937–46.

18. Beck B, Blanpain C. Unravelling cancer stem cell potential. Nat Rev Cancer. 2013 Oct;13(10):727–38.

19. Li W, Ma H, Zhang J, Zhu L, Wang C, Yang Y. Unraveling the roles of CD44/CD24 and ALDH1 as cancer stem cell markers in tumorigenesis and metastasis. Sci Rep. 2017 Oct 23;7(1):13856.

20. Al-Hajj M, Wicha MS, Benito-Hernandez A, Morrison SJ, Clarke MF. Prospective identification of tumorigenic breast cancer cells. Proc Natl Acad Sci U S A. 2003 Apr 1;100(7):3983–8.

21. Development of Radiotracers for Breast Cancer—The Tumor Microenvironment as an Emerging Target [Internet]. [cited 2025 July 18]. Available from: https://www.mdpi.com/2073-4409/9/10/2334

22. Felipe Lima J, Nofech-Mozes S, Bayani J, Bartlett JMS. EMT in Breast Carcinoma—A Review. Journal of Clinical Medicine. 2016 July;5(7):65.

23. Takebe N, Miele L, Harris PJ, Jeong W, Bando H, Kahn M, et al. Targeting Notch, Hedgehog, and Wnt pathways in cancer stem cells: clinical update. Nat Rev Clin Oncol. 2015 Aug;12(8):445–64.

24. ALDH1+ stem cells demonstrate more stem cell-like characteristics than CD44+/CD24–/low stem cells in different molecular subtypes of breast cancer - Chen - Translational Cancer Research [Internet]. [cited 2025 July 22]. Available from: https://tcr.amegroups.org/article/view/36207/html

25. Ginestier C, Hur MH, Charafe-Jauffret E, Monville F, Dutcher J, Brown M, et al. ALDH1 Is a Marker of Normal and Malignant Human Mammary Stem Cells and a Predictor of Poor Clinical Outcome. Cell Stem Cell. 2007 Nov 15;1(5):555–67.

26. Darnell JE. STATs and Gene Regulation. Science. 1997 Sept 12;277(5332):1630–5.

27. Aigner P, Just V, Stoiber D. STAT3 isoforms: Alternative fates in cancer? Cytokine. 2019 June;118:27–34.

28. Wong GL, Manore SG, Doheny DL, Lo HW. STAT family of transcription factors in breast cancer: Pathogenesis and therapeutic opportunities and challenges. Seminars in Cancer Biology. 2022 Nov 1;86:84–106.

29. Xue C, Yao Q, Gu X, Shi Q, Yuan X, Chu Q, et al. Evolving cognition of the JAK-STAT signaling pathway: autoimmune disorders and cancer. Sig Transduct Target Ther. 2023 May 19;8(1):204.

30. El-Tanani M, Al Khatib AO, Aladwan SM, Abuelhana A, McCarron PA, Tambuwala MM. Importance of STAT3 signalling in cancer, metastasis and therapeutic interventions. Cellular Signalling. 2022 Apr 1;92:110275.

31. Liu YX, Xu BW, Niu XD, Chen YJ, Fu XQ, Wang XQ, et al. Inhibition of Src/STAT3 signaling-mediated angiogenesis is involved in the anti-melanoma effects of dioscin. Pharmacological Research. 2022 Jan 1;175:105983.

32. Zhang W, Li D, Li B, Chu X, Kong B. STAT3 as a therapeutic target in the metformin-related treatment. Int Immunopharmacol. 2023 Mar;116:109770.

33. Hashemi M, Sabouni E, Rahmanian P, Entezari M, Mojtabavi M, Raei B, et al. Deciphering STAT3 signaling potential in hepatocellular carcinoma: tumorigenesis, treatment resistance, and pharmacological significance. Cellular & Molecular Biology Letters. 2023 Apr 21;28(1):33.

34. Guo S, Ramar V, Guo AA, Saafir T, Akpobiyeri H, Hudson B, et al. TRPM7 transactivates the FOSL1 gene through STAT3 and enhances glioma stemness. Cell Mol Life Sci. 2023 Aug 29;80(9):270.

35. Lefler JE, MarElia-Bennett CB, Thies KA, Hildreth BE, Sharma SM, Pitarresi JR, et al. STAT3 in tumor fibroblasts promotes an immunosuppressive microenvironment in pancreatic cancer. Life Sci Alliance. 2022 July 8;5(11):e202201460.

36. Sadrkhanloo M, Paskeh MDA, Hashemi M, Raesi R, Motahhary M, Saghari S, et al. STAT3 signaling in prostate cancer progression and therapy resistance: An oncogenic pathway with diverse functions. Biomedicine & Pharmacotherapy. 2023 Feb 1;158:114168.

37. Channon LM, Xu Z, Greening DW, Wilson JS, Perera CJ, Apte MV. Small extracellular vesicles (exosomes) and their cargo in pancreatic cancer: Key roles in the hallmarks of cancer. Biochimica et Biophysica Acta (BBA) - Reviews on Cancer. 2022 May 1;1877(3):188728.

38. Butturini E, Carcereri de Prati A, Boriero D, Mariotto S. Natural Sesquiterpene Lactones Enhance Chemosensitivity of Tumor Cells through Redox Regulation of STAT3 Signaling. Oxid Med Cell Longev. 2019 Oct 28;2019:4568964.

39. Huynh J, Chand A, Gough D, Ernst M. Therapeutically exploiting STAT3 activity in cancer — using tissue repair as a road map. Nat Rev Cancer. 2019 Feb;19(2):82–96.

40. Perugini J, Di Mercurio E, Tossetta G, Severi I, Monaco F, Reguzzoni M, et al. Biological Effects of Ciliary Neurotrophic Factor on hMADS Adipocytes. Front Endocrinol (Lausanne). 2019;10:768.

41. Eyking A, Ey B, Rünzi M, Roig AI, Reis H, Schmid KW, et al. Toll-like Receptor 4 Variant D299G Induces Features of Neoplastic Progression in Caco-2 Intestinal Cells and Is Associated With Advanced Human Colon Cancer. Gastroenterology. 2011 Dec 1;141(6):2154–65.

42. Hossain DMS, Dos Santos C, Zhang Q, Kozlowska A, Liu H, Gao C, et al. Leukemia cell–targeted STAT3 silencing and TLR9 triggering generate systemic antitumor immunity. Blood. 2014 Jan 2;123(1):15–25.

43. Lee H, Deng J, Kujawski M, Yang C, Liu Y, Herrmann A, et al. STAT3-induced S1PR1 expression is crucial for persistent STAT3 activation in tumors. Nat Med. 2010 Dec;16(12):1421–8.

44. Shuai K, Liu B. Regulation of JAK–STAT signalling in the immune system. Nat Rev Immunol. 2003 Nov;3(11):900–11.

45. Aggarwal BB, Kunnumakkara AB, Harikumar KB, Gupta SR, Tharakan ST, Koca C, et al. Signal Transducer and Activator of Transcription-3, Inflammation, and Cancer. Ann N Y Acad Sci. 2009 Aug;1171:59–76.

46. Chang R, Song L, Xu Y, Wu Y, Dai C, Wang X, et al. Loss of Wwox drives metastasis in triple-negative breast cancer by JAK2/STAT3 axis. Nat Commun. 2018 Aug 28;9(1):3486.

47. Zhou Q, Qi F, Zhou C, Ji J, Jiang J, Wang C, et al. VPS35 promotes gastric cancer progression through integrin/FAK/SRC signalling-mediated IL-6/STAT3 pathway activation in a YAP-dependent manner. Oncogene. 2024 Jan;43(2):106–22.

48. Shields BJ, Wiede F, Gurzov EN, Wee K, Hauser C, Zhu HJ, et al. TCPTP Regulates SFK and STAT3 Signaling and Is Lost in Triple-Negative Breast Cancers. Molecular and Cellular Biology. 2013 Feb 1;33(3):557–70.

49. Pfitzner E, Kliem S, Baus D, Litterst CM. The role of STATs in inflammation and inflammatory diseases. Curr Pharm Des. 2004;10(23):2839–50.

50. Moser B, Edtmayer S, Witalisz-Siepracka A, Stoiber D. The Ups and Downs of STAT Inhibition in Acute Myeloid Leukemia. Biomedicines. 2021 Aug 19;9(8):1051.

51. Banerjee K, Resat H. Constitutive activation of STAT3 in breast cancer cells: A review. Int J Cancer. 2016 June 1;138(11):2570–8.

52. Mohan CD, Rangappa S, Preetham HD, Chandra Nayaka S, Gupta VK, Basappa S, et al. Targeting STAT3 signaling pathway in cancer by agents derived from Mother Nature. Semin Cancer Biol. 2022 May;80:157–82.

53. Ma J hui, Qin L, Li X. Role of STAT3 signaling pathway in breast cancer. Cell Communication and Signaling. 2020 Feb 28;18(1):33.

54. Hanahan D, Weinberg RA. Hallmarks of Cancer: The Next Generation. Cell. 2011 Mar 4;144(5):646–74.

55. Sirkisoon SR, Carpenter RL, Rimkus T, Anderson A, Harrison A, Lange AM, et al. Interaction between STAT3 and GLI1/tGLI1 oncogenic transcription factors promotes the aggressiveness of triple-negative breast cancers and HER2-enriched breast cancer. Oncogene. 2018 May;37(19):2502–14.

56. Jhaveri K, Teplinsky E, Silvera D, Valeta-Magara A, Arju R, Giashuddin S, et al. Hyperactivated mTOR and JAK2/STAT3 Pathways: Molecular Drivers and Potential Therapeutic Targets of Inflammatory and Invasive Ductal Breast Cancers After Neoadjuvant Chemotherapy. Clinical Breast Cancer. 2016 Apr 1;16(2):113-122.e1.

57. Li H, Qian Y, Wang X, Pi R, Zhao X, Wei X. Targeted activation of Stat3 in combination with paclitaxel results in increased apoptosis in epithelial ovarian cancer cells and a reduced tumour burden. Cell Prolif. 2019 Nov 28;53(1):e12719.

58. Campos AD, Shepard RM, Ortega Z, Heumann I, Wilke AE, Nam A, et al. A STAT3/integrin axis accelerates pancreatic cancer initiation and progression. Cell Reports [Internet]. 2025 Aug 26 [cited 2025 Aug 29];44(8). Available from: https://www.cell.com/cell-reports/abstract/S2211-1247(25)00781-8

59. Brandstoetter T, Schmoellerl J, Grausenburger R, Kollmann S, Doma E, Huuhtanen J, et al. SBNO2 is a critical mediator of STAT3-driven hematological malignancies. Blood. 2023 Apr 13;141(15):1831–45.

60. Fasouli ES, Katsantoni E. Age-associated myeloid malignancies – the role of STAT3 and STAT5 in myelodysplastic syndrome and acute myeloid leukemia. FEBS Letters. 2024;598(22):2809–28.

61. Shukla S, Shishodia G, Mahata S, Hedau S, Pandey A, Bhambhani S, et al. Aberrant expression and constitutive activation of STAT3 in cervical carcinogenesis: implications in high-risk human papillomavirus infection. Mol Cancer. 2010 Oct 27;9(1):282.

62. Sayed D, Badrawy H, Gaber N, Khalaf MR. p-Stat3 and bcr/abl gene expression in chronic myeloid leukemia and their relation to imatinib therapy. Leukemia Research. 2014 Feb 1;38(2):243–50.

63. Shi S, Ma HY, Zhang ZG. Clinicopathological and prognostic value of STAT3/p-STAT3 in cervical cancer: A meta and bioinformatics analysis. Pathology - Research and Practice. 2021 Nov 1;227:153624.

64. Wang Y, Shen Y, Wang S, Shen Q, Zhou X. The role of STAT3 in leading the crosstalk between human cancers and the immune system. Cancer Letters. 2018 Feb 28;415:117–28.

65. Cheng Y, Holloway MP, Nguyen K, McCauley D, Landesman Y, Kauffman MG, et al. XPO1 (CRM1) Inhibition Represses STAT3 Activation to Drive a Survivin-Dependent Oncogenic Switch in Triple-Negative Breast Cancer. Mol Cancer Ther. 2014 Mar 9;13(3):675–86.

66. Gritsko T, Williams A, Turkson J, Kaneko S, Bowman T, Huang M, et al. Persistent Activation of Stat3 Signaling Induces Survivin Gene Expression and Confers Resistance to Apoptosis in Human Breast Cancer Cells. Clin Cancer Res. 2006 Jan 5;12(1):11–9.

67. Activation of Stat3 in Primary Tumors from High-Risk Breast Cancer Patients Is Associated with Elevated Levels of Activated Src and Survivin Expression | Clinical Cancer Research | American Association for Cancer Research [Internet]. [cited 2025 Sept 9]. Available from: https://aacrjournals.org/clincancerres/article/12/1/20/188501/Activation-of-Stat3-in-Primary-Tumors-from-High

68. Williams CB, Phelps-Polirer K, Dingle IP, Williams CJ, Rhett MJ, Eblen ST, et al. HUNK phosphorylates EGFR to regulate breast cancer metastasis. Oncogene. 2020 Jan;39(5):1112–24.

69. Béguelin W, Díaz Flaqué MC, Proietti CJ, Cayrol F, Rivas MA, Tkach M, et al. Progesterone Receptor Induces ErbB-2 Nuclear Translocation To Promote Breast Cancer Growth via a Novel Transcriptional Effect: ErbB-2 Function as a Coactivator of Stat3. Mol Cell Biol. 2010 Dec;30(23):5456–72.

70. Zhao D, Pan C, Sun J, Gilbert C, Drews-Elger K, Azzam DJ, et al. VEGF drives cancer-initiating stem cells through VEGFR-2/Stat3 signaling to upregulate Myc and Sox2. Oncogene. 2015 June;34(24):3107–19.

71. Méndez-Clemente A, Bravo-Cuellar A, González-Ochoa S, Santiago-Mercado M, Palafox-Mariscal L, Jave-Suárez L, et al. Dual STAT-3 and IL-6R inhibition with stattic and tocilizumab decreases migration, invasion and proliferation of prostate cancer cells by targeting the IL-6/IL-6R/STAT-3 axis. Oncology Reports. 2022 Aug 1;48(2):1–16.

72. Sen M, Pollock NI, Black J, DeGrave KA, Wheeler S, Freilino ML, et al. JAK Kinase Inhibition Abrogates STAT3 Activation and Head and Neck Squamous Cell Carcinoma Tumor Growth. Neoplasia. 2015 Mar 1;17(3):256–64.

73. Scuto A, Krejci P, Popplewell L, Wu J, Wang Y, Kujawski M, et al. The novel JAK inhibitor AZD1480 blocks STAT3 and FGFR3 signaling, resulting in suppression of human myeloma cell growth and survival. Leukemia. 2011 Mar;25(3):538–50.

74. Chen H, Zhou W, Bian A, Zhang Q, Miao Y, Yin X, et al. Selectively Targeting STAT3 Using a Small Molecule Inhibitor is a Potential Therapeutic Strategy for Pancreatic Cancer. Clin Cancer Res. 2023 Feb 16;29(4):815–30.

75. Small molecule inhibitors targeting the cancers - Liu - 2022 - MedComm - Wiley Online Library [Internet]. [cited 2025 Sept 10]. Available from: https://onlinelibrary.wiley.com/doi/10.1002/mco2.181

76. Turkson J, Zhang S, Palmer J, Kay H, Stanko J, Mora LB, et al. Inhibition of constitutive signal transducer and activator of transcription 3 activation by novel platinum complexes with potent antitumor activity. Mol Cancer Ther. 2005 Jan 4;3(12):1533–42.

77. Zuo D, Shogren KL, Zang J, Jewison DE, Waletzki BE, Miller AL, et al. Inhibition of STAT3 blocks protein synthesis and tumor metastasis in osteosarcoma cells. Journal of Experimental & Clinical Cancer Research. 2018 Oct 4;37(1):244.

78. Son DJ, Zheng J, Jung YY, Hwang CJ, Lee HP, Woo JR, et al. MMPP Attenuates Non-Small Cell Lung Cancer Growth by Inhibiting the STAT3 DNA-Binding Activity *via* Direct Binding to the STAT3 DNA-Binding Domain. Theranostics. 2017 Oct 16;7(18):4632–42.

79. Beebe JD, Liu JY, Zhang JT. Two decades of research in discovery of anticancer drugs targeting STAT3, how close are we? Pharmacology & Therapeutics. 2018 Nov 1;191:74–91.

80. Fagard R, Metelev V, Souissi I, Baran-Marszak F. STAT3 inhibitors for cancer therapy: Have all roads been explored? JAK-STAT. 2013 Jan 1;2(1):e22882.

81. Shao Z, Wang H, Ren H, Sun Y, Chen X, Shao Z, et al. The Anticancer Effect of Napabucasin (BBI608), a Natural Naphthoquinone. Molecules [Internet]. 2023 July 27 [cited 2025 Nov 5];28(15). Available from: https://www.mdpi.com/1420-3049/28/15/5678

82. Tian K, Liu W, Zhang J, Fan X, Liu J, Zhao N, et al. MicroRNA-125b exerts antitumor functions in cutaneous squamous cell carcinoma by targeting the STAT3 pathway. Cellular & Molecular Biology Letters. 2020 Mar 5;25(1):12.

83. Xu S, Zhao N, Hui L, Song M, Miao ZW, Jiang XJ. MicroRNA-124-3p inhibits the growth and metastasis of nasopharyngeal carcinoma cells by targeting STAT3 Retraction in /10.3892/or.2024.8807. Oncology Reports. 2016 Mar 1;35(3):1385–94.

84. Esposito CL, Nuzzo S, Catuogno S, Romano S, de Nigris F, de Franciscis V. STAT3 Gene Silencing by Aptamer-siRNA Chimera as Selective Therapeutic for Glioblastoma. Molecular Therapy - Nucleic Acids. 2018 Mar 2;10:398–411.

85. Structure-Based Discovery of SD-36 as a Potent, Selective, and Efficacious PROTAC Degrader of STAT3 Protein | Journal of Medicinal Chemistry [Internet]. [cited 2025 Sept 10]. Available from: https://pubs.acs.org/doi/10.1021/acs.jmedchem.9b01530

86. SD-91 as A Potent and Selective STAT3 Degrader Capable of Achieving Complete and Long-Lasting Tumor Regression | ACS Medicinal Chemistry Letters [Internet]. [cited 2025 Sept 10]. Available from: https://pubs.acs.org/doi/10.1021/acsmedchemlett.1c00155

87. Kim J, Park A, Hwang J, Zhao X, Kwak J, Kim HW, et al. KS10076, a chelator for redox-active metal ions, induces ROS-mediated STAT3 degradation in autophagic cell death and eliminates ALDH1+ stem cells. Cell Reports. 2022 July 19;40(3):111077.

88. Health Benefits, Pharmacological Effects, Molecular Mechanisms, and Therapeutic Potential of α-Bisabolol [Internet]. [cited 2025 Sept 11]. Available from: https://www.mdpi.com/2072-6643/14/7/1370

89. Lee SH, Cho YC, Lim JS, Lee SH, Cho YC, Lim JS. Costunolide, a Sesquiterpene Lactone, Suppresses Skin Cancer via Induction of Apoptosis and Blockage of Cell Proliferation. International Journal of Molecular Sciences [Internet]. 2021 Feb 19 [cited 2025 Nov 5];22(4). Available from: https://www.mdpi.com/1422-0067/22/4/2075

90. Butturini E, Cavalieri E, Prati AC de, Darra E, Rigo A, Shoji K, et al. Two Naturally Occurring Terpenes, Dehydrocostuslactone and Costunolide, Decrease Intracellular GSH Content and Inhibit STAT3 Activation. PLOS ONE. 2011 May 18;6(5):e20174.

91. Lyss G, Schmidt TJ, Merfort I, Pahl HL. Helenalin, an Anti-Inflammatory Sesquiterpene Lactone from Arnica, Selectively Inhibits Transcription Factor NF-κB. Biological Chemistry. 1997 Sept 1;378(9):951–62.

92. Wen L, Chan BCL, Qiu MH, Leung PC, Wong CK, Wen L, et al. Artemisinin and Its Derivatives as Potential Anticancer Agents. Molecules [Internet]. 2024 Aug 16 [cited 2025 Nov 5];29(16). Available from: https://www.mdpi.com/1420-3049/29/16/3886

93. Li Y, Zhou X, Liu J, Gao N, Yang R, Wang Q, et al. Dihydroartemisinin inhibits the tumorigenesis and metastasis of breast cancer via downregulating CIZ1 expression associated with TGF-β1 signaling. Life Sciences. 2020 May 1;248:117454.

94. Dong J, Chen Y, Yang W, Zhang X, Li L. Antitumor and anti-angiogenic effects of artemisinin on breast tumor xenografts in nude mice. Research in Veterinary Science. 2020 Apr 1;129:66–9.

95. Cui J, Cai X, Qian R, Wu L, Qi X, Cao J, et al. Tween 80 Micelles Loaded with Fe3O4 Nanoparticles and Artemisinin for Combined Oxygen-Independent Ferroptosis Therapy of Cancer. Pharmaceutics [Internet]. 2024 May 9 [cited 2025 Nov 5];16(5). Available from: https://www.mdpi.com/1999-4923/16/5/639

96. Fidyt K, Fiedorowicz A, Strządała L, Szumny A. β-caryophyllene and β-caryophyllene oxide—natural compounds of anticancer and analgesic properties. Cancer Med. 2016 Sept 30;5(10):3007–17.

97. Dickson K, Scott C, White H, Zhou J, Kelly M, Lehmann C, et al. Antibacterial and Analgesic Properties of Beta-Caryophyllene in a Murine Urinary Tract Infection Model. Molecules [Internet]. 2023 May 17 [cited 2025 Nov 5];28(10). Available from: https://www.mdpi.com/1420-3049/28/10/4144

98. Kamatou GPP, Viljoen AM. A Review of the Application and Pharmacological Properties of α-Bisabolol and α-Bisabolol-Rich Oils. Journal of the American Oil Chemists' Society. 2010;87(1):1–7.

99. Rocha NFM, Oliveira GV de, Araújo FYR de, Rios ERV, Carvalho AMR, Vasconcelos LF, et al. (−)-α-Bisabolol-induced gastroprotection is associated with reduction in lipid peroxidation, superoxide dismutase activity and neutrophil migration. European Journal of Pharmaceutical Sciences. 2011 Nov 20;44(4):455–61.

100. Schwartz MA, Swanson GC. Stereospecific syntheses of the diastereomeric (.+-.)-.alpha.-bisabolols. A caveat on the assignment of stereochemistry to natural .alpha.-bisabolol. J Org Chem. 1979 Mar 1;44(6):953–8.

101. D'Almeida APL, Pacheco de Oliveira MT, de Souza ÉT, de Sá Coutinho D, Ciambarella BT, Gomes CR, et al. α-bisabolol-loaded lipid-core nanocapsules reduce lipopolysaccharide-induced pulmonary inflammation in mice. Int J Nanomed. 2017;12:4479–91.

102. Xu C, Sheng S, Dou H, Chen J, Zhou K, Lin Y, et al. α-Bisabolol suppresses the inflammatory response and ECM catabolism in advanced glycation end products-treated chondrocytes and attenuates murine osteoarthritis. International Immunopharmacology. 2020 July 1;84:106530.

103. Oliveira F de S, Freitas TS de, Cruz RP da, Costa M do S, Pereira RLS, Quintans-Júnior LJ, et al. Evaluation of the antibacterial and modulatory potential of α-bisabolol, β-cyclodextrin and α-bisabolol/β-cyclodextrin complex. Biomedicine & Pharmacotherapy. 2017 Aug 1;92:1111–8.

104. Cavalieri E, Bergamini C, Mariotto S, Leoni S, Perbellini L, Darra E, et al. Involvement of mitochondrial permeability transition pore opening in α-bisabolol induced apoptosis. The FEBS Journal. 2009;276(15):3990–4000.

105. Cavalieri E, Mariotto S, Fabrizi C, de Prati AC, Gottardo R, Leone S, et al. α-Bisabolol, a nontoxic natural compound, strongly induces apoptosis in glioma cells. Biochemical and Biophysical Research Communications. 2004 Mar 12;315(3):589–94.

106. Wu S, Peng L, Sang H, Ping Li Q, Cheng S. Anticancer effects of α-Bisabolol in human non-small cell lung carcinoma cells are mediated via apoptosis induction, cell cycle arrest, inhibition of cell migration and invasion and upregulation of P13K/AKT signalling pathway. J BUON. 2018;23(5):1407–12.

107. Cavalieri E, Mariotto S, Fabrizi C, de Prati AC, Gottardo R, Leone S, et al. alpha-Bisabolol, a nontoxic natural compound, strongly induces apoptosis in glioma cells. Biochem Biophys Res Commun. 2004 Mar 12;315(3):589–94.

108. Cavalieri E, Mariotto S, Fabrizi C, de Prati AC, Gottardo R, Leone S, et al. α-Bisabolol, a nontoxic natural compound, strongly induces apoptosis in glioma cells. Biochemical and Biophysical Research Communications. 2004 Mar 12;315(3):589–94.

109. Mendes FB, Bergamin LS, Stuepp CDS, Braganhol E, Terroso T, Pohlmann AR, et al. Alpha-bisabolol Promotes Glioma Cell Death by Modulating the Adenosinergic System. Anticancer Research. 2017 Apr 1;37(4):1819–23.

110. Omuro A, DeAngelis LM. Glioblastoma and Other Malignant Gliomas: A Clinical Review. JAMA. 2013 Nov 6;310(17):1842–50.

111. Chen W, Hou J, Yin Y, Jang J, Zheng Z, Fan H, et al. α-Bisabolol induces dose- and time-dependent apoptosis in HepG2 cells via a Fas- and mitochondrial-related pathway, involves p53 and NFκB. Biochemical Pharmacology. 2010 July 15;80(2):247–54.

112. Stoop TF, Javed AA, Oba A, Koerkamp BG, Seufferlein T, Wilmink JW, et al. Pancreatic cancer. The Lancet. 2025 Apr 5;405(10485):1182–202.

113. Yu J, Zhang SS, Saito K, Williams S, Arimura Y, Ma Y, et al. PTEN regulation by Akt–EGR1–ARF–PTEN axis. The EMBO Journal. 2009 Jan 7;28(1):21–33.

114. Seki T, Kokuryo T, Yokoyama Y, Suzuki H, Itatsu K, Nakagawa A, et al. Antitumor effects of α-bisabolol against pancreatic cancer. Cancer Science. 2011;102(12):2199–205.

115. Uno M, Kokuryo T, Yokoyama Y, Senga T, Nagino M. α-Bisabolol Inhibits Invasiveness and Motility in Pancreatic Cancer Through KISS1R Activation. Anticancer Research. 2016 Feb 1;36(2):583–9.

116. Darra E, Abdel-Azeim S, Manara A, Shoji K, Maréchal JD, Mariotto S, et al. Insight into the apoptosis-inducing action of α-bisabolol towards malignant tumor cells: Involvement of lipid rafts and Bid. Archives of Biochemistry and Biophysics. 2008 Aug 15;476(2):113–23.

117. Cavalieri E, Rigo A, Bonifacio M, de Prati AC, Guardalben E, Bergamini C, et al. Pro-apoptotic activity of α-bisabolol in preclinical models of primary human acute leukemia cells. J Transl Med. 2011 Apr 21;9:45.

118. Rigo A, Ferrarini I, Bonalumi A, Tecchio C, Montresor A, Laudanna C, et al. Efficient lysis of B-chronic lymphocytic leukemia cells by the plant-derived sesquiterpene alcohol α-bisabolol, a dual proapoptotic and antiautophagic agent. Oncotarget. 2018 May 25;9(40):25877–90.

119. Costarelli L, Malavolta M, Giacconi R, Cipriano C, Gasparini N, Tesei S, et al. In Vivo Effect of α-Bisabolol, a Nontoxic Sesquiterpene Alcohol, on the Induction of Spontaneous Mammary Tumors in HER-2/neu Transgenic Mice. Oncology Research Featuring Preclinical and Clinical Cancer Therapeutics. 2009 Sept 1;18(9):409–18.

120. Gold nanoparticles as novel agents for cancer therapy | British Journal of Radiology | Oxford Academic [Internet]. [cited 2025 Sept 18]. Available from: https://academic.oup.com/bjr/article-abstract/85/1010/101/7450613?redirectedFrom=fulltext

121. Shi J, Kantoff PW, Wooster R, Farokhzad OC. Cancer nanomedicine: progress, challenges and opportunities. Nat Rev Cancer. 2017 Jan;17(1):20–37.

122. Kesharwani P, Gothwal A, Iyer AK, Jain K, Chourasia MK, Gupta U. Dendrimer nanohybrid carrier systems: an expanding horizon for targeted drug and gene delivery. Drug Discovery Today. 2018 Feb 1;23(2):300–14.

123. Blanco E, Shen H, Ferrari M. Principles of nanoparticle design for overcoming biological barriers to drug delivery. Nat Biotechnol. 2015 Sept;33(9):941–51.

124. Makhlouf Z, Ali AA, Al-Sayah MH. Liposomes-Based Drug Delivery Systems of Anti-Biofilm Agents to Combat Bacterial Biofilm Formation. Antibiotics. 2023 May;12(5):875.

125. Hernández-Esquivel RA, Navarro-Tovar G, Zárate-Hernández E, Aguirre-Bañuelos P, Hernández-Esquivel RA, Navarro-Tovar G, et al. Solid Lipid Nanoparticles (SLN). In: Nanocomposite Materials for Biomedical and Energy Storage Applications [Internet]. IntechOpen; 2022 [cited 2025 Sept 18]. Available from: https://www.intechopen.com/chapters/80519

126. Chauhan I, Yasir M, Verma M, Singh AP. Nanostructured Lipid Carriers: A Groundbreaking Approach for Transdermal Drug Delivery. Adv Pharm Bull. 2020 June;10(2):150–65.

127. Kim T, Hyeon T. Applications of inorganic nanoparticles as therapeutic agents. Nanotechnology. 2013 Dec;25(1):012001.

128. Yaqoob SB, Adnan R, Rameez Khan RM, Rashid M. Gold, Silver, and Palladium Nanoparticles: A Chemical Tool for Biomedical Applications. Front Chem [Internet]. 2020 June 3 [cited 2025 Sept 18];8. Available from: https://www.frontiersin.org/journals/chemistry/articles/10.3389/fchem.2020.00376/full

129. Ali A, Shah T, Ullah R, Zhou P, Guo M, Ovais M, et al. Review on Recent Progress in Magnetic Nanoparticles: Synthesis, Characterization, and Diverse Applications. Front Chem [Internet]. 2021 July 13 [cited 2025 Sept 18];9. Available from: https://www.frontiersin.org/journals/chemistry/articles/10.3389/fchem.2021.629054/full

130. Cotta MA. Quantum Dots and Their Applications: What Lies Ahead? ACS Appl Nano Mater. 2020 June 26;3(6):4920–4.

131. Selvarajan V, Obuobi S, Ee PLR. Silica Nanoparticles—A Versatile Tool for the Treatment of Bacterial Infections. Front Chem [Internet]. 2020 July 15 [cited 2025 Sept 18];8. Available from: https://www.frontiersin.org/journals/chemistry/articles/10.3389/fchem.2020.00602/full

132. Javadzadeh Y, Azharshekoufeh Bahari L. Chapter 8 - Therapeutic Nanostructures for Dermal and Transdermal Drug Delivery. In: Grumezescu AM, editor. Nano- and Microscale Drug Delivery Systems [Internet]. Elsevier; 2017 [cited 2025 Sept 18]. p. 131–46. Available from: https://www.sciencedirect.com/science/article/pii/B978032352727900008X

133. Kumar SSA, M. NB, Batoo KM, Wonnie Ma IA, Ramesh K, Ramesh S, et al. Fabrication and characterization of graphene oxide-based polymer nanocomposite coatings, improved stability and hydrophobicity. Sci Rep. 2023 June 2;13(1):8946.

134. Polymer Nanoparticles - an overview | ScienceDirect Topics [Internet]. [cited 2025 Sept 18]. Available from: https://www.sciencedirect.com/topics/materials-science/polymer-nanoparticles

135. Sadhu P, Kumari M, Rathod F, Shah N, Patel S. A Review on Poly(amidoamine) Dendrimers: Properties, Synthesis, and Characterization Prospects. Archives of Pharmacy Practice. 2022;13(4–2022):1–6.

136. Polydopamine nanomaterials for overcoming current challenges in cancer treatment - Cerca con Google [Internet]. [cited 2025 Sept 18]. Available from: https://www.google.com/search?client=firefox-b-d&q=Polydopamine+nanomaterials+for+overcoming+current+challenges+in+cancer+treatment

137. Vargas-Bernal R, He P, Zhang S. Hybrid Nanomaterials: Flexible Electronics Materials. BoD – Books on Demand; 2020. 150 p.

138. Masood F. Polymeric nanoparticles for targeted drug delivery system for cancer therapy. Materials Science and Engineering: C. 2016 Mar 1;60:569–78.

139. Rezvantalab S, Drude NI, Moraveji MK, Güvener N, Koons EK, Shi Y, et al. PLGA-Based Nanoparticles in Cancer Treatment. Front Pharmacol [Internet]. 2018 Nov 2 [cited 2025 Sept 24];9. Available from: https://www.frontiersin.org/journals/pharmacology/articles/10.3389/fphar.2018.01260/full

140. Makadia HK, Siegel SJ. Poly Lactic-co-Glycolic Acid (PLGA) as Biodegradable Controlled Drug Delivery Carrier. Polymers. 2011 Sept;3(3):1377–97.

141. Razavi MS, Abdollahi A, Malek-Khatabi A, Ejarestaghi NM, Atashi A, Yousefi N, et al. Recent advances in PLGA-based nanofibers as anticancer drug delivery systems. Journal of Drug Delivery Science and Technology. 2023 Aug 1;85:104587.

142. Li J, Kataoka K. Chemo-physical Strategies to Advance the in Vivo Functionality of Targeted Nanomedicine: The Next Generation. J Am Chem Soc. 2021 Jan 20;143(2):538–59.

143. Kim KT, Lee JY, Kim DD, Yoon IS, Cho HJ. Recent Progress in the Development of Poly(lactic-co-glycolic acid)-Based Nanostructures for Cancer Imaging and Therapy. Pharmaceutics. 2019 June 14;11(6):280.

144. Sharifnia Z, Bandehpour M, Hamishehkar H, Mosaffa N, Kazemi B, Zarghami N. In-vitro Transcribed mRNA Delivery Using PLGA/PEI Nanoparticles into Human Monocyte-derived Dendritic Cells. Iran J Pharm Res. 2019;18(4):1659–75.

145. Shen Y, TanTai J. Co-Delivery Anticancer Drug Nanoparticles for Synergistic Therapy Against Lung Cancer Cells. Drug Des Devel Ther. 2020 Oct 23;14:4503–10.

146. Fonseca C, Simões S, Gaspar R. Paclitaxel-loaded PLGA nanoparticles: preparation, physicochemical characterization and in vitro anti-tumoral activity. Journal of Controlled Release. 2002 Oct 4;83(2):273–86.

147. Wu J, Wang X, Wang Y, Xun Z, Li S. Application of PLGA in Tumor Immunotherapy. Polymers. 2024 Jan;16(9):1253.

148. Global Cancer Statistics 2020: GLOBOCAN Estimates of Incidence and Mortality Worldwide for 36 Cancers in 185 Countries - Sung - 2021 - CA: A Cancer Journal for Clinicians - Wiley Online Library [Internet]. [cited 2025 June 5]. Available from: https://acsjournals.onlinelibrary.wiley.com/doi/10.3322/caac.21660

149. Wu S, Peng L, Sang H, Li QP, Cheng S. Anticancer effects of α-Bisabolol in human non-small cell lung carcinoma cells are mediated via apoptosis induction, cell cycle arrest, inhibition of cell migration and invasion and upregulation of P13K/AKT signalling pathway.

150. Wei S, Li J, Tang M, Zhang K, Gao X, Fang L, et al. STAT3 and p63 in the Regulation of Cancer Stemness. Front Genet [Internet]. 2022 Aug 17 [cited 2025 Nov 16];13. Available from: https://www.frontiersin.org/journals/genetics/articles/10.3389/fgene.2022.909251/full

151. Wang T, Fahrmann JF, Lee H, Li YJ, Tripathi SC, Yue C, et al. JAK/STAT3-Regulated Fatty Acid β-Oxidation Is Critical for Breast Cancer Stem Cell Self-Renewal and Chemoresistance. Cell Metabolism. 2018 Jan 9;27(1):136-150.e5.

152. Arunachalam S, Meeran MFN, Azimullah S, Jha NK, Saraswathiamma D, Subramanya S, et al. α-Bisabolol Attenuates Doxorubicin Induced Renal Toxicity by Modulating NF-κB/MAPK Signaling and Caspase-Dependent Apoptosis in Rats. International Journal of Molecular Sciences [Internet]. 2022 Sept 10 [cited 2025 Nov 15];23(18). Available from: https://www.mdpi.com/1422-0067/23/18/10528

153. Cavalieri E, Bergamini C, Mariotto S, Leoni S, Perbellini L, Darra E, et al. Involvement of mitochondrial permeability transition pore opening in alpha-bisabolol induced apoptosis. FEBS J. 2009 Aug;276(15):3990–4000.

154. Cavalieri E, Bergamini C, Mariotto S, Leoni S, Perbellini L, Darra E, et al. Involvement of mitochondrial permeability transition pore opening in alpha-bisabolol induced apoptosis. FEBS J. 2009 Aug;276(15):3990–4000.

155. Aslan M, Hsu EC, Liu S, Stoyanova T. Quantifying the invasion and migration ability of cancer cells with a 3D Matrigel drop invasion assay. Biology Methods and Protocols. 2021 Jan 1;6(1):bpab014.

156. Marongiu L, Donini M, Bovi M, Perduca M, Vivian F, Romeo A, et al. The inclusion into PLGA nanoparticles enables α-bisabolol to efficiently inhibit the human dendritic cell pro-inflammatory activity. J Nanopart Res. 2014 July 18;16(8):2554.

157. Danhier F, Ansorena E, Silva JM, Coco R, Le Breton A, Préat V. PLGA-based nanoparticles: An overview of biomedical applications. Journal of Controlled Release. 2012 July 20;161(2):505–22.

158. Gaonkar RH, Ganguly S, Dewanjee S, Sinha S, Gupta A, Ganguly S, et al. Garcinol loaded vitamin E TPGS emulsified PLGA nanoparticles: preparation, physicochemical characterization, in vitro and in vivo studies. Sci Rep. 2017 Apr 3;7(1):530.

159. Butturini E, Prati AC de, Mariotto S, Butturini E, Prati AC de, Mariotto S. Redox Regulation of STAT1 and STAT3 Signaling. International Journal of Molecular Sciences [Internet]. 2020 Sept 24 [cited 2025 Nov 17];21(19). Available from: https://www.mdpi.com/1422-0067/21/19/7034

160. Chen W, Hou J, Yin Y, Jang J, Zheng Z, Fan H, et al. α-Bisabolol induces dose- and time-dependent apoptosis in HepG2 cells via a Fas- and mitochondrial-related pathway, involves p53 and NFκB. Biochemical Pharmacology. 2010 July 15;80(2):247–54.

161. Cavalieri E, Rigo A, Bonifacio M, de Prati AC, Guardalben E, Bergamini C, et al. Pro-apoptotic activity of α-bisabolol in preclinical models of primary human acute leukemia cells. Journal of Translational Medicine. 2011 Apr 21;9(1):45.

162. Ponomarev AS, Gilazieva ZE, Solovyova VV, Rizvanov AA. Molecular Mechanisms of Tumor Cell Stemness Modulation during Formation of Spheroids. Biochemistry Moscow. 2023 July 1;88(7):979–94.

163. Altundag-Erdogan Ö, Çelebi-Saltik B. Niclosamide Treatment Suppressed Metastatic, Apoptotic, and Proliferative Characteristics of MDA-MB-231 Cancer Stem Cells. ACS Omega. 2025 June 10;10(22):23629–38.

164. Chung SS, Giehl N, Wu Y, Vadgama JV. [Corrigendum] STAT3 activation in HER2-overexpressing breast cancer promotes epithelial-mesenchymal transition and cancer stem cell traits. International Journal of Oncology. 2025 Aug 1;67(2):1–3.

165. Schaijik B van, Davis PF, Wickremesekera AC, Tan ST, Itinteang T. Subcellular localisation of the stem cell markers OCT4, SOX2, NANOG, KLF4 and c-MYC in cancer: a review. Journal of Clinical Pathology. 2018 Jan 1;71(1):88–91.

166. Lee S, Wottrich S, Bonavida B. Crosstalks between Raf-kinase inhibitor protein and cancer stem cell transcription factors (Oct4, KLF4, Sox2, Nanog). Tumour Biol. 2017 Apr 1;39(4):1010428317692253.

167. Kaur B, Mukhlis Y, Natesh J, Penta D, Musthapa Meeran S. Identification of hub genes associated with EMT-induced chemoresistance in breast cancer using integrated bioinformatics analysis. Gene. 2022 Jan 30;809:146016.

168. Marongiu L, Donini M, Bovi M, Perduca M, Vivian F, Romeo A, et al. The inclusion into PLGA nanoparticles enables α-bisabolol to efficiently inhibit the human dendritic cell pro-inflammatory activity. J Nanopart Res. 2014 July 18;16(8):2554.

169. Kiruthiga C, Balan DJ, Prasath NH, Manikandakrishnan M, Jafni S, Prabhu NM, et al. Synergistic induction of apoptosis in lung cancer cells through co-delivery of PLGA phytol/α-bisabolol nanoparticles. Naunyn-Schmiedeberg's Arch Pharmacol. 2024 July 1;397(7):5131–44.

170. Mulè C, Caputo TM, Montefusco A, Romanelli AM, Caputo I, Paolella G, et al. PLGA nanoparticles for capsaicin delivery: enhanced encapsulation efficiency and pro-apoptotic activity in HEPG2 cells. Front Bioeng Biotechnol [Internet]. 2025 July 18 [cited 2025 Nov 4];13. Available from: https://www.frontiersin.org/journals/bioengineering-and-biotechnology/articles/10.3389/fbioe.2025.1617022/full

171. Noorain L, Nguyen V, Kim HW, Nguyen LTB, Noorain L, Nguyen V, et al. A Machine Learning Approach for PLGA Nanoparticles in Antiviral Drug Delivery. Pharmaceutics [Internet]. 2023 Feb 2 [cited 2025 Nov 4];15(2). Available from: https://www.mdpi.com/1999-4923/15/2/495

172. Markowski A, Migdał P, Zygmunt A, Zaremba-Czogalla M, Gubernator J, Markowski A, et al. Evaluation of the In Vitro Cytotoxic Activity of Ursolic Acid PLGA Nanoparticles against Pancreatic Ductal Adenocarcinoma Cell Lines. Materials [Internet]. 2021 Aug 29 [cited 2025 Nov 4];14(17). Available from: https://www.mdpi.com/1996-1944/14/17/4917

173. Makadia HK, Siegel SJ, Makadia HK, Siegel SJ. Poly Lactic-co-Glycolic Acid (PLGA) as Biodegradable Controlled Drug Delivery Carrier. Polymers. 2011 Aug 26;3(3):1377–97.

174. Zundert IV, Fortuni B, Rocha S, Zundert IV, Fortuni B, Rocha S. From 2D to 3D Cancer Cell Models—The Enigmas of Drug Delivery Research. Nanomaterials [Internet]. 2020

Nov 11 [cited 2025 Nov 13];10(11). Available from: https://www.mdpi.com/2079-4991/10/11/2236

175. Munir MU. Nanomedicine Penetration to Tumor: Challenges, and Advanced Strategies to Tackle This Issue. Cancers [Internet]. 2022 June 13 [cited 2025 Nov 13];14(12). Available from: https://www.mdpi.com/2072-6694/14/12/2904

176. Priwitaningrum DL, Blondé JBG, Sridhar A, van Baarlen J, Hennink WE, Storm G, et al. Tumor stroma-containing 3D spheroid arrays: A tool to study nanoparticle penetration. Journal of Controlled Release. 2016 Dec 28;244:257–68.

177. Li X, Strietz J, Bleilevens A, Stickeler E, Maurer J. Chemotherapeutic Stress Influences Epithelial-Mesenchymal Transition and Stemness in Cancer Stem Cells of Triple-Negative Breast Cancer. Int J Mol Sci. 2020 Jan 8;21(2):404.

178. Limiting dilution assay to quantify the self-renewal potential of cancer stem cells in hepatocellular carcinoma. In: Methods in Cell Biology [Internet]. Academic Press; 2022 [cited 2025 Nov 16]. p. 197–213. Available from: https://www.sciencedirect.com/science/chapter/bookseries/pii/S0091679X22000577

179. Cavalieri E, Rigo A, Bonifacio M, de Prati AC, Guardalben E, Bergamini C, et al. Pro-apoptotic activity of α-bisabolol in preclinical models of primary human acute leukemia cells. Journal of Translational Medicine. 2011 Apr 21;9(1):45.

180. Li Y, Wei J, Sun Y, Zhou W, Ma X, Guo J, et al. DLGAP5 Regulates the Proliferation, Migration, Invasion, and Cell Cycle of Breast Cancer Cells via the JAK2/STAT3 Signaling Axis. International Journal of Molecular Sciences [Internet]. 2023 Oct 31 [cited 2025 Nov 21];24(21). Available from: https://www.mdpi.com/1422-0067/24/21/15819

181. Song Y, Zhao H, Yu R, Zhang Y, Zou Y, Liu X, et al. Wogonin suppresses proliferation, invasion and migration in gastric cancer cells via targeting the JAK-STAT3 pathway. Sci Rep. 2024 Dec 28;14(1):30803.

Appendix

During my 1st year as a PhD student in the Biomolecular Medicine Program, I was also involved in a second project in the laboratory of Prof. S. Mariotto.
Specifically, this project aimed to study the effect of a vegetable extract on the chronic hypoxia-resistant breast cancer cell line chMDA-MB231. This project was presented in the poster session at the SIB 2023 congress (September 5-7, 2023). Hereafter, the research output of this project is presented.

Background

Tumor microenvironment (TME) is composed of a complex network of components that regulate tumor initiation, malignancy, and metastasis. Due to rapid cell growth and poor vascularization, TME is often characterized by hypoxic regions that induce genetic instability and adaptive changes of cancer cells associated with aggressiveness (1).
Tumor hypoxia can be classified into acute**,** chronic, and cycling forms.
Acute hypoxia results from short exposure to low oxygen for a few hours or days, inducing metabolic reprogramming of glycolysis genes, cell migration, and extracellular matrix remodeling. These events are specifically mediated by the family of transcription factors known as hypoxia-inducible factor 1 (HIF-1). In contrast, chronic hypoxia induces long-term cellular changes, including DNA breaks and a metabolic shift from oxidative phosphorylation to anaerobic glycolysis (2–4). Finally, cycling hypoxia, characterized by a period of hypoxia followed by reoxygenation, induces several survival mechanisms of the cells, such as autophagy (5), and is considered the condition that more closely reflects *in vivo* oxygen fluctuations.
Our research group established and characterized chMDA-MB-231 cells obtained by culturing parental MDA-MB-231 cells under chronic hypoxia for at least 40 days. These cells stably survive under 1% O_2 conditions by entering into a dormant state from which they recover their normal proliferation rate once returned to normoxic conditions. Furthermore, we proposed that autophagy serves as a survival mechanism of chMDA-MB-231 cells (6). Dormant cells are a poorly understood

state in cancer progression, characterized by mitotic arrest in the G0/G1 phase, low metabolism, and stem cell–like properties, such as spheroid formation capacity and expression of stem cell markers. Because dormant tumor cells may be the founders of metastasis, one hypothesis is that these cells, or at least a subset of them, exhibit stem cell-like characteristics that may be responsible for their prolonged survival. Literature evidence associates tumor relapse with tumor dormancy. In recent years, considerable progress has been made in understanding the factors that determine whether these cells survive, remain dormant, or become metastatic.
The aim of this project is to propose new precision therapeutic strategies for breast cancer by selectively targeting dormant cancer cells using the in-house dormant cell model chMDA-MB-231 treated with different vegetable extracts.

Material and Methods

Cell line and cell culture

Human breast cancer cell line MDA-MB-231 were purchased from American Type Culture Collection. The MDA-MB-231 cells were cultured in DMEM (LifeTechnologies) supplemented with 10%FBS, 100 IU/mL streptomycin and 40 µg/mL gentamycin (LifeTechnologies) in 5% CO_2 atmosphere at 37°C. Hypoxic culture was archived by incubating cells with 1% O_2 and 5% CO_2 in a Multigas Incubator (RUSKINN C300, RUSKINN Technology Ltd) in DMEM (LifeTechnologies) supplemented with 10%FBS, 100 IU/mL streptomycin and 40 µg/mL gentamycin (LifeTechnologies).

Cells viability with Trypan Blue

The viability of MDA-MB-231 and chMDA-MB-231 cells were evaluated with the 0.1% Trypan Blue exclusion test using a TC20 Automated Cell Counter (Bio-Rad).

Morphological Analyses of Dormant Cells and Spheroids

The MDA-MB-231 and chMDA-MB-231 cells were cultured under the conditions described above and after 45 days images of cells were acquired with phase-contrast microscope (Carl Zeiss™ Axio Vert.A1).
The viable floating chMDA-MB-231 cells were collected, seeded on a 96-well plate coated with 1% of agar, and cultured in hypoxic conditions for 10 days. Each day, the spheroids images, were acquired by phase contrast microscope and analyzed by ImageJ software (Rasband, W.S. ImageJ, U.S. National Istitute of Health, Bethsda, Maryland).

Immunophenotype

1 x 10^5 cells were washed in PBS, and stained with anti-human CD44-PE (BD Pharmingen, San Jose, CA, USA) at 37°C for 15 mins. After incubation, the cells were washed with PBS, acquired on a BD FACSCanto II (BD Biosciences, San Jose, CA, USA), and analyzed using FlowJo v10 software (BD Biosciences). Data were expressed as the Median Fluorescence Intensity (MFI) difference between stained and unstained cells.

Western Blot

Cells were washed with ice-cold PBS and lysed at 4 °C in 20 mM HEPES (pH 7.4) containing 420 mM NaCl, 1 mM EDTA, 1 mM EGTA, 1% Igepal, 20% glycerol, and protease and phosphatase inhibitor cocktails. Protein concentration was quantified using Bradford reagent (Thermo Fisher Scientific). 50 µg/lane of total protein extracted was resolved by 7.5% or 10% SDS-polyacrylamide gel electrophoresis and transferred to a polyvinylidene difluoride (PVDF) membrane (Immobilon P, Millipore, Bedford, MA, USA). Membranes were blocked with 5% fat dry milk or BSA in Tris-buffered saline with 0.1% Tween 20 (TBST) at room temperature (RT) for 1 hour and then incubated with primary antibodies specific for p-AKT and p-ERK (Cell Signalling Technology, Beverly, MA, USA. After washings with TBST, the membranes were hybridised with anti-rabbit or anti-mouse IgG

peroxidase-conjugated secondary antibody (Cell Signalling Technology) and developed by Western Chemiluminescent HRP Substrate (Millipore) using ChemiDoc MP Imaging System (Bio-Rad, Hercules, CA, USA). Blotted proteins were quantified using ImageLab (Bio-Rad).

Monodansylcadaverine staining

The MDA-MB-231 and chMDA-MB-231 cells were incubated with the fluorescent probe monodansylcadaverine (MDC; Sigma), a selective marker for acidic vesicular organelles, such as autophagic vacuoles. Briefly, cells were seeded in 96-well plates (3 × 10^4 cells/well) and, after 24 hours, were incubated in culture medium containing 50 mM MDC at 37°C for 15 minutes. Cells were then washed with Hanks buffer (20 mM Hepes pH 7.2, 10 mM glucose, 118 mM NaCl, 4.6 mM KCl, and 1 mM CaCl2) and fluorescence was measured using a multimode plate reader (Ex 340 nm and Em 535nm) (GENios Pro, Tecan). The values were normalized for cell proliferation by the Crystal Violet assay.

Real-Time PCR

For hypoxia and normoxia-regulated genes the Real-Time PCR procedure was carried out, and RPL13a was used as the internal control. RNA extraction was performed using the RNeasy Mini Kit (Qiagen) according to the manufacturer's instructions, and the RNA was quantified using a Nano Drop spectrophotometer (NanoDrop, Thermo Scientific, Waltham, MA, USA) Following the manufacturer's protocol, 1 g of total RNA was reverse-transcribed using ImProm-II™ Reverse Transcription System kit ((Promega Corporation, Madison, WI, USA). Aliquots of the cDNAs (corresponding to 25 ng of the original RNA) were used for real-time PCR with the GoTaq qPCR Master Mix (Promega, USA) CFX96 Real-Time PCR System (Bio-Rad Laboratories, Hercules, CA, USA). The specificity of the amplified products was monitored by performing melting curves at the end of each amplification reaction. All amplicons generated a single peak, thus reflecting the specificity of the primers.

Statistical analysis

Data are reported as means ± SD of three independent experiments; statistical analyses were performed using Student's t-test.

Results and Discussion

Chronic hypoxia selects a dormant cell population

To establish an *in vitro* model of a dormant cancer cell line, we cultured MDA-MB-231 cells in hypoxic conditions (1% O_2). After 40 days, the cell population exhibits low proliferation rate, distinct morphology, stem-like properties, and altered protein expression. These cells were designed by the chMDA-MB-231 cell line.

As revealed by phase-contrast microscopy analysis, the chMDA-MB-231 cells show a longer and tapered shape compared to parental cells (Figure 1A). It has been described that dormant cells exhibit a typical profile of cancer stem cells (CSCs), characterized by the differential expression of CD44, CD24, ESA, and ALDH1. CD44 is a cell surface transmembrane glycoprotein, and its overexpression represents one of the CSCs' features, such as self-renewal and epithelial-mesenchymal transition (EMT) capability (7). ChMDA-MB-231 cells displayed an upregulation of CD44 expression after 40 days of hypoxia, as determined by flow cytometry (Figure 1B). To confirm the stemness of hypoxia-selected cells, the sphere-forming capacity was assessed. The viable chMDA-MB-231 floating cells were collected, seeded on a coated 96 plate, and cultured in hypoxic conditions. The spheroid's size was 30 µm after 3 days and reached at least 170 µm after 10 days. Due to their irregular shape, diameters were measured using ellipse fitting in ImageJ (Figure 1C).

Recently, Endo et al. identified protein kinase AKT as a key molecular regulator involved in the induction of cellular dormancy, showing that its suppression helps to preserve cellular energy by reducing metabolic demand (8). Furthermore, studies have reported that the phospho-ERK/p38 ratio functions as a molecular switch controlling tumor cell dormancy: a high ratio promotes proliferation and metastatic progression, whereas in restrictive microenvironments, a low phospho-ERK/p38 ratio induces prolonged dormancy and G0/G1 cell-cycle arrest (9). Consistent with previous reports, we observed reduced serine phosphorylation of AKT and decreased

tyrosine/threonine phosphorylation of ERK in chMDA-MB-231 cells (Figure 1D). To evaluate different stemness markers that could be modulated after hypoxic conditions in chMDA-MB-231 cells, qRT-PCR analysis was performed. Exposure to hypoxia decreases the expression of stemness- and EMT-associated genes, such as E-*cadherin, N-cadherin, SOX9, TGF-β*, and *NOTCH1* (Figure 1E).

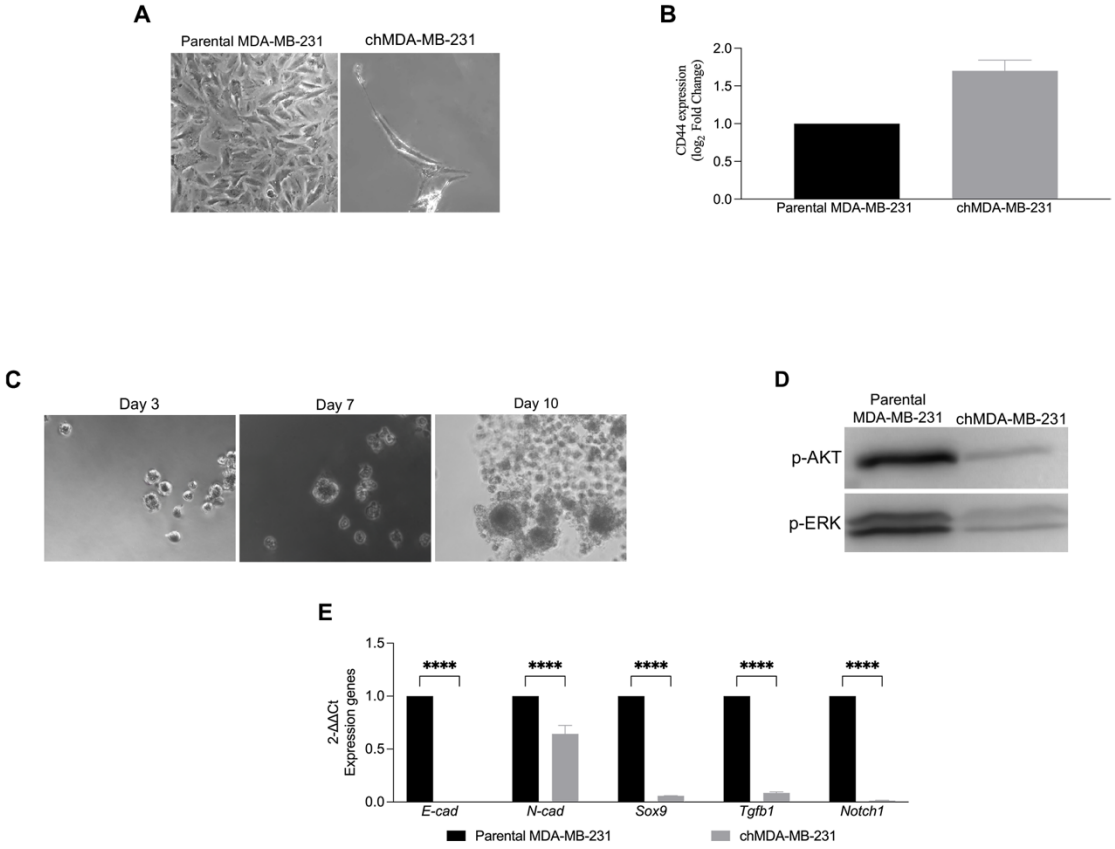

Figure 1. Chronic hypoxia selects the dormant cell population. A) Phase-contrast microscopy analysis showed morphology of MDA-MB-231 and chMDA-MB-231. B) Flow cytometry analysis of the immunophenotype of the $CD44^{+}/CD24^{-}$ using the FACScan cytometer (Becton Dickinson). The parental cells MDA-MB231 cultured under normoxia were used as a control. C) Phase-contrast microscopy analysis shows spheroids after chronic hypoxia. D) Western blot analysis for the expression of pAKT and pERK in MDA-MB-231 and chMDA-MB-231. The shown image is representative of three independent experiments. E) qPCR analysis of stemness- and EMT-related genes expression in chMDA-MB-23 and MDA-MB-231 cells. The data were normalized against RLP13A RNA, and the levels of mRNA are expressed as arbitrary units. Each bar represents the mean±SD of four independent experiments performed in triplicate, and a Two-way ANOVA test with Dunnett's multiple comparison was performed to determine statistical significance, $p < 0.00001$ (****), $p < 0.0001$ (***), $p < 0.001$ (**), $p < 0.01$(*).

Effect of vegetable extract CC on dormant cancer cell

The chMDA-MB-231 cell line was treated with a vegetable extract, referred to in this work as CC. For confidentiality reasons, the company that prepared the extract (Natural Biomedicine S.r.l.) did not disclose the plant source. The MDA-MB-231 and chMDA-MB-231 cells were treated with different concentrations of CC for 24 hours, and then cell viability was evaluated. The results demonstrated a dose-dependent decrease in cell viability of chMDA-MB-231 cells, with an EC_{50} of approximately 0.2 mg/mL, while the parental cells remained unaffected at the tested concentrations (Figure 2A). The ability of CC to specifically target CSCs was assessed by examining the expression of CD44, a key marker of CSCs, by flow cytometry. As shown in Figure 29B, 0,2 mg/mL CC vegetable extract decreases the expression of CD44, which returns to the same value as that of the parental cells (Figure 2B). Our previous report describes that hypoxia promotes autophagy as a survival mechanism in dormant cells (6). To test if CC vegetable extract affects autophagy, the chMDA-MB-231 cells were treated with the indicated concentration of CC extract for 24 hours, and autophagosome formation was evaluated using MDC analysis. The results indicate that 0.2 mg/mL of CC vegetable extract induced an increase in autophagosome formation, suggesting that autophagy switches from a survival to a death mechanism. This effect is even pronounced with 0.2 mg/mL of CC vegetable extract (Figure 2C).

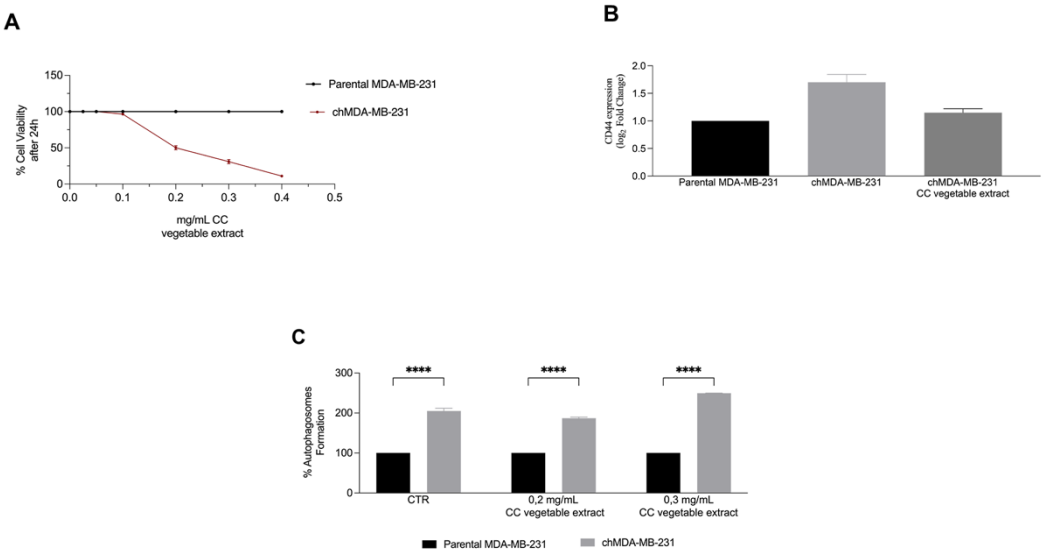

Figure 2. Effect of vegetable extract CC of dormant cancer cells. A) Cell viability assay at 24 hours after CC treatment in parental MDA-MB-231 and chMDA-MB-231 cells. Data are presented as mean ± SD from three independent experiments. B) Flow cytometry analysis of the $CD44^{+}/CD24^{-}$ immunophenotype of MDA-MB-231 and chMDA-MB-231 cells after CC treatment. C) MDC analysis of autophagosome formation after treatment with 0.2 mg/mL and 0.3 mg/mL CC vegetable extract. Incorporated MDC was measured using a multimode plate reader (Ex 340 nm and Em 535 nm) (GENios Pro, Tecan). The values were normalized for cell proliferation by the crystal violet assay. Data are presented as mean ± SD from three independent experiments.

Conclusion

In summary, the results obtained in this study demonstrate that prolonged exposure to chronic hypoxia (1% O_2 for 45 days) of MDA-MB-231 cells leads to the selection of a dormant subpopulation, designated as chMDA-MB-231. Moreover, the CC vegetable extract exhibits a cytotoxic effect toward these dormant cells, with an EC_{50} value of 0.2 mg/mL. The extract also reduces CD44 expression, indicating a potential impact on the stem-like features typically associated with dormant cancer cells. Finally, treatment with the CC enhances autophagosome formation, a mechanism that may contribute to the induction of cell death in dormant cancer cells.

References

1. Bejarano L, Jordão MJC, Joyce JA. Therapeutic Targeting of the Tumor Microenvironment. Cancer Discovery. 2021 Apr 1;11(4):933–59.

2. Lee P, Chandel NS, Simon MC. Cellular adaptation to hypoxia through hypoxia inducible factors and beyond. Nat Rev Mol Cell Biol. 2020 May;21(5):268–83.

3. Bayer C, Vaupel P. Acute versus chronic hypoxia in tumors. Strahlenther Onkol. 2012 July 1;188(7):616–27.

4. Bellot G, Garcia-Medina R, Gounon P, Chiche J, Roux D, Pouysségur J, et al. Hypoxia-Induced Autophagy Is Mediated through Hypoxia-Inducible Factor Induction of BNIP3 and BNIP3L via Their BH3 Domains. Molecular and Cellular Biology. 2009 May 1;29(10):2570–81.

5. Michiels C, Tellier C, Feron O. Cycling hypoxia: A key feature of the tumor microenvironment. Biochimica et Biophysica Acta (BBA) - Reviews on Cancer. 2016 Aug 1;1866(1):76–86.

6. Carcereri de Prati A, Butturini E, Rigo A, Oppici E, Rossin M, Boriero D, et al. Metastatic Breast Cancer Cells Enter Into Dormant State and Express Cancer Stem Cells Phenotype Under Chronic Hypoxia. Journal of Cellular Biochemistry. 2017;118(10):3237–48.

7. Hassn Mesrati M, Syafruddin SE, Mohtar MA, Syahir A. CD44: A Multifunctional Mediator of Cancer Progression. Biomolecules. 2021 Dec;11(12):1850.

8. Endo H, Okuyama H, Ohue M, Inoue M. Dormancy of Cancer Cells with Suppression of AKT Activity Contributes to Survival in Chronic Hypoxia. PLOS ONE. 2014 June 6;9(6):e98858.

9. Adam AP, George A, Schewe D, Bragado P, Iglesias BV, Ranganathan AC, et al. Computational Identification of a p38SAPK-Regulated Transcription Factor Network Required for Tumor Cell Quiescence. Cancer Research. 2009 July 15;69(14):5664–72.